WORLD METEOROLOGICAL ORGANIZATION

GLOBAL ATMOSPHERE WATCH

WORLD DATA CENTRE FOR GREENHOUSE GASES

WMO WDCGG DATA SUMMARY

WDCGG No. 41

GAW DATA

Volume IV-Greenhouse Gases and Other Atmospheric Gases

PUBLISHED BY
JAPAN METEOROLOGICAL AGENCY
IN CO-OPERATION WITH
WORLD METEOROLOGICAL ORGANIZATION

MARCH 2017

Acknowledgments

This issue of *Data Summary* reports the latest status of greenhouse and related gases in the global atmosphere. This *Data Summary* has been prepared by the World Data Centre for Greenhouse Gases (WDCGG), established under the Global Atmosphere Watch (GAW) Programme of the World Meteorological Organization (WMO) and operated by the Japan Meteorological Agency (JMA). This *Data Summary* is based on the data submitted by many contributors worldwide (Appendix: LIST OF CONTRIBUTORS). These contributors include both organizations and individuals involved in observations and research of greenhouse and related gases at stations and laboratories operating within the framework of GAW and some other monitoring and research programmes. The WDCGG thanks all of these organizations and individuals, including those from the global air sampling network of the National Oceanic and Atmospheric Administration (NOAA), for their efforts in maintaining the observation programme and continuous provision of observational data. Not all of the contributors may be explicitly acknowledged in this publication, owing to lack of space, but all the organizations and individuals that have submitted data to the WDCGG are nevertheless here acknowledged as invaluable contributors to this latest issue of *Data Summary*.

CONTENTS

	Page
SUMMARY	1
1. INTRODUCTION	3
2. ANALYSIS	5
3. CARBON DIOXIDE	7
4. METHANE	15
5. NITROUS OXIDE	21
6. HALOCARBONS AND OTHER HALOGENATED SPECIES	27
7. CARBON MONOXIDE	35
REFERENCES	41
APPENDICES	45
CALIBRATION AND STANDARD SCALES	46
LIST OF ABBREVIATIONS IN THE CALIBRATION AND STANDARD SCALES	55
LIST OF OBSERVATIONAL STATIONS	58
LIST OF CONTRIBUTORS	69
ACRONYMS	93
LIST OF WMO/ WDCGG PUBLICATIONS	94

SUMMARY

This *Data Summary* reports the results of basic analyses of greenhouse and related gas data submitted to the WMO World Data Centre for Greenhouse Gases (WDCGG) by contributing organizations and individuals. This issue covers observations from 1968 through 2015, based on data reported to the WDCGG by September 2016. The *Data Summary* includes analyses of global, hemispheric and latitudinal monthly mean mole fractions of greenhouse and related gases calculated using data from observations at marine and continental surface-based stations, and provides current information on the state of mole fractions of these gases.

Although monthly mean mole fractions were mainly used for the analyses, the WDCGG greatly appreciates those stations that submit daily, hourly and occasional mean mole fractions, which are important for analysis of variations on shorter time scales. All data submitted to the WDCGG are available on its website, http://ds.data.jma.go.jp/gmd/wdcgg/. In this *Data Summary*, data are reported as dry air mole fractions defined as the number of molecules of a target gas species divided by the number of all molecules in the air including the target itself, but excluding water vapor. Mole fractions are expressed as parts per million (ppm), parts per billion (ppb), and parts per trillion (ppt), which correspond to the SI units of μmol/mol, nmol/mol and pmol/mol, respectively.

Variations in the mole fractions of some gases are presented as combinations of seasonal cycles and deseasonalized long-term trends. Growth rates are presented as time derivatives of the long-term trends. Global average mole fractions are presented with accompanying uncertainty. The analytical results are summarized below for each greenhouse and related gas.

Carbon Dioxide (CO_2)

The level of carbon dioxide (CO_2), which contributes the most to increases in anthropogenic induced radiative forcing, has been increasing since the beginning of the industrial era. The global average mole fraction of CO_2 reached a new high of 400.0±0.1 ppm in 2015, which constitutes 144% of the pre-industrial level (in 1750). The annual increase of 2.3 ppm from 2014 to 2015 was larger than that observed from 2013 to 2014 and that averaged over the past decade (about 2.1 ppm/year).

The global growth rate of CO_2 shows significant interannual variability driven by natural processes. Large interannual changes in 1987/1988, 1997/1998, 2002/2003, 2009/2010 and 2014/2015 resulted from warmer conditions caused by El Niño-Southern Oscillation (ENSO) events. The anomalously strong El Niño event in 1997/1998 resulted in greater annual increases in CO_2 worldwide in 1998 than during any other one-year period. The high growth rate in 2012/2013 and the smaller one in 2013/2014 were most likely related to changes in fluxes between the atmosphere and terrestrial biosphere, particularly in tropical and subtropical regions (WMO, 2015). The exceptionally low growth rate in 1992, including negative values in northern high latitudes, may have been due to low global temperatures following the eruption of Mount Pinatubo in 1991.

Variations in CO_2 mole fraction can be seen on seasonal scales. The seasonal amplitudes are large in northern high and mid-latitudes and small in the Southern Hemisphere. In southern low latitudes, there is no clear annual cycle, but a semiannual cycle can be determined.

Methane (CH_4)

Methane (CH_4) is the second most significant greenhouse gas which is largely influenced by anthropogenic activity and whose level has been increasing since the beginning of the industrial era. The annual average mole fraction was 1845±2 ppb in 2015, an increase of 11 ppb since 2014. The mean annual absolute increase during the last 10 years was 6.0 ppb/year. The mole fraction is now 256% of that in the pre-industrial period.

The latitudinal gradient of CH_4 mole fraction is large from the northern mid-latitudes to the tropics, suggesting that the major sources of CH_4 are located in the Northern Hemisphere.

In the 1990s, CH_4 growth rates decreased significantly in all latitudinal zones. However, both hemispheres experienced high growth rates in 1998, caused by the higher than average global mean temperature. The global growth rates were generally low from 1999 to 2006, except during the El Niño event of 2002/2003, but since 2007 they have been high again. In the last nine years through 2015, the global mole fraction increased by 6.7 ppb/year.

CH_4 mole fractions vary seasonally, being relatively high in winter and low in summer. The seasonal amplitudes of CH_4 are large, not only in the Northern Hemisphere but also in southern high and mid-latitudes which are associated with methane sinks. In southern low latitudes, a distinct secondary maximum in boreal winter overlies the annual cycle.

Nitrous Oxide (N_2O)

Nitrous oxide (N_2O) is an important greenhouse gas whose level is increasing globally. N_2O data submitted to the WDCGG show that mole fractions are increasing in both hemispheres. The global mean

mole fraction reached a new high of 328.0±0.1 ppb in 2015, which is 1.0 ppb higher than that in the previous year. This mole fraction corresponds to 121% of that in the pre-industrial period. The mean annual absolute increase during the last 10 years was 0.89 ppb/year and the interhemispheric difference in mole fraction is 1.0 ppb (averaged over the years 1980 to 2015), indicating that the majority of N_2O sources are situated in the Northern Hemisphere.

Halocarbons and Other Halogenated Species

Halocarbons, most of which are anthropogenic and generated since the 20th century, are potent greenhouse gases, with some also acting as ozone-depleting compounds. Levels of some halocarbons (*e.g.* CFCs) increased in the 1970s and 1980s, but this increase has almost ceased by now, due to the production and consumption control of halocarbons under the Montreal Protocol on Substances that Deplete the Ozone Layer and its subsequent Adjustments and Amendments. However, some substances targeted by the Kyoto Protocol but not regulated by the Montreal Protocol, such as HFCs and SF_6, are increasing.

The mole fraction of CFC-11 peaked around 1992 and then started decreasing. The mole fraction of CFC-12 increased until around 2005 and then started decreasing gradually. The mole fraction of CFC-113 stopped increasing in the 1990s, followed by a slight decrease over about twenty years. The mole fractions of HCFCs, used mainly as substitutes for CFCs, have increased significantly during the last decade. The growth of HCFC-141b decelerated around 2005, but has accelerated over the last several years. The mole fraction of Halon-1211 has decreased since 2005, whereas the mole fraction of Halon-1301 is increasing. The mole fraction of CCl_4 was maximal around 1991 and has since decreased slowly. The mole fraction of CH_3CCl_3 peaked around 1992 and decreased thereafter. The mole fractions of HFC-134a, HFC-152a and SF_6 are increasing, but the growth of HFC-152a has decelerated over the last several years.

Carbon Monoxide (CO)

Carbon monoxide (CO) is not a greenhouse gas itself but influences the mole fractions of greenhouse gases by affecting hydroxyl radicals (OH). Beginning in 1950, the CO mole fraction increased at a rate of 1% per year but started to decrease in the late 1980s (WMO, 1999). In 2015, the global mean mole fraction of CO was 91±2 ppb. The mole fraction is high in the Northern Hemisphere and low in the Southern Hemisphere, suggesting substantial anthropogenic emissions in the Northern Hemisphere.

There is a large interannual variability of CO growth rates. The growth rate increases are mainly attributed to biomass burning emissions during El Niño conditions.

The monthly mean mole fractions show seasonal variations, with large amplitudes in the Northern Hemisphere and small amplitudes in the Southern Hemisphere with opposite phase.

1. INTRODUCTION

Human activities have had major impacts on the global environment. Since the beginning of the industrial era, mankind has increasingly made use of land, water, minerals and other natural resources, and continuous growth of the world human population and economies may further increase our impact on the environment. As the climate, biogeochemical processes and natural ecosystems are closely interlinked, changes in any one of these may affect the others and be detrimental to humans and other organisms. Emissions of anthropogenic gaseous species and particulate matter alter the energy balance of the atmosphere, which in turn has implications for the multiple interactions within the complex Earth's system. These interactions are not fully understood, partly due to the lack of high quality observations.

The World Meteorological Organization (WMO) established the Global Atmosphere Watch (GAW) Programme in 1989 to promote systematic and reliable observations of the global environment, including greenhouse gases (*e.g.*, CO_2, CH_4, CFCs, and N_2O) and some reactive gases (*e.g.*, O_3, CO, VOCs, NO_x, and SO_2) in the atmosphere. In October 1990, WMO designated the Japan Meteorological Agency (JMA) in Tokyo to serve as the World Data Centre for Greenhouse Gases (WDCGG). The WDCGG is responsible for collecting, archiving and providing data of greenhouse gases in the atmosphere and oceans from a number of observational sites throughout the world that participate in GAW and other scientific monitoring programmes (Appendix: LIST OF OBSERVATIONAL STATIONS).

The WDCGG had dealt with reactive gases as well as greenhouse gases by 2015. In January 2016, however, the newly established GAW World Data Centre for Reactive Gases (WDCRG) hosted by the Norwegian Institute for Air Research (NILU) took over responsibility for the reactive gases apart from CO. The WDCGG remains the primary archive for CO data which is a reactive gas by definition (not a greenhouse gas), but is of key importance to carbon cycle interpretation because CO influences greenhouse gases through its reaction with hydroxyl radicals (OH).

With regard to the issue of climate change the Kyoto Protocol to the United Nations Framework Convention on Climate Change came into force in February 2005. In March 2006, WMO commenced annual publication of the WMO Greenhouse Gas Bulletin, which summarizes the state of greenhouse gases in the atmosphere. The twelfth issue of the Bulletin was published in October 2016. The WDCGG contributes to the production of the Bulletin through timely and adequate collection and analysis of data in cooperation with the contributors of the data.

Since its establishment, the WDCGG has provided its users with data and other information through its regular publications, including the *Data Summary* (Appendix: LIST OF WMO WDCGG PUBLICATIONS). In accordance with the GAW Implementation Plan 2016-2023, all observational data and information on greenhouse gases are available on the WDCGG website, improving the accessibility of data, information and products (WMO, 2017). The WDCGG published the Data Submission and Dissemination Guide in 2007 (WMO, 2007), which, with its revision in 2009 (WMO, 2009b), is designed to facilitate submission of observational data and access to archived data in the WDCGG. Clear guidelines for data submission are included in the measurement guidelines published by GAW for the variables, which are under the responsibility of the WDCGG.

The WDCGG provides global and integrated diagnostics on the state of greenhouse and related gases as analytical information in the *Data Summary*. The WDCGG global analysis method in the *Data Summary* has been described in a GAW technical report (WMO, 2009a). The content of the *Data Summary* is revised and improved based on comments from data contributors and scientists. We hope the diagnostic information presented here will promote the use of data on greenhouse and related gases and will enhance appreciation of the value of the GAW Programme.

All users are required to accept the following statement endorsed by the Commission for Atmospheric Sciences (CAS) at its thirteenth session: "For scientific purposes, access to these data is unlimited and provided without charge. By their use you accept that an offer of co-authorship will be made through personal contact with the data providers or owners whenever substantial use is made of their data. In all cases, an acknowledgment must be made to the data providers or owners and to the data centre when these data are used within a publication." The WDCGG requests data users to make appropriate acknowledgments. The principal investigators and other contacts can be obtained from the WDCGG website, as well as from the GAW Station Information System (GAWSIS) website (https://gawsis.meteoswiss.ch). Information on these websites is updated in cooperation with the data contributors and the WMO Secretariat.

Finally, the WDCGG would like to thank all data contributors worldwide, including those involved in on-site measurements, for their efforts in maintaining the observational programmes and for continuous data provision.

Mailing address:

WMO World Data Centre for Greenhouse Gases (WDCGG)
c/o Japan Meteorological Agency
1-3-4, Otemachi, Chiyoda-ku, Tokyo 100-8122, Japan

E-mail: wdcgg@met.kishou.go.jp
Telephone: +81-3-3287-3439
Facsimile: +81-3-3211-4640
Website: http://ds.data.jma.go.jp/gmd/wdcgg/

2. ANALYSIS

The WDCGG gathers, archives and provides observational data on the mole fractions of greenhouse and related gases, and publishes diagnostic information on these gases based on the reported data.

The long-term trends and seasonal variations in the mole fractions of CO_2, CH_4, N_2O and CO are calculated for the whole globe (global means) and for latitudinal belts (zonal means). For halocarbons, only monthly mean mole fractions over time are presented without global, hemispheric or zonal averaging, due to insufficient number of reporting sites.

Mole fractions are expressed as parts per million (ppm), parts per billion (ppb), and parts per trillion (ppt), which correspond to the SI units of μmol/mol, nmol/mol and pmol/mol, respectively.

The method of analysis for CO_2, CH_4, N_2O and CO is summarized below. The details of the global analysis method are provided in the *Technical Report of Global Analysis Method for Major Greenhouse Gases by the World Data Centre for Greenhouse Gases*, published as a GAW technical report (WMO, 2009a). Additional uncertainty can be expected in the result of CO global analysis due to diversity of scales. When assessing long-term trends for CO_2, CH_4 and N_2O, the growth rates at both ends of the period were assumed to be simple linear extensions of the adjacent year, thus avoiding end effects. For simplicity, the growth rates for the rest of the period were approximated using linear regressions.

(1) Site selection

For CO_2, CH_4 and N_2O, the diagnostic analyses, including global, hemispheric and zonal means, were based on data from sites that have adopted a standard scale traceable to the Primary Standard designated by WMO. These analyses also utilize data on other standard scales that are convertible to the WMO scale through a proven equation. Letters informing data submitters of the most recent WMO scales are sent out regularly by the WDCGG as well as discussed at the regular expert meetings (WMO, 2016a).

Selection of observational sites is also based on whether they provide data representing a reasonably large geographical area, considering the fact that some sites may be susceptible to local sources and sinks. Sites are selected objectively using data submitted to the WDCGG. For CO_2, CH_4 and CO, only those sites that provide annual mean mole fractions falling within a range of $\pm 3\sigma$ from a curve fitted to the LOESS model curve (Cleveland and Devlin, 1988) have been selected in an iterative manner until no outliers are detected. This procedure does not affect the datasets residing in the WDCGG, and these data may be useful for purposes other than global analysis, such as identification of sources and sinks.

The sites selected according to the above criteria are marked with asterisks in Plate 3.1 for CO_2, Plate 4.1 for CH_4, Plate 5.1 for N_2O and Plate 7.1 for CO, which represent 125 (63%), 123 (72%), 33 (39%) and 111 (74%) of the submitted datasets respectively (detailed in 'LIST OF OBSERVATIONAL STATIONS' in this issue).

(2) Analysis of long-term trends

The mole fractions of greenhouse and related gases, measured under unpolluted conditions, exhibit variations on different time scales. The two major components are seasonal variations and long-term trends. Several attempts have been made to separate these variations from the measured data, including objective curve fitting (Keeling *et al.*, 1989), digital filtering (Thoning *et al.*, 1989; Nakazawa *et al.*, 1991), or both (Conway *et al.*, 1994; Dlugokencky *et al.*, 1994).

In this report, seasonal variations derived from components of Fourier harmonics and long-term trends are extracted by low-pass filtering with a cut-off frequency of 0.48 $year^{-1}$ for each selected site. Details are described in WDCGG *Data Summary* No. 22 (WMO, 2000).

(3) Estimation for missing periods and gaps

The number and distribution of sites used to assess trends during the analysis period should be kept to avoid the effects of changes in the availability of data over time. However, only a small number of sites provided data throughout the entire analysis period; others cover shorter periods or have gaps in measurements due to various reasons. To use as many sites as possible, data for missing values are estimated using interpolation and extrapolation in the calculation of zonal means as described below.

Gaps in some data were filled by linear interpolation based on available data in the long-term trends, which were derived by subtracting the seasonal variation calculated from the longest consecutive period of data with Lanczos filters (Duchon, 1979). The subtracted variation was added back to the data to obtain estimated mole fractions.

In the case of extrapolation, long-term trends from the existing or interpolated series of data were extrapolated using zonal mean growth rates calculated from other sites in the same latitudinal zone. The seasonal variation was added to the extrapolated long-term trend to obtain estimated mole fractions for the entire period of analysis.

Using these statistical procedures, the future addition of new stations should not affect the consistency in

global estimates over time.

(4) Calculation of global, hemispheric and zonal means

Zonal means were calculated by determining the arithmetic average of the mole fractions in each latitudinal zone, based on consistent datasets derived as above.

Global and hemispheric means were calculated as the weighted averages of the zonal means taking account of the area of each latitudinal zone.

Deseasonalized long-term trends and growth rates for the globe, each hemisphere and each latitudinal zone were calculated from the global, hemispheric and zonal means, respectively, using the low-pass filter mentioned above and the time derivatives after filtering.

Uncertainty in global means of major GHGs (CO_2, CH_4, N_2O and CO) was estimated using a method described in Conway *et al*. (1994) as the standard deviation of averages from a targeting observation network with its uneven geographical distribution of stations. The calculation procedure is as follows:

(i). Select a set of stations at random from the targeting network. A set comprises *n* observation stations, including at least one from each of six latitudinal bands of 30 degree width (90°N~60°N, 60°N~30°N, and so on). Any station may appear twice or more times in one set. In our case, *n* equals the number of stations in the GAW global network (number of stations after the site selection procedure described in this chapter).

(ii). Calculate the global mean *M* from the set in (i).

(iii). Repeat steps (i) and (ii) *m* times to obtain set M_m. We take *m* as 200 because the standard deviation becomes relatively stable compared to that for a smaller *m*.

(iv). Calculate the standard deviation of set M_m.

3.

CARBON DIOXIDE

(CO_2)

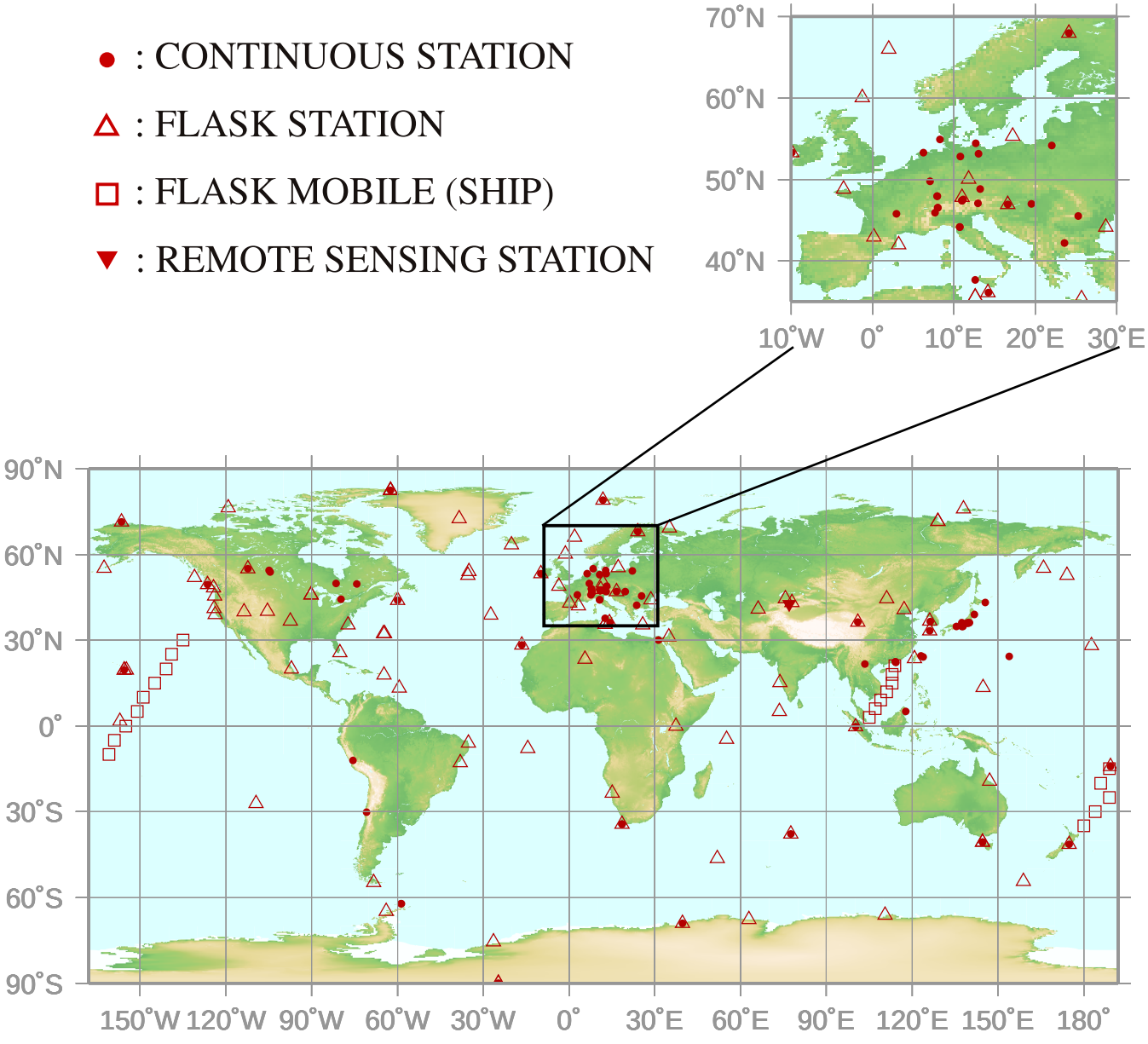

This map shows locations of the stations that have submitted data for monthly mean mole fractions.

CO_2 Monthly Data

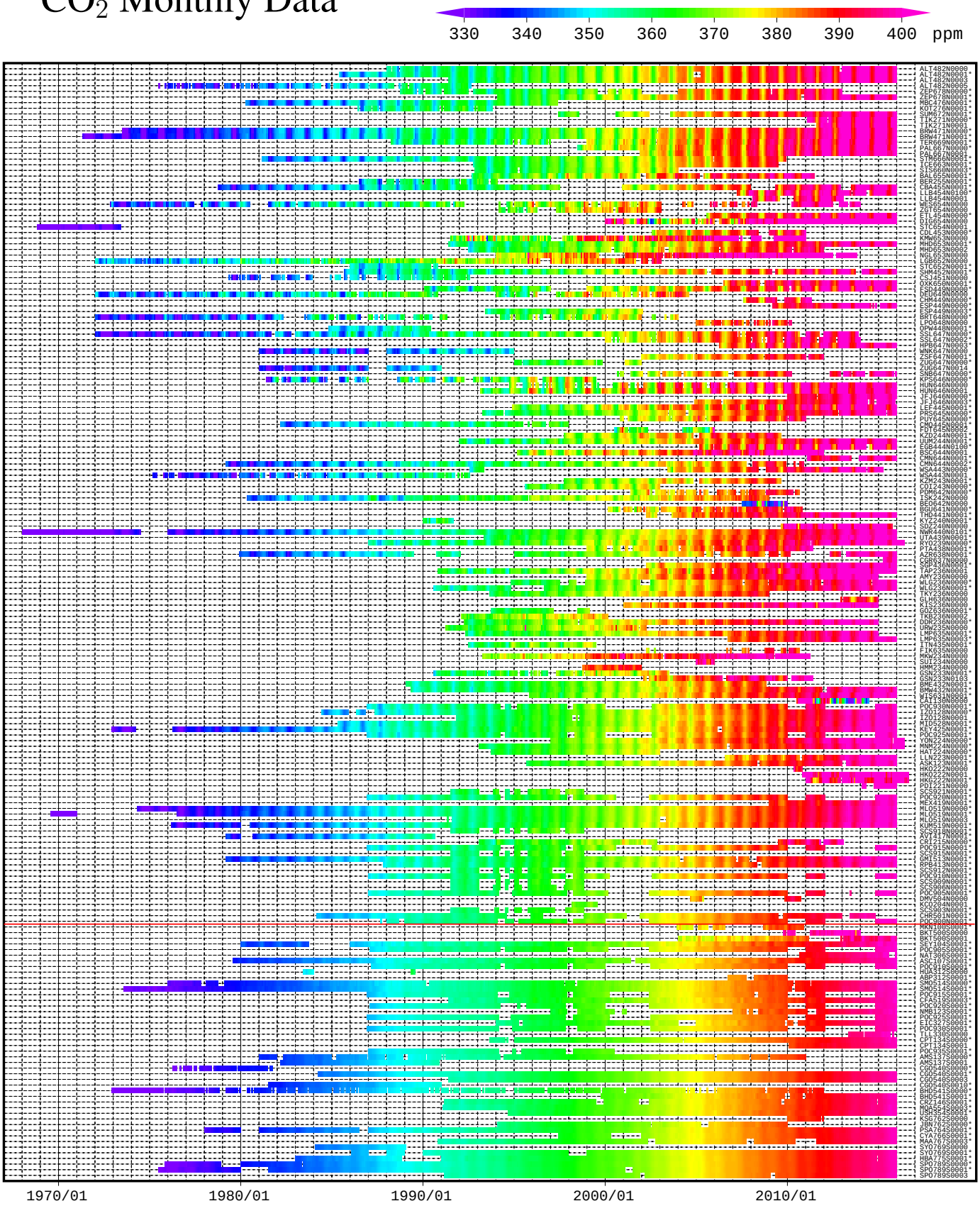

Plate 3.1 Monthly mean CO_2 mole fractions that have been reported to the WDCGG. The mole fractions are illustrated in different colors. The sites are listed in order from north to south. The red line indicates the equator. In cases where data are reported for two or three different altitudes, only the data at the highest altitudes are illustrated. In cases where monthly means are not reported, the WDCGG calculates them from hourly or other mole fractions reported to the WDCGG by simple arithmetic mean. The data from the sites with an asterisk at the end of the station index were used for the analyses shown in Plate 3.2. (see Chapter 2)

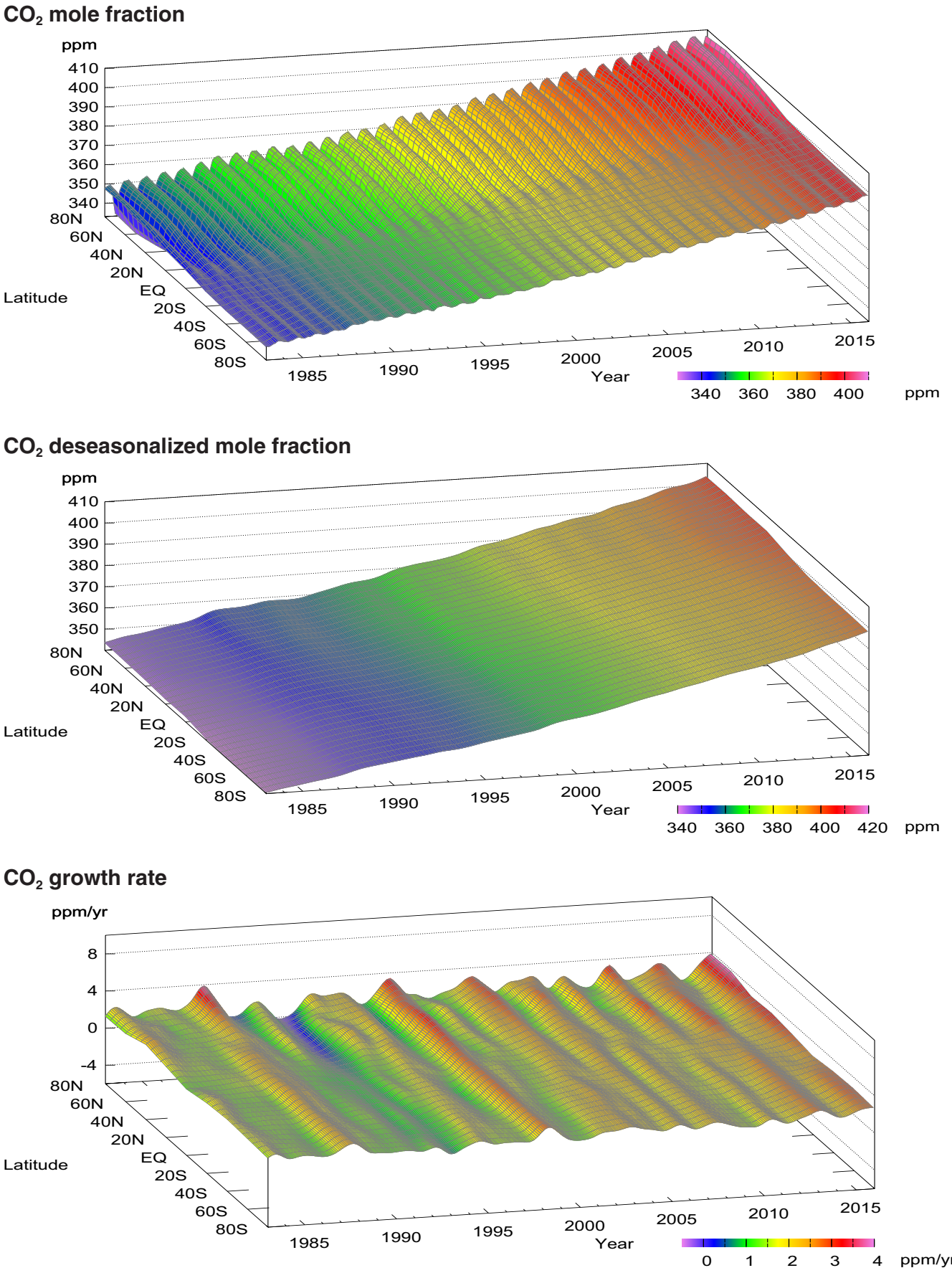

Plate 3.2 Variation of zonally averaged monthly mean CO_2 mole fractions (top), deseasonalized long-term trends (middle), and growth rates (bottom). The zonally averaged mole fractions were calculated for each 20° zone. The deseasonalized trends and growth rates were derived as described in Chapter 2.

3. CARBON DIOXIDE (CO_2)

Basic information on CO_2 with regard to environmental issues

Carbon dioxide (CO_2) has strong absorption bands in the infrared region and is the biggest anthropogenic contributor to anthropogenic greenhouse effect. CO_2 accounts for about 65% of total increase in the radiative forcing (since 1750) due to long-lived greenhouse gases in the atmosphere. It is responsible for 81% of the increase in radiative forcing over the past decade and 82% over the past five years (WMO, 2016b).

The balance of the fluxes between the atmosphere, the oceans and the biosphere determines the mole fraction of CO_2 in the atmosphere. An amount of 515 [445 to 585] PgC was emitted between 1870 and 2011 (IPCC, 2013) and annual anthropogenic emissions mainly due to fossil fuel combustion and cement production reached 9.9±0.5 PgC in 2015 (Le Quéré *et al.*, 2016). Carbon in the atmosphere is exchanged with two other large reservoirs, the terrestrial biosphere and the oceans. CO_2 exchanges between the atmosphere and terrestrial biosphere occur mainly through absorption by photosynthesis and emission from the respiration of plants and the decomposition of organic soils. These biogenic activities vary seasonally, resulting in large seasonal variations in the level of CO_2. The direction of CO_2 exchange between the atmosphere and oceans is determined by the gradient of CO_2 mole fraction, and varies in time and space.

Globally averaged mole fraction of CO_2 in the atmosphere reached the symbolic and significant milestone of 400 ppm for the first time in 2015. The current mole fraction far exceeds historic records, dating back at least 2.1 million years (Tans, 2009). Based on the results of ice core studies, the mole fraction of atmospheric CO_2 in pre-industrial times was about 278 ppm (IPCC, 2013). The emission of CO_2 due to human activities has increased dramatically since the beginning of the industrial era, impacting CO_2 exchange rates between different reservoirs and CO_2 levels not only in the atmosphere but in the oceans and terrestrial biosphere. The global carbon cycle, which is comprised mainly of CO_2, is not fully understood. About half of anthropogenic CO_2 emissions has remained in the atmosphere, with the remainder removed by sinks, including the terrestrial biosphere and oceans. The amount of CO_2 removed from the atmosphere varies significantly over time (Figure 3.1) and shows an increasing trend (Levin, 2012).

Carbon isotopic studies have shown the importance of the terrestrial biosphere and oceans as sources and sinks of CO_2 (Francey *et al.*, 1995; Keeling *et al.*, 1995; and Nakazawa *et al.*, 1993, 1997). In contrast, the atmospheric content of O_2 depends primarily on its removal by the burning of fossil fuels and on its release from the terrestrial biosphere. Therefore, the uptake of carbon by the terrestrial biosphere and oceans can be estimated from the combination of measurements of O_2 (O_2/N_2) and CO_2 (Manning and Keeling, 2006; WMO, 2014). A quasi-equilibrium amount of CO_2 is expected to be retained in the atmosphere by the end of the millennium that is surprisingly large: typically 40% of the peak concentration enhancement over pre-industrial values (278 ppm) (Solomon *et al.*, 2009).

Large amounts of CO_2 are exchanged among the reservoirs in nature, and the global carbon cycle is coupled with the climate system on seasonal, yearly and decadal time scales. Complete understanding of the global carbon cycle is essential for estimating future CO_2 mole fractions in the atmosphere.

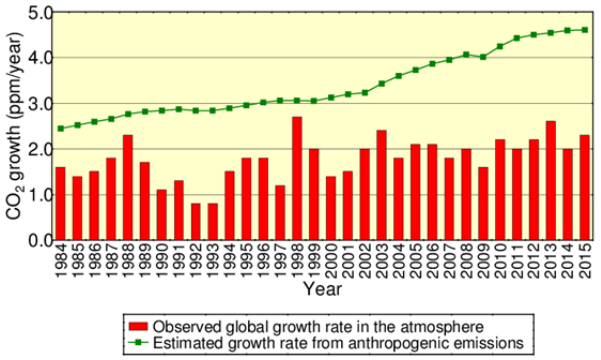

Fig. 3.1 Annual mean growth rates of CO_2 in the atmosphere, calculated from observational data (red columns) and that estimated from anthropogenic emissions (green curve). The estimated growth rates were calculated taking CO_2 emissions as a proxy (from Carbon Dioxide Information Analysis Center (CDIAC) (Boden *et al.*, 2016) for period 1984 to 2013 and from Global Carbon Project (Le Quéré *et al.*, 2016) for period 2014 to 2015), expressed as moles divided by the total mass of gas in the atmosphere (5.2 petatonnes) converted to moles based on the mean molar mass of dry air (about 29.0 g/mol). The observed growth rates were calculated by the WDCGG. CO_2 abundance from observational data is expressed as mole fractions with respect to dry air, while that estimated from anthropogenic emissions is based on the atmosphere, including water vapor, usually in a proportion less than 1%.

Mole fractions of CO_2 can be analyzed utilizing data submitted to the WDCGG from fixed stations and some ships. The observational sites from which data were used for the analysis are shown on the map at the beginning of this chapter. They include fixed stations

performing continuous measurements as well as flask-sampling stations, including those in the NOAA/ESRL cooperative air sampling network. In addition, mobile platforms such as ships and aircraft and other stations observing on an event basis report their data to the WDCGG (see Appendix: LIST OF OBSERVATIONAL STATIONS), which are not used for global analysis.

Annual variation of CO_2 mole fraction in the atmosphere

The monthly mean mole fractions of CO_2 used in the analysis are shown in Plate 3.1, with mole fraction levels illustrated in different colors. Global, hemispheric and zonal mean mole fractions were analyzed based on data from selected stations under unpolluted conditions (see the caption for Plate 3.1). Zonally averaged mole fractions of atmospheric CO_2, together with their deseasonalized components and growth rates, are shown as three-dimensional representations in Plate 3.2. These plots show that the seasonal variations in mole fraction are large in northern high and mid-latitudes, but are indistinct in the Southern Hemisphere. The increases in the Northern Hemisphere precede those in the Southern Hemisphere by one or two years, and the interannual variations in growth rate are larger in the Northern Hemisphere.

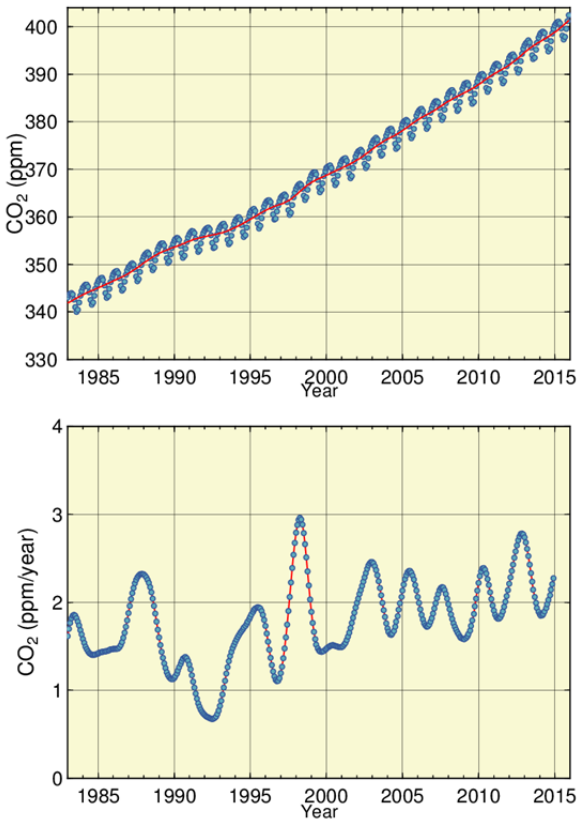

Fig. 3.2 Global monthly mean mole fraction of CO_2 from 1983 to 2015 and the deseasonalized long-term trend shown as a red line (top), and annual growth rate (bottom).

Figure 3.2 shows global monthly mean CO_2 mole fractions and their growth rates from 1983 to 2015. The global average mole fraction reached a new high of 400.0±0.1 ppm in 2015, which is 144% of the pre-industrial level of 278 ppm. The 2.3 ppm annual increase in 2014-2015 was greater than that observed in 2013-2014 and that averaged over the last decade (about 2.1 ppm/year).

The global growth rate shows large interannual variations, with an instantaneous maximum of about 3 ppm/year in 1998 and a minimum below 1 ppm/year in 1992. There were short periods of high rates in 1987/1988, 1997/1998, 2002/2003, 2005/2006, 2007, 2009/2010, 2012/2013 and 2014.

Figure 3.3 shows monthly mean mole fractions and long-term trends from 1983 to 2015 for each 30° latitudinal zone, indicating that there were clear long-term increases in both hemispheres and seasonal variations in the Northern Hemisphere.

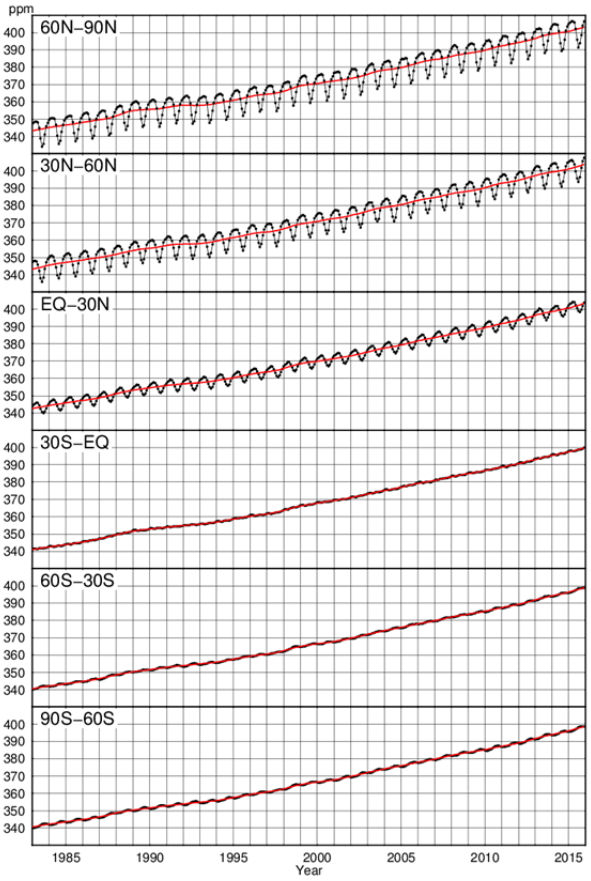

Fig. 3.3 Monthly mean mole fractions of CO_2 from 1983 to 2015 for each 30° latitudinal zone (dots) and their deseasonalized long-term trends (red lines).

As shown in Figure 3.4, the growth rates for each 30° latitudinal zone fluctuated between –0.3 and 3.6 ppm/year, with the largest interannual variability in

northern high latitudes. High growth rates for all 30° latitudinal zones were observed in 1987/1988, 1997/1998, 2002/2003, 2005, 2007, 2010 and 2012/2013, with negative rates recorded in northern high latitudes in 1992.

Changes in growth rate are partly associated with ENSO. Apart from that in 1991/1992, the El Niño events in 1982/1983, 1986–1988, 1997/1998, 2002/2003, 2009/2010 and 2014-2016 coincided with high growth rates of CO_2, whereas no El Niño event was reported in 2005/2006 and 2012/2013 when high growth rates of CO_2 were recorded. The larger increase of 2.3 ppm in annual mean mole fraction from 2014 to 2015, compared to those in previous years is due to increased natural emissions of CO_2 related to the El Niño event (WMO, 2016b). The growth rates of CO_2 observed by aircraft at high altitudes (8–13 km) over the Pacific Ocean were also associated with ENSO (Matsueda *et al.*, 2002).

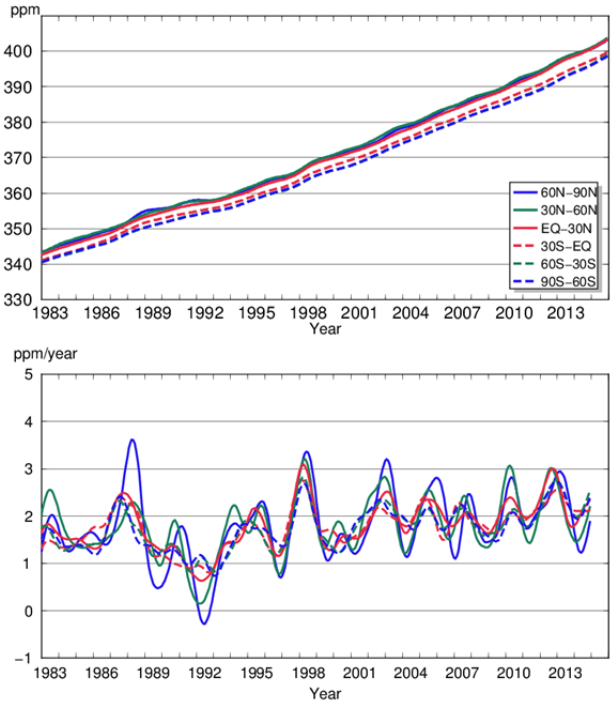

Fig. 3.4 Long-term trends in the mole fractions of CO_2 for each 30° latitudinal zone (top) and their growth rates (bottom).

During El Niño events, the up-welling of CO_2-rich ocean water in the eastern equatorial Pacific is suppressed, resulting in reduced CO_2 emissions from this area. El Niño events induce high temperature anomalies in many areas, particularly in the tropics, resulting in increased CO_2 emissions from the terrestrial biosphere due to the enhanced respiration of plants and activated decomposition of organic matter in soil (Keeling *et al.*, 1995). This effect is enhanced by the suppression of plant photosynthesis in areas of anomalously low precipitation, particularly in the tropics. These oceanic and terrestrial processes during El Niño events have opposing effects, but Heimann and Reichstein (2008) suggested that the latter was the main cause of the variation in the CO_2 growth rate.

However, an exceptionally low CO_2 growth rate occurred during the El Niño event in 1991/1992. The injection of 14 - 20 megatonnes (Mt) of SO_2 aerosols into the stratosphere by the Mount Pinatubo eruption in June 1991 affected the radiation budget and atmospheric circulation (Hansen *et al.*, 1992; Stenchikov *et al.*, 2002), resulting in a drop in global temperature. Angert *et al.* (2004) suggested that the low CO_2 growth rate observed during this El Niño event was due to reduced CO_2 emissions caused by consequent changes in the respiration of terrestrial vegetation and the decomposition of organic matter (Conway *et al.*, 1994; Lambert *et al.*, 1995; Rayner *et al.*, 1999), and by enhanced CO_2 absorption due to intensive photosynthesis caused by an increase in diffuse radiation (Gu *et al.*, 2003).

In contrast, exceptionally high CO_2 growth rates occurred in 2005/2006. This may have been related to the global high temperature. The high growth rate in 2012/2013 and the smaller growth rate in 2013/2014 are most likely related to changes in fluxes between the atmosphere and terrestrial biosphere, particularly in tropical and subtropical regions (WMO, 2015).

Seasonal cycle of CO_2 mole fraction in the atmosphere

Figure 3.5 shows average seasonal cycles in the mole fraction of CO_2 for each 30° latitudinal zone. The seasonal cycles are clearly large in amplitude in northern high and mid-latitudes and small in the Southern Hemisphere. The seasonal cycle in the Northern Hemisphere is mainly dominated by the land biosphere (Nevison *et al.*, 2008), and it is characterized by rapid decreases from June to August and large returns from September to December.

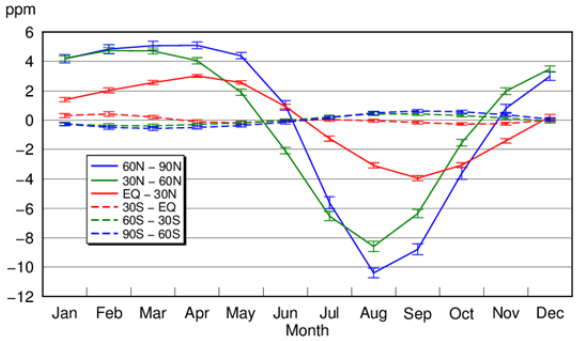

Fig. 3.5 Average seasonal cycles in the mole fractions of CO_2 for each 30° latitudinal zone obtained by subtracting long-term trends from the zonal mean time series. Vertical error bars represent the range of ±1σ which was calculated for each month. (period 1983 to 2015).

The mole fractions of CO_2 in northern low latitudes lagged behind that in high latitudes by one or two months. Minimum values appeared in August in northern high and mid-latitudes and in September in northern low latitudes.

In the Southern Hemisphere, seasonal variations showed small amplitudes with a half-year delay due to small amounts of net emission and absorption by the terrestrial biosphere. Seasonal variations in both northern and southern mid-latitudes were apparently superimposed in southern low latitudes (0–30°S). The direct influence of sources and sinks in the Southern Hemisphere may be partially cancelled by the propagation of an antiphase variation from the Northern Hemisphere.

Figure 3.6 shows latitudinal distributions of the mole fractions of CO_2 in January, April, July and October 2015, from sites marked with an asterisk in Plate 3.1. In latitudes north of 30°N, the mole fractions increased towards higher latitudes in January and April, and decreased towards higher latitudes in July, corresponding to the large seasonal variations in northern high and mid-latitudes, variations associated with activities of the terrestrial biosphere.

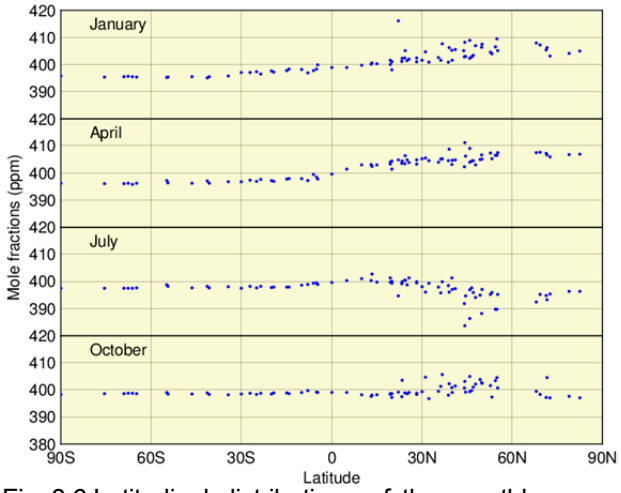

Fig. 3.6 Latitudinal distributions of the monthly mean mole fractions of CO_2 in January, April, July and October 2015.

4.

METHANE

(CH_4)

● : CONTINUOUS STATION

△ : FLASK STATION

□ : FLASK MOBILE (SHIP)

▼ : REMOTE SENSING STATION

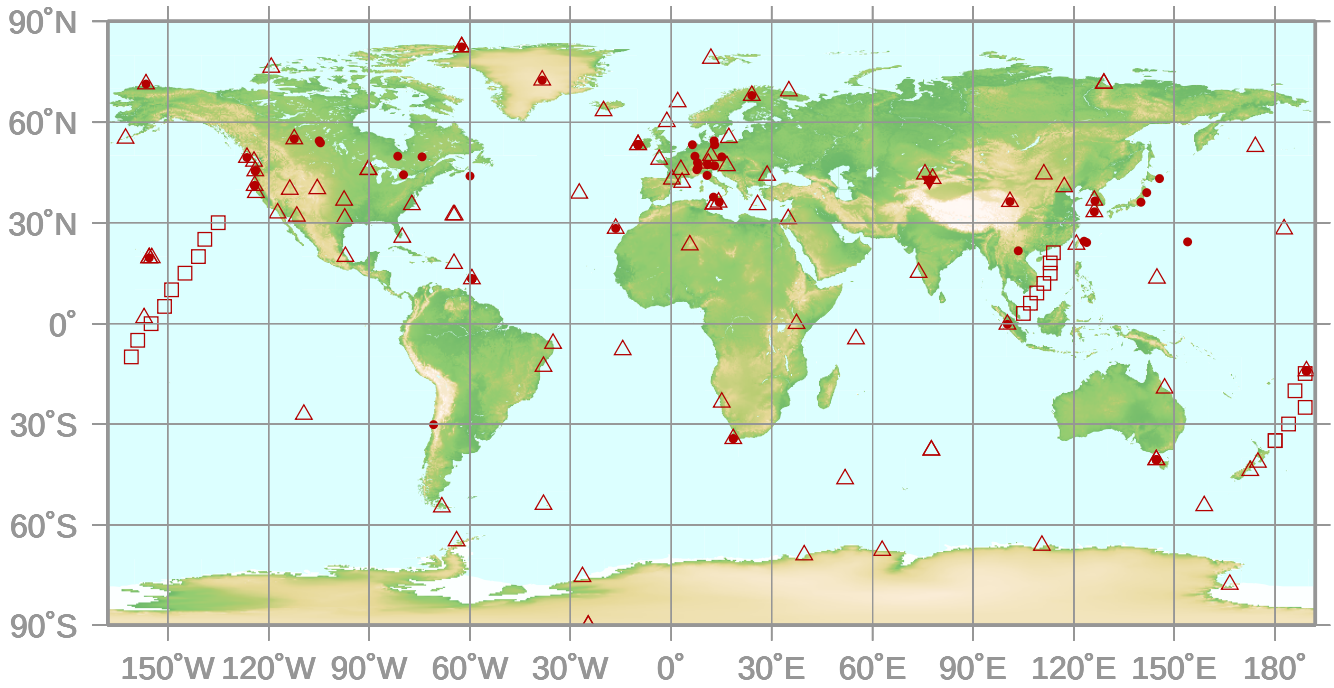

This map shows locations of the stations that have submitted data for monthly mean mole fractions.

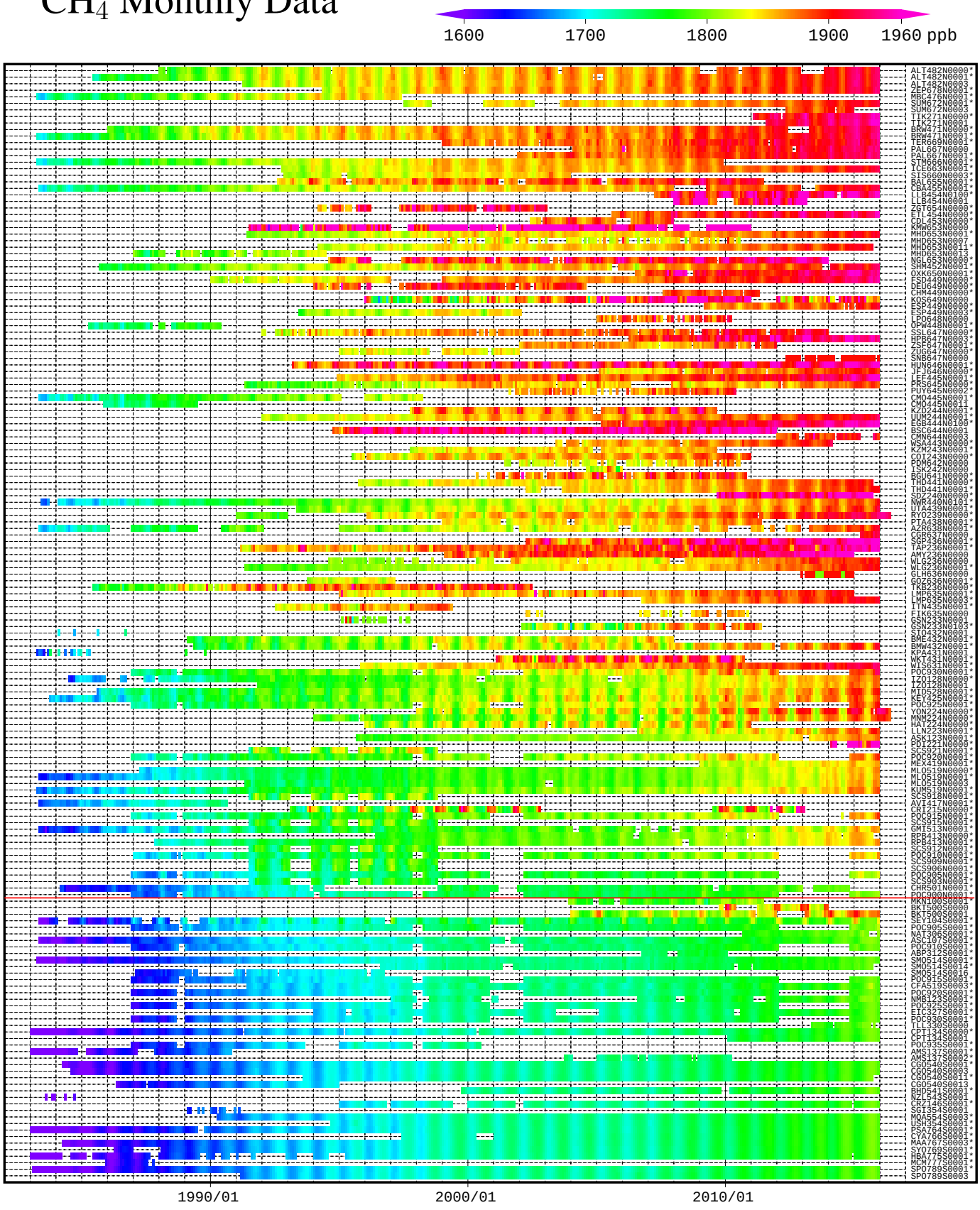

Plate 4.1 Monthly mean CH_4 mole fractions that have been reported to the WDCGG. The mole fractions are illustrated in different colors. The sites are listed in order from north to south. The red line indicates the equator. In cases where data are reported for two or three different altitudes, only the data at the highest altitudes are illustrated. In cases where monthly means are not reported, the WDCGG calculates them from hourly or other mole fractions reported to the WDCGG by simple arithmetic mean. The data from the sites with an asterisk at the end of the station index were used for the analyses shown in Plate 4.2. (see Chapter 2)

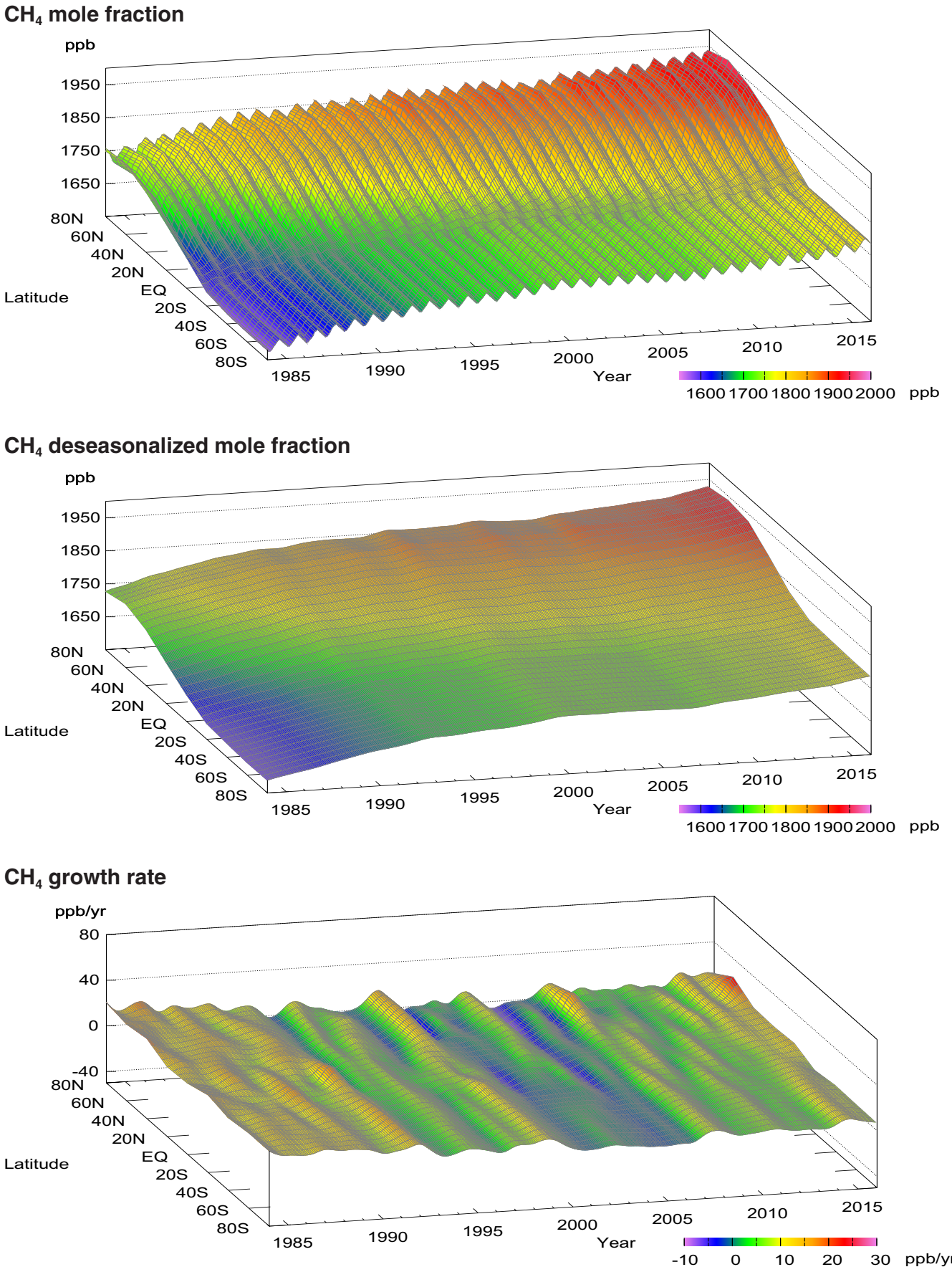

Plate 4.2 Variation of zonally averaged monthly mean CH_4 mole fractions (top), deseasonalized long-term trends (middle), and growth rates (bottom). The zonally averaged mole fractions were calculated for each 20° zone. The deseasonalized trends and growth rates were derived as described in Chapter 2.

4. METHANE (CH_4)

Basic information on CH_4 with regard to environmental issues

Methane (CH_4) is the second most important anthropogenic greenhouse gas, with an estimated global warming potential per molecule 28 times greater over a 100 year horizon and 84 times greater over a 20 year horizon than CO_2 (IPCC, 2013). Between 1750 and 2015, CH_4 accounted for about 17% of the total increase in radiative forcing due to long-lived greenhouse gases in the atmosphere (WMO, 2016b).

Analyses of air trapped in ice cores from Antarctica and the Arctic revealed that the current atmospheric CH_4 mole fraction is the highest over the last 680,000 years (Nisbet *et al.*, 2014). The mole fraction of CH_4 remained at about 700 ppb from 1000 A.D. until the start of the industrial era when it started increasing. Measurements in ice cores have shown that interpolar differences in CH_4 mole fractions between Greenland and Antarctica ranged from 24 to 58 ppb between 1000 and 1800 A.D. (Etheridge *et al.*, 1998). Atmospheric observations show that difference of the mole fractions between the high latitudinal belts of the Northern and Southern Hemispheres (see Fig. 4.3) averaged over the years 1984 to 2015 reached about 140 ppb. Increase in the interhemispheric gradient reflects the dominant impact of the emissions from the Northern Hemisphere, where major anthropogenic and natural sources are situated. Increased emissions from the Arctic have not contributed to the continued increase in atmospheric CH_4 since 2007 (WMO, 2013), when they last had an impact on the annual increase.

CH_4 is emitted by both natural and anthropogenic sources, including natural wetlands, oceans, landfills, rice paddies, enteric fermentation, fossil fuel production and consumption and biomass burning. The global emission of CH_4 was 558 teragrams (Tg) CH_4 per year for 2003-2012, with about 60% related to anthropogenic activities (Saunois *et al.*, 2016). CH_4 is removed from the atmosphere by reaction with hydroxyl radicals (OH) in both the troposphere and stratosphere, and by reaction with chlorine atoms and $O(^1D)$, an excited state of oxygen, in the stratosphere. CH_4 is one of the most important sources of water vapor in the stratosphere and has an atmospheric lifetime of about 10 years. More information regarding sources and sinks of CH_4 must be collected to better understand the budget of atmospheric CH_4.

Mole fractions of CH_4 are analyzed using data submitted to the WDCGG from fixed stations and some ships. These observational sites are shown on the map at the beginning of this chapter.

Annual variation of CH_4 mole fraction in the atmosphere

The monthly mean dry mole fractions of CH_4 used in this analysis are shown in Plate 4.1, with the mole fraction levels illustrated in different colors. Global, hemispheric and zonal mean mole fractions have been calculated based on data from selected stations under unpolluted conditions (see the caption for Plate 4.1). Zonally averaged atmospheric CH_4 mole fractions, together with their deseasonalized components and growth rates, are shown as three-dimensional representations in Plate 4.2. These plots show that the seasonal variations in CH_4 mole fraction are larger in the Northern than in the Southern Hemisphere and that the increase in the Northern Hemisphere propagates to the Southern Hemisphere. The growth rates vary on a global scale with the patterns similar to those for CO_2 (see Chapter 3). There is a large latitudinal gradient in CH_4 mole fraction from the northern mid-latitudes to the tropics, suggesting major sinks in the tropics, where the mole fraction of OH radicals is higher.

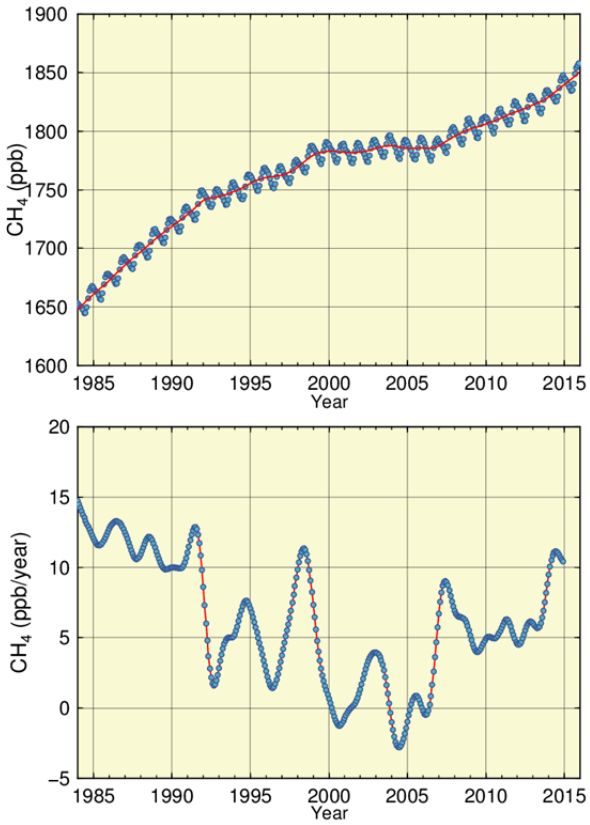

Fig. 4.1 Global monthly mean mole fraction of CH_4 from 1984 to 2015 and the deseasonalized long-term trend plotted by red line (top), and annual growth rate (bottom).

Figure 4.1 shows globally averaged monthly mean mole fractions and the growth rates for CH_4 from 1984 to 2015. The global average mole fraction was 1845±2 ppb in 2015, an increase of 11 ppb from 2014. The mole fraction changed little between 1999 and 2006. The mean annual absolute increase during the last 10 years was 6.0 ppb/year. The current mole fraction is 256% of its pre-industrial level of 722 ppb.

Figure 4.2 shows monthly mean mole fractions from 1984 to 2015 for each 30° latitudinal zone. The smallest magnitude of the seasonal variations occurred in the latitudinal zone between the equator and 30°S.

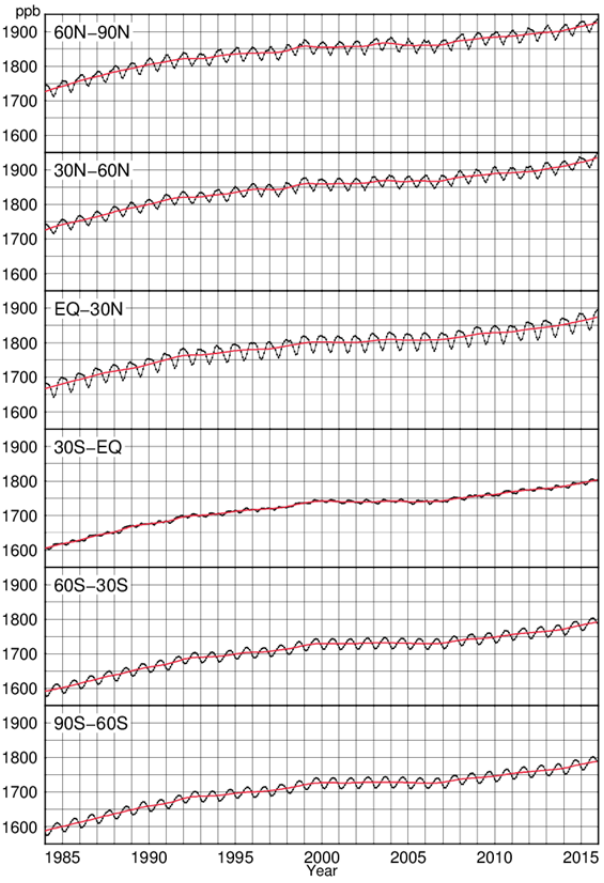

Fig. 4.2 Monthly mean mole fractions of CH_4 from 1984 to 2015 for each 30° latitudinal zone (dots) and their deseasonalized long-term trends (red lines).

Figure 4.3 summarizes deseasonalized long-term trends for each 30° latitudinal zone and their growth rates. A latitudinal gradient between the high and mid-latitudes of the Northern and Southern Hemispheres is almost absent, while the difference between high/mid-latitudes and low latitudes of the Northern Hemisphere is larger than that in the Southern Hemisphere. Fig. 4.3 also shows that mole fractions in most latitudinal belts have similar tendencies. In the 1990s, the growth rates clearly decreased in all latitudinal zones, but remained positive. The declined growth rate was especially evident during the second half of 1992, in 1996, and almost even in 2000 and in 2004/2005, when growth rates were less than 5 ppb/year in all latitudes. During the year 1998, the maximum global growth rate reached about 11 ppb/year (Fig. 4.1). Maximum increases occurred in high and mid-latitudes of the Northern Hemisphere, where the growth rates exceeded 15 ppb/year. In 2000, the global growth rate decreased to around -1 ppb/year. Around 2002/2003, the growth rates increased in the Northern Hemisphere, especially in northern high latitudes where they exceeded 10 ppb/year. The global growth rate was as low as -3 ppb/year in 2004 and 1 ppb/year in 2005. Despite the large growth rates in 1998 and 2002/2003, during El Niño events, the global mean mole fraction was relatively stable between 1999 and 2006. However, since 2007, the mole fraction has been increasing. The average growth rates over the last nine years through 2015 were 6.7 ppb/year. In 2014, growth rates exceeded 9 ppb/year in all latitudinal zones, contributing to a global growth rate almost as high as that in 1998.

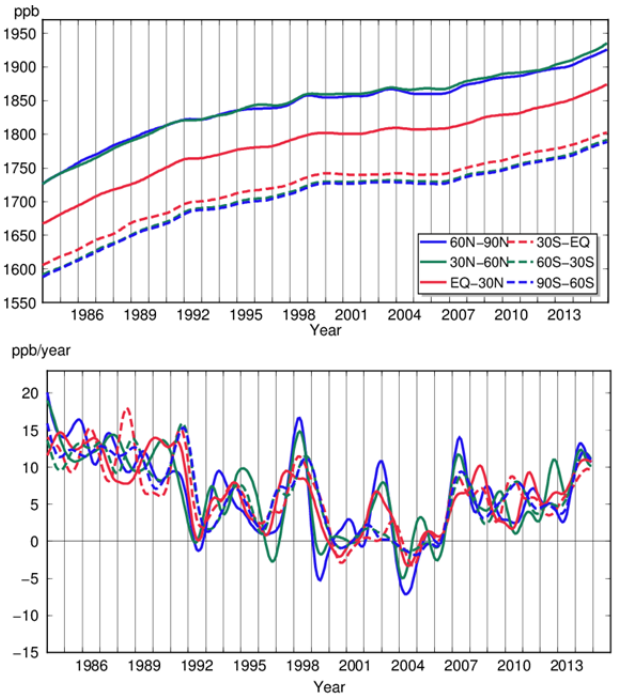

Fig. 4.3 Long-term trends in the mole fractions of CH_4 for each 30° latitudinal zone (top) and their growth rates (bottom).

The large increase in CH_4 growth rate in 1991 may have been caused by decreased levels of OH radicals in the atmosphere due to reduced UV radiation resulting from the eruption of Mt. Pinatubo in 1991 (Dlugokencky *et al.*, 1996), and the subsequent decrease in 1992 may have been due to an increase in OH radicals resulting from the depletion of stratospheric ozone following this eruption (Bekki *et*

al., 1994).

In 1998, the growth rates were high in all latitudes, which may have been due to increased emissions in northern high latitudes and tropical wetlands caused by high temperatures and increased precipitation, as well as by biomass burning in boreal forests, mainly in Siberia (Dlugokencky *et al.*, 2001). In contrast, Morimoto *et al.* (2006) estimated from isotope observations that the contribution of biomass burning to the increase in 1998 was about half that of wetlands. The growth rates were low from 1999 to 2006, with an exception during the El Niño event of 2002/2003. The causes of these decreases and increases in CH_4 growth rates are not yet determined.

Since 2007, atmospheric CH_4 has increased significantly throughout the entire monitoring network (Rigby *et al.*, 2008; Dlugokencky *et al.*, 2009). This is due to increased emissions in the tropical and mid-latitude Northern Hemisphere (Nisbet *et al.*, 2014). The attribution of this increase to anthropogenic and natural sources is difficult because the current network is insufficient to characterize emissions by region and source process (Bergamaschi *et al.*, 2013).

The WMO/GAW observational network includes the observations of carbon stable isotopes in methane, with 15 datasets submitted to the WDCGG. Such observations can be useful for the identification of primary methane sources.

Seasonal cycle of CH_4 mole fraction in the atmosphere

Figure 4.4 shows seasonal cycles in the mole fraction of CH_4 for each 30° latitudinal zone. The seasonal cycles are driven mainly by reaction with OH radicals, a major CH_4 sink in the atmosphere. Seasonal cycles are also affected by the magnitude and timing of CH_4 emissions from sources such as wetlands and biomass burning as well as by its atmospheric transport. The seasonal cycles are large in amplitude in the Northern Hemisphere. Unlike CO_2, amplitudes were also large in high and mid-latitudes of the Southern Hemisphere. Seasonally, the Northern Hemisphere shows minima in summer and maxima in winter, while the Southern Hemisphere shows a seasonal cycle lagging two-thirds to three-quarter years behind. The seasonal variations in the mole fraction of CH_4 were almost consistent with those of the OH radical that reacts with CH_4. Southern low latitudes have a distinct antiphase annual component with that of the seasonal cycle arising from southern mid-latitudes. The maximum in the former component occurs in boreal winter due to the interhemispheric transport of CH_4 from the Northern Hemisphere.

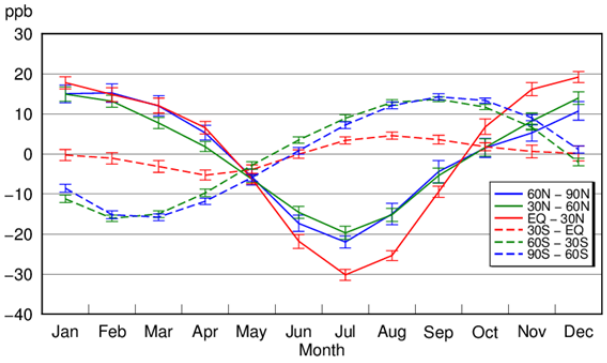

Fig. 4.4 Average seasonal cycles of CH_4 mole fractions for each 30° latitudinal zone obtained by subtracting long-term trends from the zonal mean time series. Vertical error bars represent the range of ±1σ calculated for each month. (period 1984 to 2015).

5.

NITROUS OXIDE

(N_2O)

● : CONTINUOUS STATION

△ : FLASK STATION

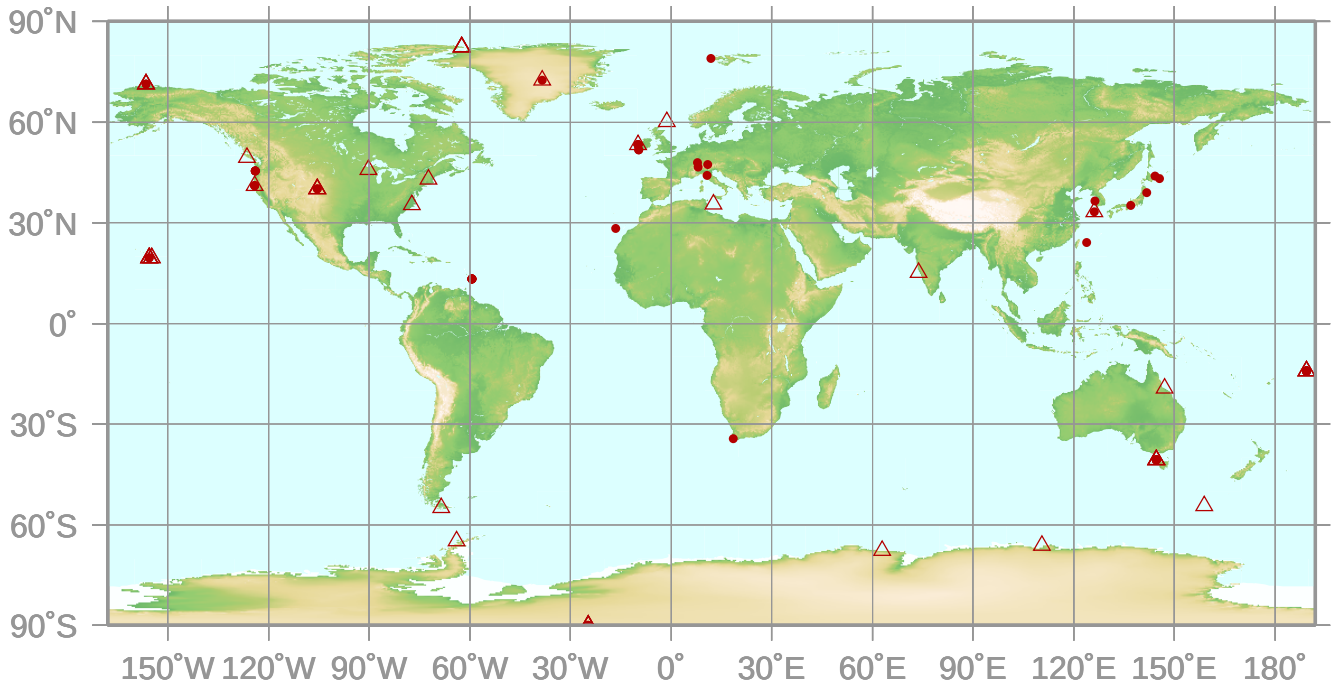

This map shows locations of the stations that have submitted data for monthly mean mole fractions.

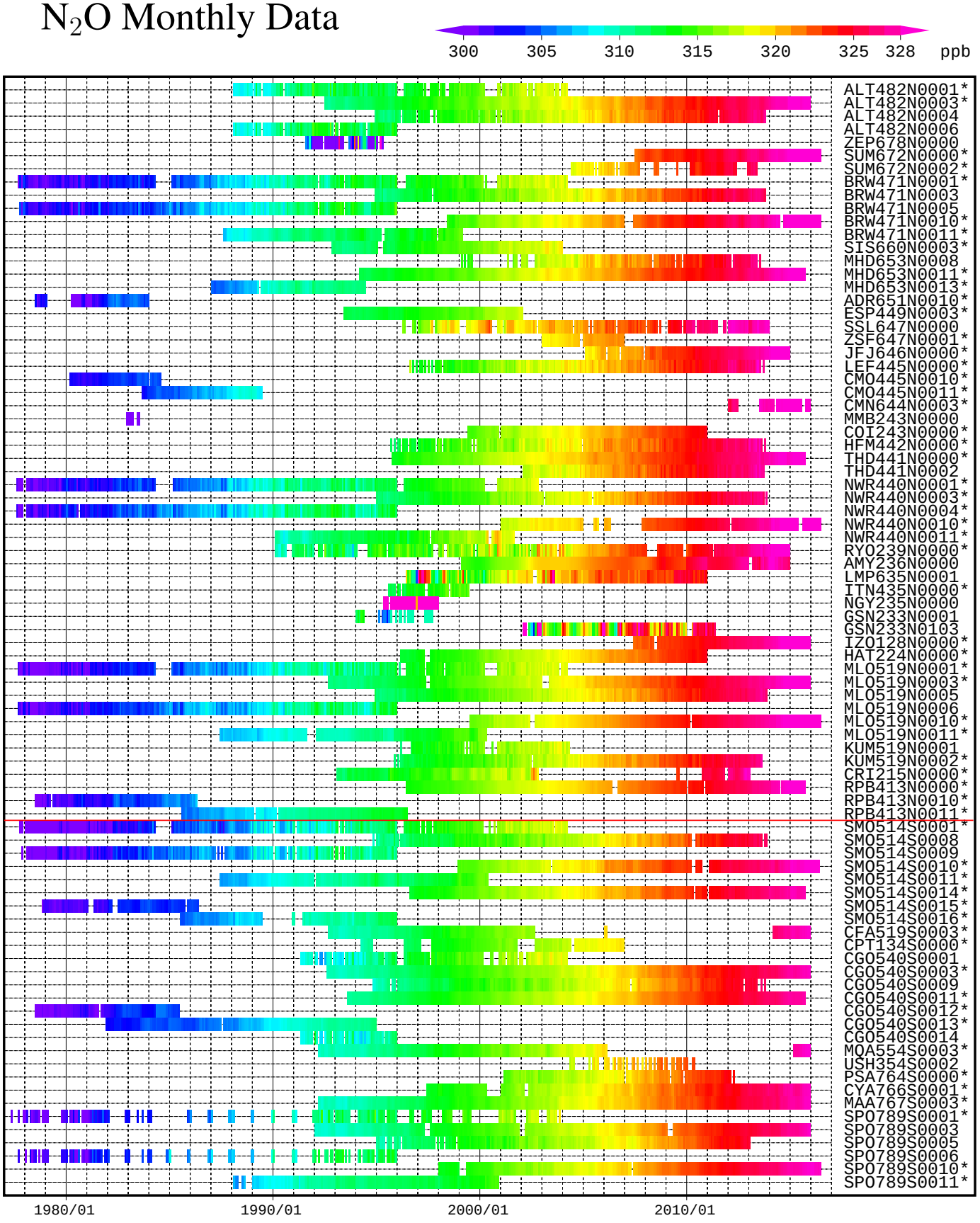

Plate 5.1 Monthly mean N_2O mole fractions that have been reported to the WDCGG. The mole fractions are illustrated in different colors. The sites are listed in order from north to south. The red line indicates the equator. The data from the sites with an asterisk at the end of the station index were used for the analyses shown in Plate 5.2. (see Chapter 2)

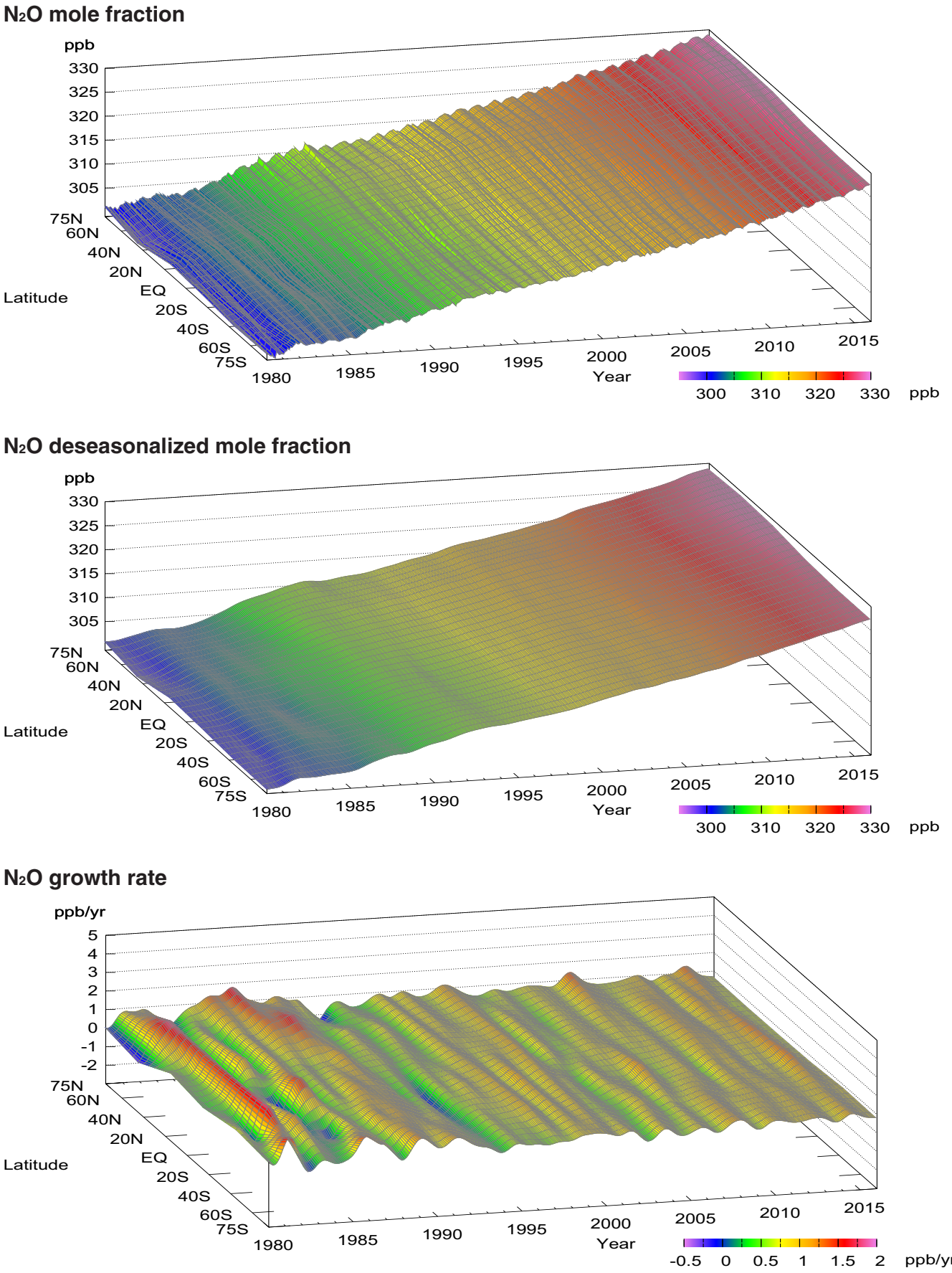

Plate 5.2 Variation of zonally averaged monthly mean N_2O mole fractions (top), deseasonalized long-term trends (middle), and growth rates (bottom). The zonally averaged mole fractions were calculated for each 30° zone. The deseasonalized trends and growth rates were derived as described in Chapter 2.

5. NITROUS OXIDE (N_2O)

Basic information on N_2O with regard to environmental issues

Nitrous oxide (N_2O) is a relatively stable greenhouse gas in the troposphere with a lifetime of 121 years (IPCC, 2013). Between 1750 and 2015, N_2O accounted for about 6% of the total increase in radiative forcing due to long-lived greenhouse gases (WMO, 2016b). N_2O is the third most important anthropogenic greenhouse gas in the atmosphere. It also plays an important role in stratospheric ozone depletion (Ravishankara *et al*., 2009). The mole fraction of N_2O in the atmosphere has increased steadily from its pre-industrial level of 270 ppb to its current value, which is 21% higher. Prior to industrialization, the atmospheric N_2O burden reflected the balance between emissions from natural systems (soils and oceans) and chemical losses in the stratosphere. In the industrial era, additional emissions result from the use of synthetic nitrogen fertilizers (direct emissions from agricultural fields and indirect emissions from waterways affected by agricultural runoff), fossil fuel combustion, biomass burning and other minor processes.

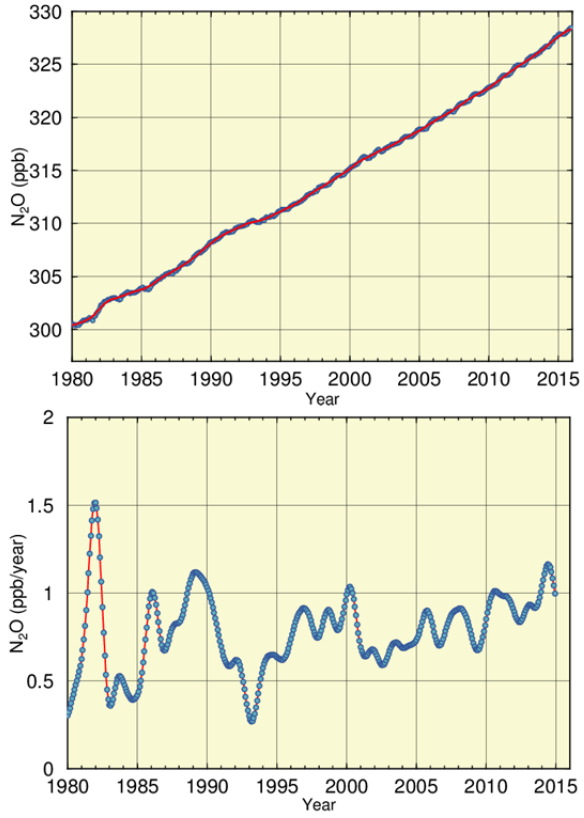

Fig. 5.1 Globally averaged monthly mean mole fraction of N_2O from 1980 to 2015 and the deseasonalized long-term trend shown as a red line (top), and annual growth rate (bottom).

Currently, anthropogenic sources are responsible for ~40% of total emissions (WMO, 2016b). Most of the anthropogenic N_2O enters the atmosphere from the transformation of fertilizer nitrogen into N_2O and its subsequent emission from agricultural soils.

However, more research is needed to understand the role of N_2O in the global nitrogen cycle.

Long-term trend of N_2O mole fraction in the atmosphere

Dry mole fractions of N_2O are analyzed using the data submitted to the WDCGG from fixed stations and some ships. The observational sites that supplied data used for this analysis are shown on the map at the beginning of this chapter. The monthly mean mole fractions of N_2O, including the ones used in the global analysis, are shown in Plate 5.1, with the various mole fraction levels illustrated in different colors. The data submitted to the WDCGG show that N_2O mole fractions have increased at almost all stations. Zonally averaged atmospheric N_2O mole fractions, together with their deseasonalized components and growth rates, are shown as three-dimensional representations from 1980 to 2015 in Plate 5.2.

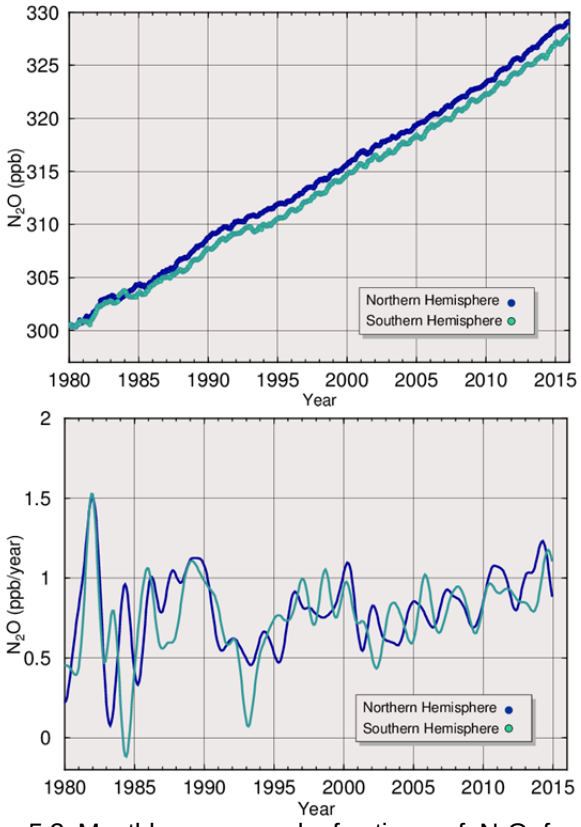

Fig. 5.2 Monthly mean mole fractions of N_2O from 1980 to 2015 (top) and annual growth rates (bottom), averaged over the Northern and Southern Hemispheres.

Figure 5.1 shows globally averaged monthly mean N_2O mole fractions from 1980 to 2015 and its long-term trend. The global average mole fraction reached a new high of 328.0±0.1ppb in 2015, an increase of 1.0 ppb over the previous year. The mean annual absolute increase during the last 10 years was 0.89 ppb/year. Annual averages of atmospheric growth rate showed substantial variability (from 0.4 to 1.1 ppb/year) from the beginning of observations. The interhemispheric difference in mole fraction of N_2O averaged over year 1980 to 2015 is 1.0 ppb (Figure 5.2 upper panel), indicating that the majority of N_2O sources are situated in the Northern Hemisphere.

6.

HALOCARBONS AND OTHER HALOGENATED SPECIES

● : CONTINUOUS STATION

△ : FLASK STATION

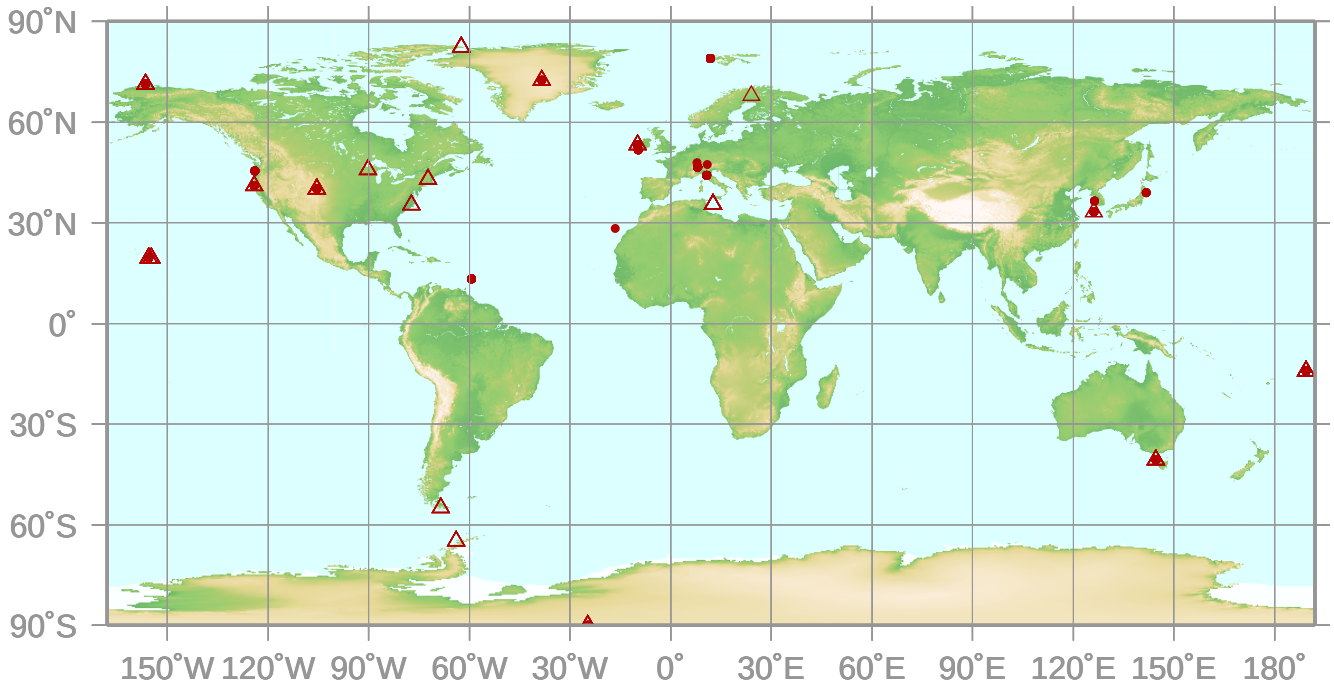

This map shows locations of the stations that have submitted data for monthly mean mole fractions.

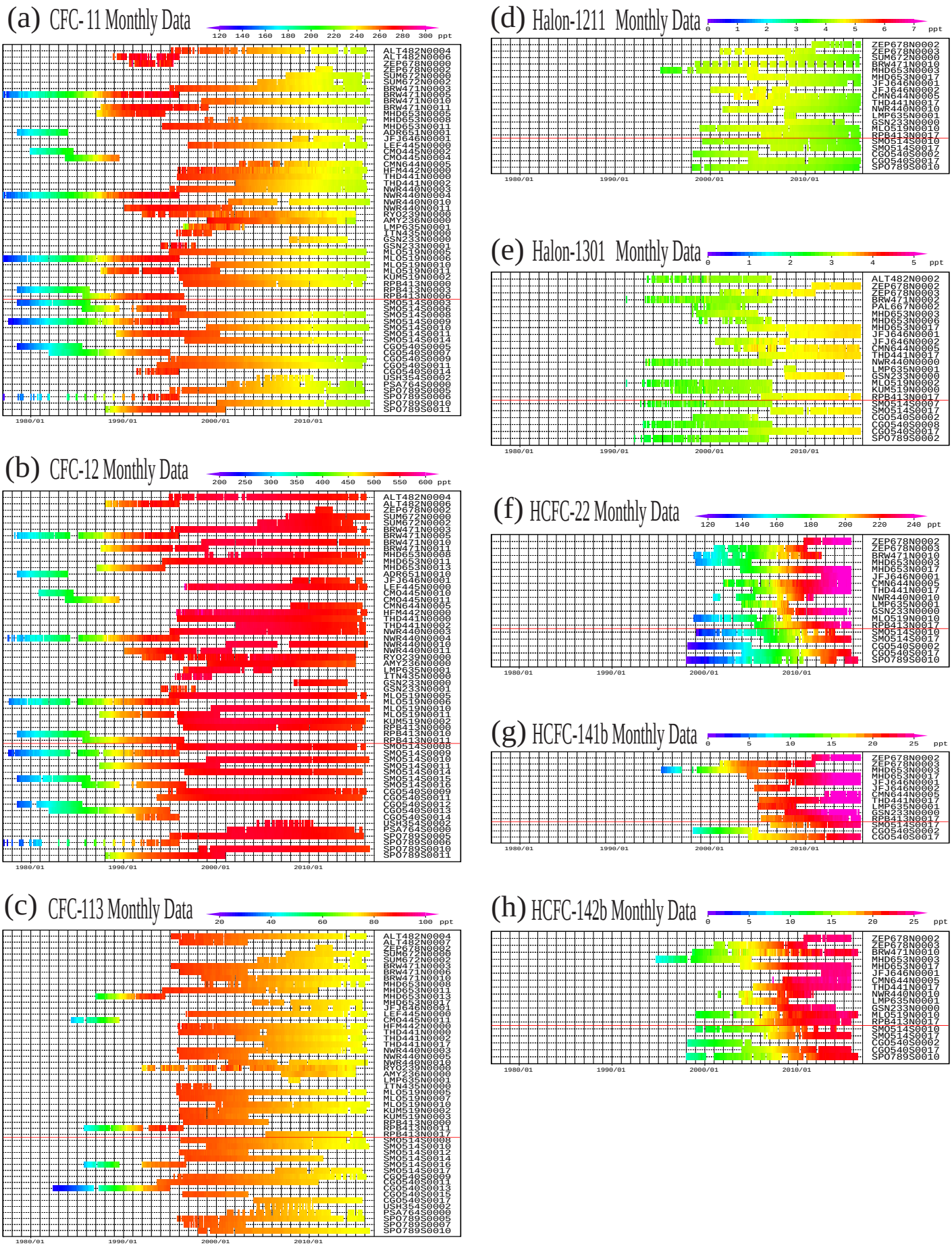

Plate 6.1 Monthly mean (a) CFC-11, (b) CFC-12, (c) CFC-113, (d) Halon-1211, (e) Halon-1301, (f) HCFC-22, (g) HCFC-141b, (h) HCFC-142b mole fractions that have been reported to the WDCGG. The mole fractions are illustrated in different colors. The sites are listed in order from north to south. The red line indicates the equator.

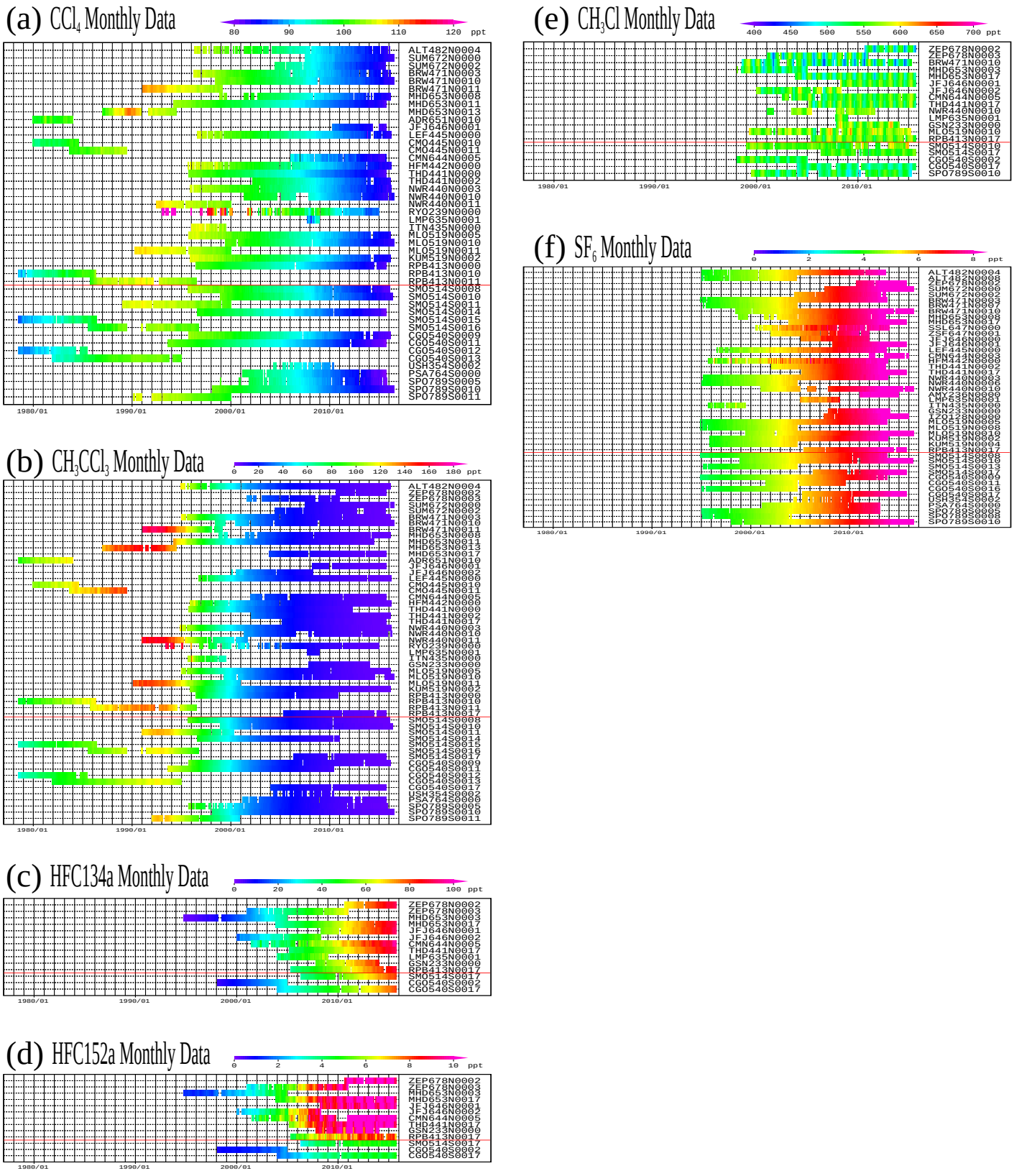

Plate 6.2 Monthly mean (a) CCl_4, (b) CH_3CCl_3, (c) HFC134a, (d) HFC152a, (e) CH_3Cl, (f) SF_6 mole fractions that have been reported to the WDCGG. The mole fractions are illustrated in different colors. The sites are listed in order from north to south. The red line indicates the equator.

6. HALOCARBONS AND OTHER HALOGENATED SPECIES

Basic information on halocarbons with regard to environmental issues

Halocarbons are carbon compounds containing one or more halogens, *i.e.*, fluorine, chlorine, bromine or iodine, with most being industrial products. Halocarbons are classified into chlorofluorocarbons (CFCs), which contain fluorine and chlorine; the hydrochlorofluorocarbons (HCFCs), which contain hydrogen in addition to fluorine and chlorine; and the halons, which contain bromine and other halogens. Perfluorocarbons (PFCs) are carbon compounds in which all hydrogen atoms are replaced by fluorine atoms, and hydrofluorocarbons (HFCs) are halocarbons that contain hydrogen and fluorine but no chlorine. Most halocarbons (HFCs, CCl_4, CH_3CCl_3, etc.) are produced industrially, whereas some species (*e.g.*, CH_3Cl) have natural sources. Although the mole fractions of the halocarbons are relatively low in the atmosphere, they have high global warming potentials. The halocarbons have been shown to account for about 12% of the total increase in radiative forcing due to long-lived greenhouse gases from 1750 to 2015 (WMO, 2016b).

The halocarbons are colorless, odorless and innocuous substances that can be readily gasified and liquefied and have low surface tension. Thus, they were commonly used as refrigerants, propellants and detergents for semiconductors, resulting in a rapid increase in their mole fractions in the atmosphere until the 1980s. Halocarbons containing chlorine and bromine led to the depletion of the ozone layer. Since the mid-1990s, the Montreal Protocol on Substances that Deplete the Ozone Layer and its subsequent Adjustments and Amendments have progressively tightened the regulations for the production, consumption and trade of ozone-depleting substances.

The CFCs are destroyed mainly by ultraviolet radiation in the stratosphere, and their lifetimes are generally long (*e.g.*, about 50 years for CFC-11). However, the HCFCs and CH_3CCl_3, which contain hydrogen, react with hydroxyl radicals (OH) in the troposphere and have relatively short lifetimes (*e.g.*, about 5 years for CH_3CCl_3). As the reaction with OH in the troposphere is a major sink for CH_3CCl_3, global measurements of CH_3CCl_3 provide an accurate estimate of the global mole fraction of OH (Prinn *et al.*, 2001). However, due to a substantial decrease of CH_3CCl_3 mole fraction in the atmosphere, reconstruction of OH levels using this molecule is becoming increasingly difficult and other compounds are now used as reference tracers for OH mole fraction determination.

The Kyoto Protocol to the United Nations Framework Convention on Climate Change (UNFCCC), which came into force on 16 February 2005, specifies HFCs, PFCs and sulfur hexafluoride (SF_6) as targets for quantified emission limitation and reduction commitments.

SF_6, although not a halocarbon, behaves similarly to halocarbons and is a potent long-lived greenhouse gas. Its emissions are almost entirely anthropogenic, and it is used mainly as an electrical insulator in power distribution equipment. SF_6 current mole fraction is about twice the level observed in the mid-1990s (WMO, 2016b). It has a very long atmospheric lifetime, 3,200 years, so emissions accumulate in the atmosphere. These emissions can be determined utilizing atmospheric observations of SF_6 and the rate of mole fraction in inverse modelling (Levin *et al.*, 2010).

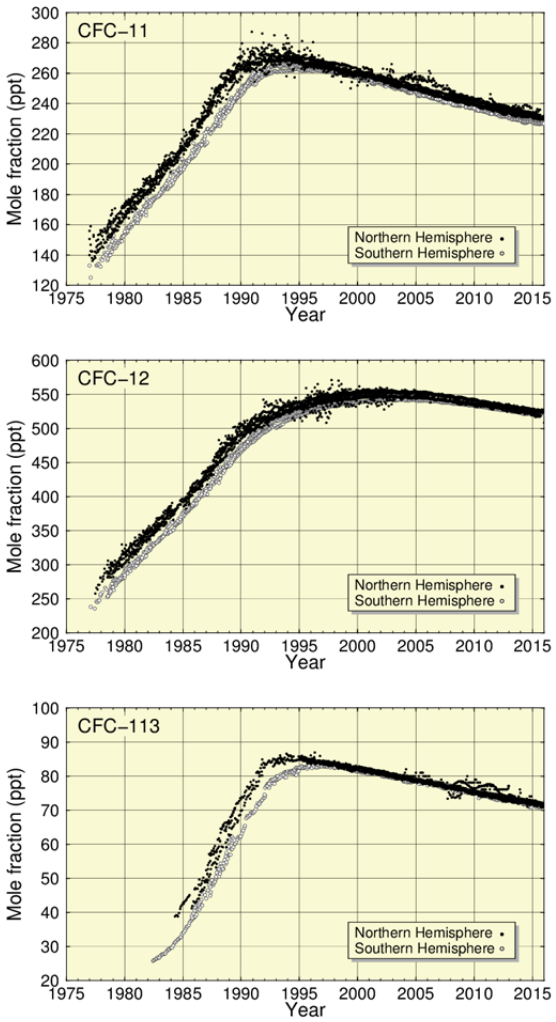

Fig. 6.1 Time series of the monthly mean mole fractions of CFC-11, CFC-12 and CFC-113 at individual stations. Solid circles show mole fractions in the Northern Hemisphere and open circles show those measured in the Southern Hemisphere.

Annual changes in the levels of halocarbons in the atmosphere

The cover map of this chapter shows observational sites that have submitted data on halocarbons and other halogenated species to the WDCGG. Although the number of stations measuring these species is rather limited, halocarbons are generally well mixed in the atmosphere and the data may be sufficient to reflect their global tendencies. Plates 6.1 and 6.2 show all the monthly mean mole fractions of these gases submitted to the WDCGG. The figures (6.1 – 6.7) in this chapter show the monthly mean data reported to the WDCGG without spatial averaging. Some discrepancies in the absolute mole fractions were observed between several stations, suggesting that these stations may have adopted different standard scales. Observational data expressed on the same standard scales revealed that the differences in the mole fractions between the two hemispheres were large in the 1980s for CFCs, CCl_4 and CH_3CCl_3 but have since narrowed as the emissions have been suppressed and the existing constituents have been mixed between the hemispheres.

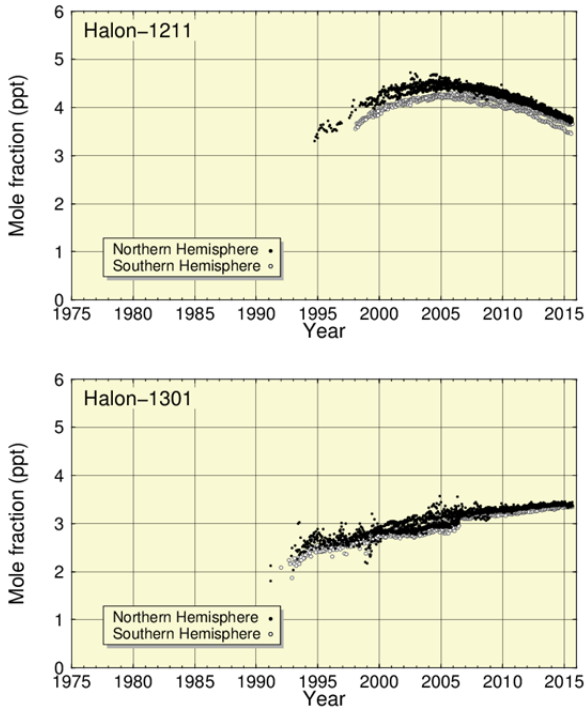

Fig. 6.2 Time series of the monthly mean mole fractions of Halon-1211 and Halon-1301 at individual stations. Solid circles show mole fractions measured in the Northern Hemisphere and open circles show those measured in the Southern Hemisphere.

Figure 6.1 shows monthly mean mole fractions of CFC-11 (CCl_3F), CFC-12 (CCl_2F_2) and CFC-113 (CCl_2FCClF_2) over time. The mole fractions of CFC-11 peaked around 1992 in the Northern Hemisphere, followed by a maximum about one year later in the Southern Hemisphere. The mole fractions of CFC-113 were maximal around 1992 in the Northern Hemisphere and around 1997 in the Southern Hemisphere. The mole fractions of these gases have since been decreasing slowly in both hemispheres. The mole fraction of CFC-12 increased until around 2005 and then started decreasing gradually.

Figure 6.2 shows time series of the monthly mean mole fractions of Halon-1211 ($CBrClF_2$) and Halon-1301 ($CBrF_3$). The mole fraction of Halon-1211 has decreased since 2005, whereas the mole fraction of Halon-1301 has been increasing.

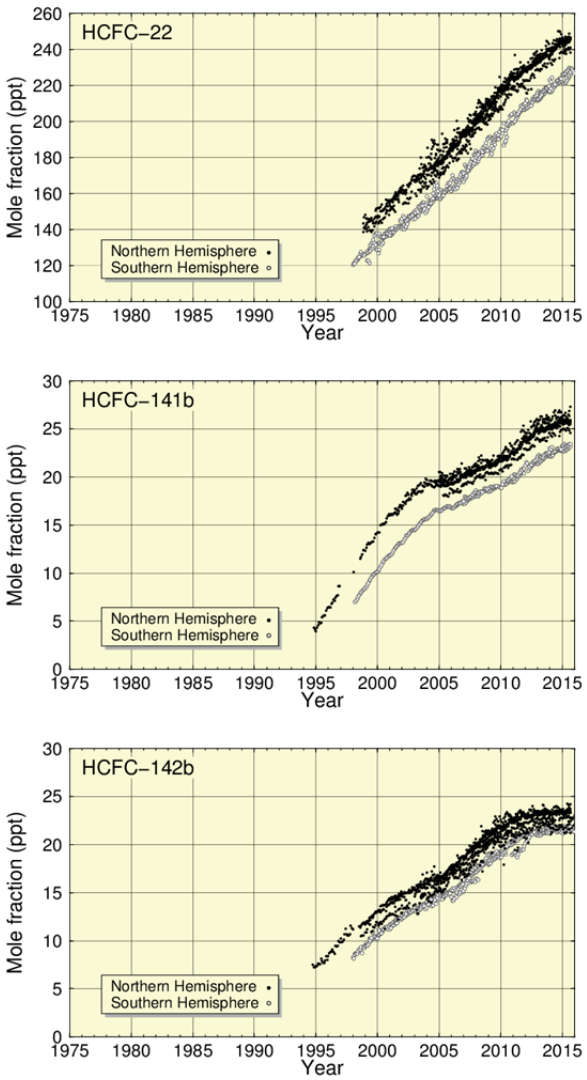

Fig. 6.3 Time series of the monthly mean mole fractions of HCFC-22, HCFC-141b and HCFC-142b at individual stations. Solid circles show mole fractions measured in the Northern Hemisphere and open circles show those measured in the Southern Hemisphere.

Figure 6.3 shows time series of the mole fractions of HCFC-22 ($CHClF_2$), HCFC-141b (CH_3CCl_2F) and

HCFC-142b (CH_3CClF_2). The mole fractions of these gases increased significantly during the last decade as a result of their continued use as substitutes for CFCs. The growth of HCFC-141b decelerated around 2005, but has slightly accelerated again over the last several years.

Figure 6.4 shows time series of the mole fractions of CCl_4 and CH_3CCl_3. The mole fractions of CCl_4 in both hemispheres peaked around 1991. The mole fractions of CH_3CCl_3 were at a maximum around 1992 in the Northern Hemisphere and around 1993 in the Southern Hemisphere. The mole fractions of these gases have since been decreasing.

Figure 6.5 shows time series of the monthly mean mole fractions of HFC-134a (CH_2FCF_3) and HFC-152a (CH_3CHF_2). The mole fractions of HFC-134a and HFC-152a have risen twofold over the last 10 years, increasing sooner in the Northern than in the Southern Hemisphere suggesting their predominant sources are located in the Northern Hemisphere. The growth of HFC-152a has decelerated over the last several years.

Figure 6.6 shows time series of the monthly mean mole fractions of methyl chloride (CH_3Cl). The mole fraction of CH_3Cl does not show any particular long-term tendency although clear seasonal cycle can be seen in the dataset.

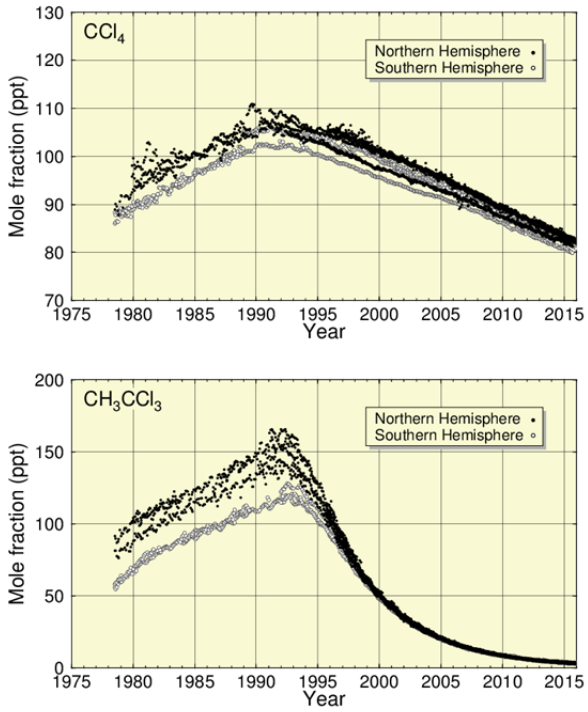

Fig. 6.4 Time series of the monthly mean mole fractions of CCl_4 and CH_3CCl_3 at individual stations. Solid circles show mole fractions measured in the Northern Hemisphere and open circles show those measured in the Southern Hemisphere.

Figure 6.7 shows a time series of the monthly mean mole fractions of SF_6. The mole fraction of SF_6 in 2015 was over twice that observed in 1995 and has increased at an almost linear rate (WMO, 2016b).

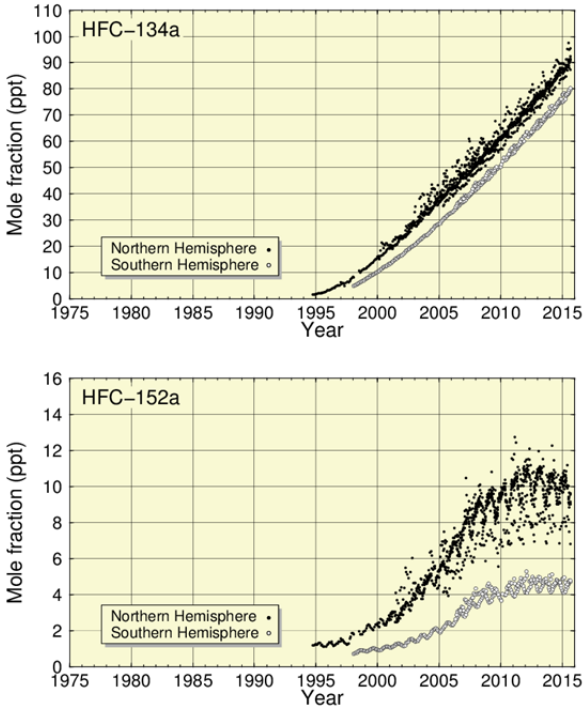

Fig. 6.5 Time series of the monthly mean mole fractions of HFC-134a and HFC-152a at individual stations. Solid circles show mole fractions measured in the Northern Hemisphere and open circles show those measured in the Southern Hemisphere.

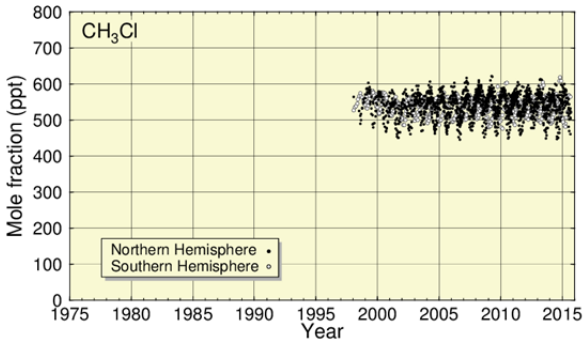

Fig. 6.6 Time series of the monthly mean mole fractions of CH_3Cl at individual stations. Solid circles show mole fractions measured in the Northern Hemisphere and open circles show those measured in the Southern Hemisphere.

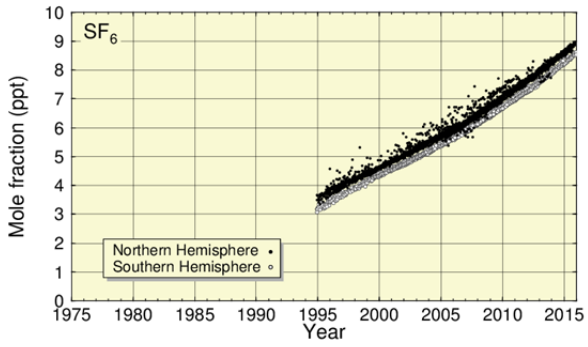

Fig. 6.7 Time series of the monthly mean mole fractions of SF_6 at individual stations. Solid circles show mole fractions measured in the Northern Hemisphere and open circles show those measured in the Southern Hemisphere.

7.

CARBON MONOXIDE

(CO)

● : CONTINUOUS STATION

△ : FLASK STATION

□ : FLASK MOBILE (SHIP)

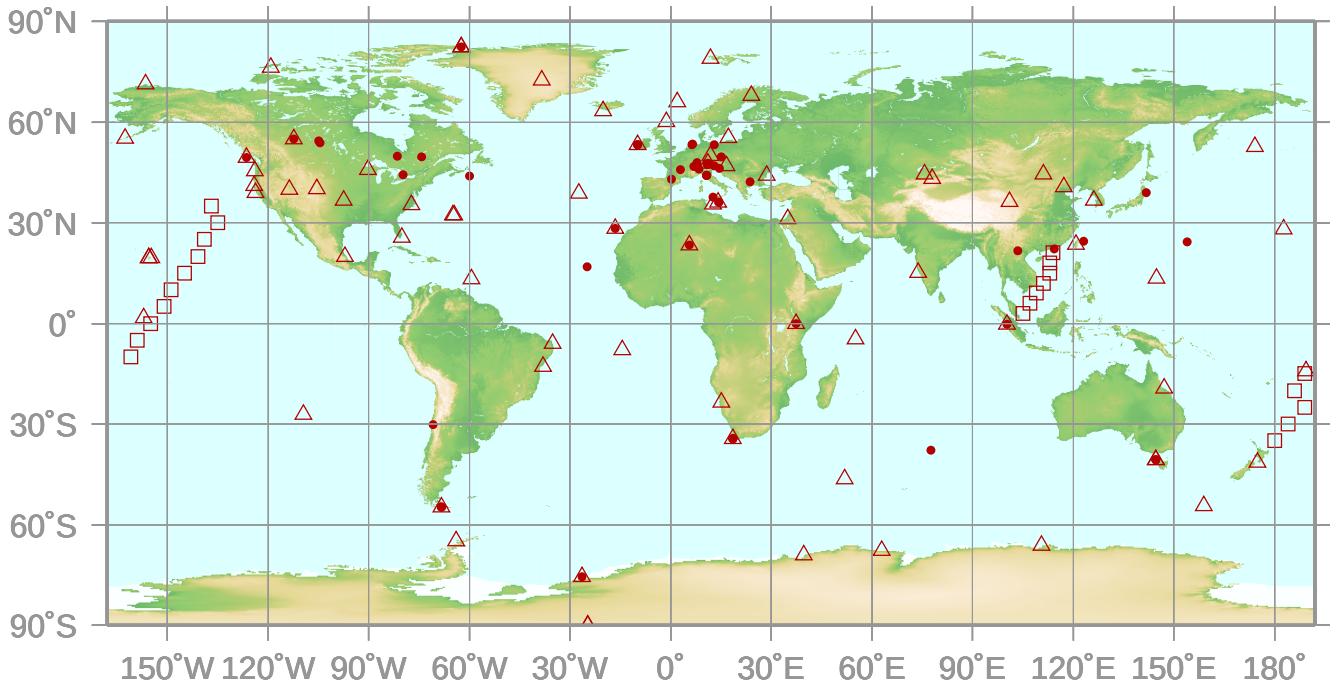

This map shows locations of the stations that have submitted data for monthly mean mole fractions.

CO Monthly Data

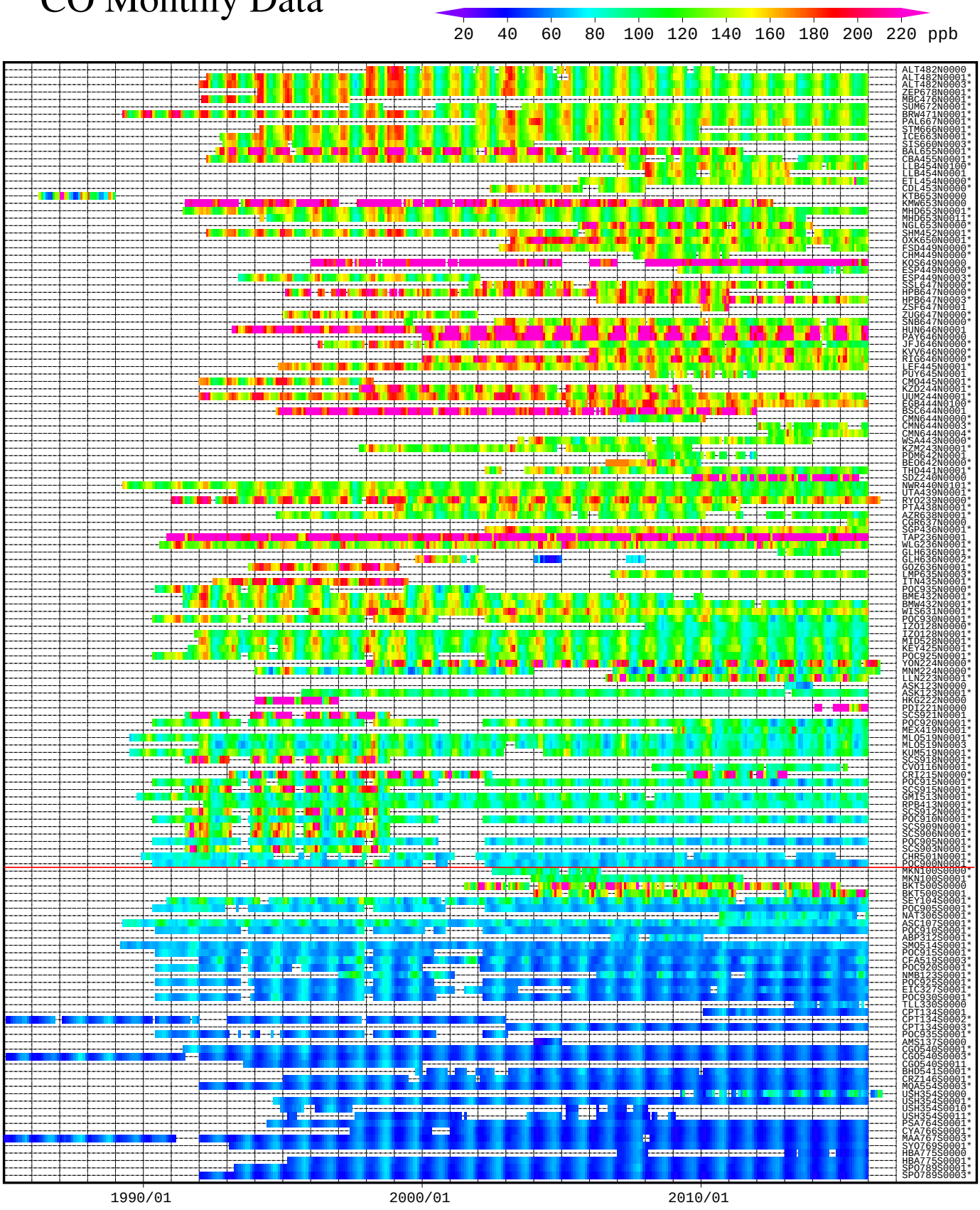

Plate 7.1 Monthly mean CO mole fractions that have been reported to the WDCGG. The mole fractions are illustrated in different colors. The sites are listed in order from north to south. The red line indicates the equator. The data from the sites with an asterisk at the end of the station index were used for the analyses shown in Plate 7.2. (see Chapter 2)

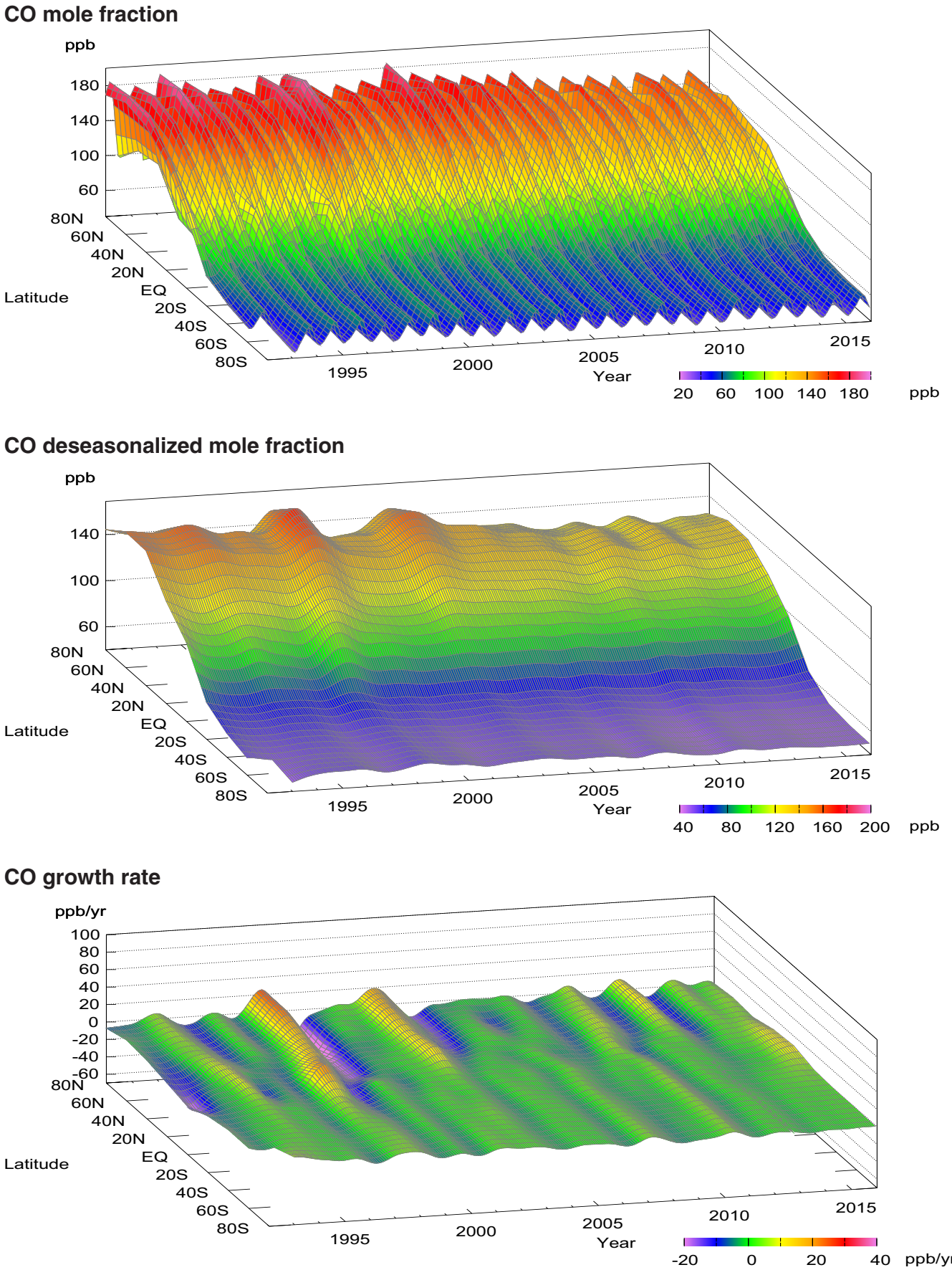

Plate 7.2 Variation of zonally averaged monthly mean CO mole fractions (top), deseasonalized long-term trends (middle), and growth rates (bottom). The zonally averaged mole fractions were calculated for each 20° zone. The deseasonalized trends and growth rates were derived as described in Chapter 2.

7. CARBON MONOXIDE (CO)

Basic information on CO with regard to environmental issues

Carbon monoxide (CO) is not a greenhouse gas; it absorbs hardly any infrared radiation from the Earth. However, CO influences the oxidation capacity of the atmosphere through its reaction with hydroxyl radicals (OH), which control the lifetimes of other greenhouse gases including methane and halocarbons. CO has been monitored due to its indirect influence on greenhouse gases through such reactions.

Sources of atmospheric CO include fossil fuel combustion and biomass burning, along with the oxidation of methane and non-methane hydrocarbons. Major sinks include reaction with OH and surface deposition; the reaction of CO with OH accounts for all of the chemical loss of CO in the troposphere (Seinfeld and Pandis, 1998). CO has a relatively short atmospheric lifetime, ranging from 10 days in summer in the tropics to more than a year over the polar regions in winter. Thus anthropogenic CO emissions do not lead to CO accumulation in the atmosphere. Furthermore, the uneven distribution of sources causes large spatial and temporal variations in CO mole fraction.

Measurements of trapped air in ice cores have shown that the pre-industrial CO mole fraction over central Antarctica during the last two millennia was about 50 ppb and the CO level increased to 110 ppb by 1950 in Greenland (Haan and Raynaud, 1998). Beginning in 1950, the global average CO mole fraction increased at a rate of 1% per year but started to decrease in the late 1980s (WMO, 1999). Between 1991 and 2001, the global average mole fraction of CO decreased at an annual rate of about 0.5 ppb, excluding temporal enhancements from large biomass burning events (Novelli *et al*., 2003). In last decade, a slightly negative trend of CO mole fraction has been dominant in the Northern Hemisphere with significant interannual variability, which is well reproduced by earth system models (Yoon and Pozzer, 2014).

Annual variation of CO mole fraction in the atmosphere

The monthly mean mole fractions of CO that have been reported from fixed stations and some ships to the WDCGG are shown in Plate 7.1, in which different mole fraction levels are plotted in different colors. The observational sites that provide data for global analysis are shown on the map at the beginning of this chapter.

Latitudinally averaged mole fractions of CO in the atmosphere, together with their deseasonalized mole fractions and growth rates, are shown in Plate 7.2 as three-dimensional representations.

Data for the mole fractions of CO are reported in various units, *i.e.*, ppb, μg/m^3-25°C, μg/m^3-20°C and mg/m^3-25°C. Units other than ppb were converted to ppb using the formulas:

$$X_p\,[\text{ppb}] = (R \times T / M / P_0) \times 10 \times X_g\,[\mu\text{g/m}^3]$$
$$X_p\,[\text{ppb}] = (R \times T / M / P_0) \times 10^4 \times X_g\,[\text{mg/m}^3]$$

where R is the molar gas constant (8.31451 [J/K/mol]),
T is the absolute temperature reported from each station,
M is the molecular weight of CO (28.0101) and
P_0 is the standard pressure (1013.25 [hPa]).

If temperature is not reported by a station, T is taken to be 298K (25 °C).

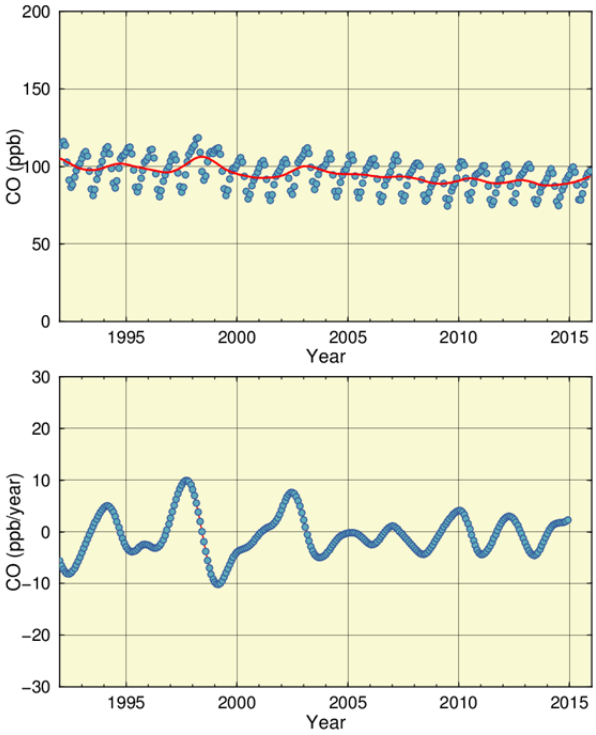

Fig. 7.1 Globally averaged monthly mean mole fraction of CO from 1992 to 2015 and the deseasonalized long-term trend in red line (top), and annual growth rate (bottom).

Figure 7.1 shows globally averaged monthly mean CO mole fractions and their growth rates. Growth rates were high in 1993/1994, 1997/1998 and 2002, and low in 1992 and 1998/1999. The global annual mean mole fraction was 91±2 ppb in 2015, which was calculated irrespective of the difference in observation scales.

Plate 7.2 shows that the seasonal variations of CO were larger in the Northern Hemisphere and smaller in the Southern Hemisphere, and that the deseasonalized mole fractions were the highest in mid-latitudes of the Northern Hemisphere and the lowest in the Southern Hemisphere, with a large latitudinal gradient from northern mid- to southern low-latitudes. This is likely due to the presence of numerous anthropogenic sources of CO in the northern mid-latitudes, combined with the destruction of CO in the tropics, where OH radicals are abundant.

Figure 7.2 shows monthly mean mole fractions of CO for each 30° latitudinal zone. Seasonal variations were observed in both hemispheres, with mole fractions being higher in winter. Amplitudes of the seasonal cycle were larger in the Northern Hemisphere than in the Southern Hemisphere.

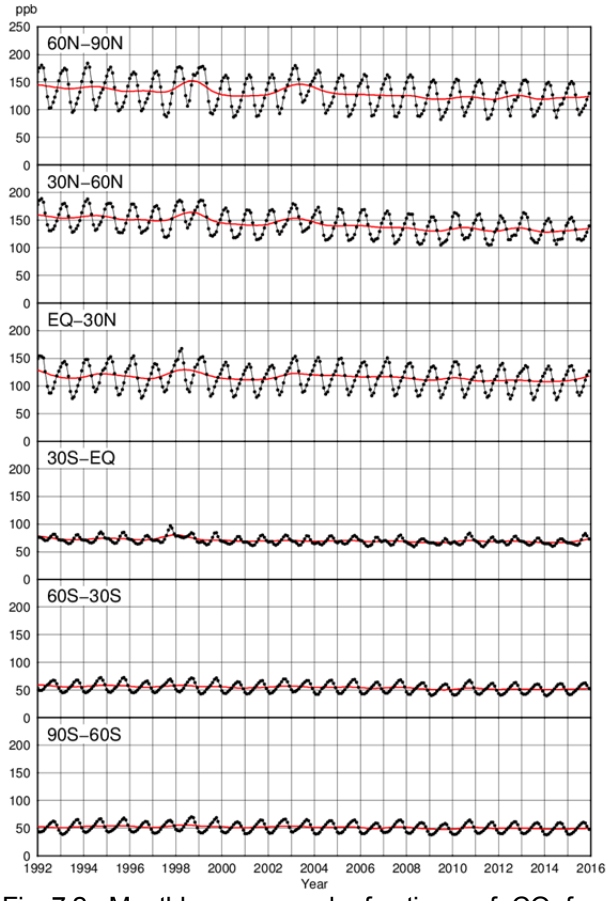

Fig. 7.2 Monthly mean mole fractions of CO from 1992 to 2015 for each 30° latitudinal zone (dots) and their deseasonalized long-term trends (red lines).

Figure 7.3 summarizes deseasonalized long-term trends for each 30° latitudinal zone and their growth rates. There was a decline in CO mole fractions around 1992, almost coinciding with the decrease in the growth rate of CH_4 mole fractions, most likely due to variations in their common sink (reaction with OH). The enhanced stratospheric ozone depletion due to increased volcanic aerosols following the eruption of Mt. Pinatubo in 1991 may have increased atmospheric OH radicals, which react with both CO and CH_4 (Dlugokencky *et al.*, 1996).

Increases in CO mole fractions were observed from 1997 to 1998 in the Northern Hemisphere and in the low latidutes of the Southern Hemisphere. These increases were attributed to large biomass burning events in Indonesia in late 1997 and in Siberia in the summer and autumn of 1998 (Novelli *et al.*, 1998).

The CO mole fractions returned to normal after 1999, but the growth rates in the Northern Hemisphere increased substantially again in 2002. The latter may have been due to large biomass burning events. Large-scale boreal forest fires occurred in Siberia and North America from 2002 to 2003. Large forest fires also occurred in Russia in summer 2010 which is reflected in the data in the bottom panel of Figure 7.3.

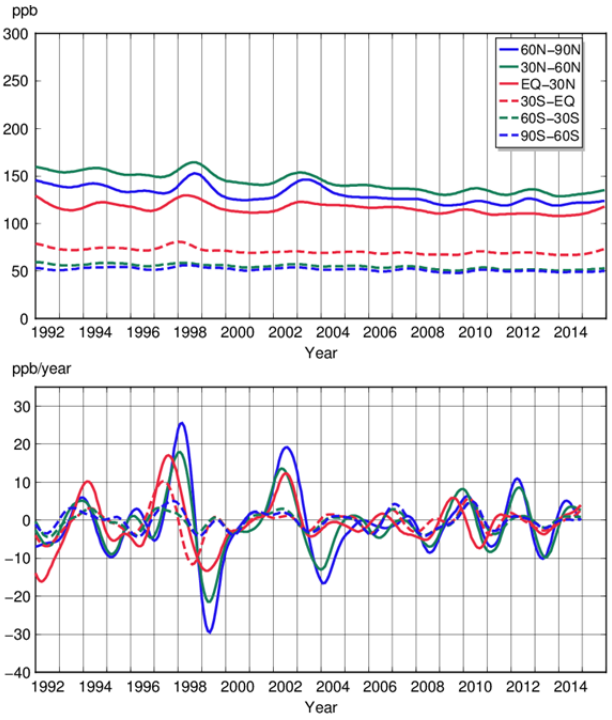

Fig. 7.3 Deseasonalized long-term trends of CO for each 30° latitudinal zone (top) and their growth rates (bottom).

Seasonal cycle of CO mole fraction in the atmosphere

Figure 7.4 shows average seasonal cycles in the mole fraction of CO for each 30° latitudinal zone. The seasonal cycle is driven mainly by seasonal variations in OH abundance as a CO sink. This seasonality and a short lifetime of about a few months resulted in a sharp decrease in early summer followed by a relatively slow increase in autumn. The levelling-off in the beginning of the year observed in the southern low latitudes may be attributed to the transport of CO from the Northern Hemisphere.

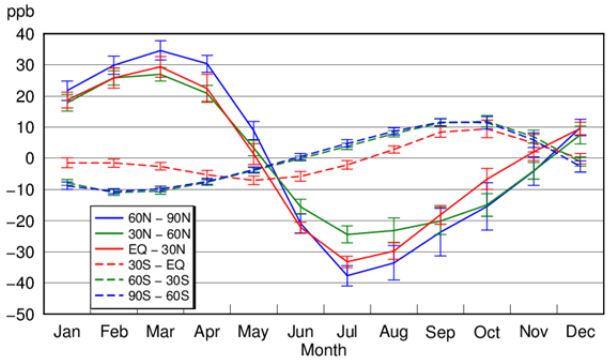

Fig. 7.4 Average seasonal cycles of CO mole fractions for each 30° latitudinal zone obtained by subtracting long-term trends from the zonal mean time series. Error bars represent the range of ±1σ calculated for each month. (period 1992 to 2015).

REFERENCES

References

Angert, A., S. Biraud, C. Bonfils, W. Buermann, and I. Fung, CO_2 seasonality indicates origins of post-Pinatubo sink, *Geophys. Res. Lett.*, **31**, L11103, doi:10.1029/2004GL019760, 2004.

Bekki, S., K. S. Law, and J. A. Pyle, Effect of ozone depletion on atmospheric CH_4 and CO concentrations, *Nature*, **371**, 595–597, 1994.

Bergamaschi, P., S. Houweling, A. Segers, M. Krol, C. Frankenberg, R. A. Scheepmaker, E. Dlugokencky, S. C. Wofsy, E. A. Kort, C. Sweeney, T. Schuck, C. Brenninkmeijer, H. Chen, V. Beck, and C. Gerbig, Atmospheric CH_4 in the first decade of the 21st century: Inverse modeling analysis using SCIAMACHY satellite retrievals and NOAA surface measurements, *J. Geophys. Res. Atmos.*, **118**, 7350–7369, 2013.

Boden, T. A., G. Marland, and R. J. Andres, Global, Regional, and National Fossil-Fuel CO_2 Emissions. Carbon Dioxide Information Analysis Center, Oak Ridge National Laboratory, U.S. Department of Energy, Oak Ridge, Tenn., USA, doi: 10.3334/CDIAC/00001_V2016, 2016.

Cleveland, W. S., and S. J. Devlin, Locally weighted regression: an approach to regression analysis by local fitting, *J. Amer. Statist. Assn.*, **83**, 596–610, 1988.

Conway, T. J., P. P. Tans, L. S. Waterman, K. W. Thoning, D. R. Kitzis, K. A. Masarie, and N. Zhang, Evidence for interannual variability of the carbon cycle from the National Oceanic and Atmospheric Administration/Climate Monitoring and Diagnostics Laboratory global air sampling network, *J. Geophys. Res.*, **99**, 22831–22855, 1994.

Dlugokencky, E. J., L. P. Steele, P. M. Lang, and K. A. Masarie, The growth rate and distribution of atmospheric methane, *J. Geophys. Res.*, **99**, 17021–17043, 1994.

Dlugokencky, E. J., E. G. Dutton, P. C. Novelli, P. P. Tans, K. A. Masarie, K. O. Lantz, and S. Mardronich, Changes in CH_4 and CO growth rates after the eruption of Mt. Pinatubo and their link with changes in tropical tropospheric UV flux, *Geophys. Res. Lett.*, **23**, 2761–2764, 1996.

Dlugokencky, E. J., B. P. Walter, K. A. Masarie, P. M. Lang, and E. S. Kasischke, Measurements of an anomalous global methane increase during 1998, *Geophys. Res. Lett.*, **28**, 499–502, 2001.

Dlugokencky, E. J., L. Bruhwiler, J. W. C. White, L. K. Emmons, P. C. Novelli, S. A. Montzka, K. A. Masarie, P. M. Lang, A. M. Crotwell, J. B. Miller, and L. V. Gatti, Observational constraints on recent increases in the atmospheric CH_4 burden, *Geophys. Res. Lett.*, **36**, L18803, 2009.

Duchon, C. E., Lanczos filtering in one and two dimensions, *J. Appl. Meteor.*, **18**, 1016-1022, 1979.

Etheridge, D. M., L. P. Steele, R. J. Francey, and R. L. Langenfelds, Atmospheric methane between 1000 A.D. and present: Evidence of anthropogenic emissions and climatic variability, *J. Geophys. Res.*, **103**, 15979–15993, 1998.

Francey, R. J., P. P. Tans, C. E. Allison, I. G. Enting, J. W. C. White, and M. Trolier, Changes in oceanic and terrestrial carbon uptake since 1982, *Nature*, **373**, 326–330, 1995.

Gu, L., D. D. Baldocchi, S. C. Wofsy, J. W. Munger, J. J. Michalsky, S. P. Urbanski, and T. A. Boden, Response of a deciduous forest to the Mount Pinatubo eruption: enhanced photosynthesis, *Science*, **299**, 2035–2038, 2003.

Haan, D. and D. Raynaud, Ice core record of CO variations during the last two millennia: atmospheric implications and chemical interactions within the Greenland ice, *Tellus*, **50B**, 253–262, 1998.

Hansen, J., A. Lacis, R. Ruedy, and M. Sato, Potential Climate Impact of Mount-Pinatubo Eruption, *Geophys. Res. Lett.*, **19**, 215–218, 1992.

Heimann, M. and M. Reichstein, Terrestrial ecosystem carbon dynamics and climate feedbacks, *Nature*, **451**, 289–292, 2008.

IPCC, Climate Change 2013: The Physical Science Basis. Contribution of Working Group I to the Fifth Assessment Report of the Intergovernmental Panel on Climate Change [Stocker, T. F., D. Qin, G.-K. Plattner, M. Tignor, S. K. Allen, J. Boschung, A. Nauels, Y. Xia, V. Bex, and P. M. Midgley (eds.)]. Cambridge University Press, Cambridge, United Kingdom and New York, NY, USA, 2013.

Keeling, C. D., R. B. Bacastow, A. F. Carter, S. C. Piper, T. P. Whorf, M. Heimann, W. G. Mook, and H. Roeloffzen, A three-dimensional model of atmospheric CO_2 transport based on observed winds: 1. Analysis of observational data, in aspects of climate variability in the Pacific and the Western Americas, edited by D. H. Peterson, *Geophysical Monograph* **55**, 165–236, American Geophysical Union, Washington, D.C., 1989.

Keeling, C. D., T. P. Whorf, M. Wahlen, and J. van der Plicht, Interannual extremes in the rate of rise of atmospheric carbon dioxide since 1980, *Nature*, **375**, 666–670, 1995.

Lambert, G., P. Monfray, B. Ardouin, G. Bonsang, A. Gaudry, V. Kazan and G. Polian, Year-to-year changes in atmospheric CO_2, *Tellus*, **47B**, 35–55, 1995.

Le Quéré C., R. M. Andrew, J. G. Canadell, S. Sitch, J. I. Korsbakken, G. P. Peters, A. C. Manning, T. A. Boden, P. P. Tans, R. A. Houghton, R. F. Keeling, S.

Alin, O. D. Andrews, P. Anthoni, L. Barbero, L. Bopp, F. Chevallier, L. P. Chini, P. Ciais, K. Currie, C. Delire, S. C. Doney, P. Friedlingstein, T. Gkritzalis, I. Harris, J. Hauck, V. Haverd, M. Hoppema, K. K. Goldewijk, A. K. Jain, E. Kato, A. Körtzinger, P. Landschützer, N. Lefèvre, A. Lenton, S. Lienert, D. Lombardozzi, J. R. Melton, N. Metzl, F. Millero, P. M. S. Monteiro, D. R. Munro, J. E. M. S. Nabel, S. Nakaoka, K. O'Brien, A. Olsen, A. M. Omar, T. Ono, D. Pierrot, B. Poulter, C. Rödenbeck, J. Salisbury, U. Schuster, J. Schwinger, R. Séférian, I. Skjelvan, B. D. Stocker, A. J. Sutton, T. Takahashi, H. Tian, B. Tilbrook, I. T. van der Laan-Luijkx, G. R. van der Werf, N. Viovy, A. P. Walker, A. J. Wiltshire, and S. Zaehle, Global Carbon Budget 2016, *Earth Syst. Sci. Data*, **8**, 605-649, doi:10.5194/essd-8-605-2016, 2016. (Further information is available on: http://www.globalcarbonproject.org/)

Levin, I., T. Naegler, R. Heinz, D. Osusko, E. Cuevas, A. Engel, J. Ilmberger, R. L. Langenfelds, B. Neininger, C. v. Rohden, L. P. Steele, R. Weller, D. E. Worthy, and S. A. Zimov, The global SF_6 source inferred from long-term high precision atmospheric measurements and its comparison with emission inventories, *Atmos. Chem. Phys.*, **10**, 2655–2662, 2010.

Levin, I., Earth science: The balance of the carbon budget, *Nature*, **488**, 35–36, 2012.

Manning, A. C., and R. F. Keeling, Global oceanic and land biotic carbon sinks from the Scripps atmospheric oxygen flask sampling network, *Tellus*, **58B**, 95–116, 2006.

Matsueda, H., S. Taguchi, H. Y. Inoue, and M. Ishii, A large impact of tropical biomass burning on CO and CO_2 in the upper troposphere, *Science in China (Series C)*, **45**, 116–125, 2002.

Morimoto, S., S. Aoki, T. Nakazawa, and T. Yamanouchi, Temporal variations of the carbon isotopic ratio of atmospheric methane observed at Ny Ålesund, Svalbard from 1996 to 2004, *Geophys. Res. Lett.*, **33**, L01807, doi:10.1029/2005GL024648, 2006.

Nakazawa, T., K. Miyashita, S. Aoki, and M. Tanaka, Temporal and spatial variations of upper tropospheric and lower stratospheric carbon dioxide, *Tellus*, **43B**, 106–117, 1991.

Nakazawa, T., S. Morimoto, S. Aoki and M. Tanaka, Time and space variations of the carbon isotopic ratio of tropospheric carbon dioxide over Japan, *Tellus*, **45B**, 258–274, 1993.

Nakazawa, T., S. Morimoto, S. Aoki and M. Tanaka, Temporal and spatial variations of the carbon isotopic ratio of atmospheric carbon dioxide in the western Pacific region, *J. Geophys. Res.*, **102**, 1271–1285, 1997.

Nevison, C. D., N. M. Mahowald, S. C. Doney, I. D. Lima, G. R. van der Werf, J. T. Randerson, D. F. Baker, P. Kasibhatla, and G. A. McKinley, Contribution of ocean, fossil fuel, land biosphere, and biomass burning carbon fluxes to seasonal and interannual variability in atmospheric CO_2, *J. Geophys. Res.*, **113**, doi:10.1029/2007JG000408, 2008.

Nisbet, E. G., E. J. Dlugokencky, and P. Bousquet, Methane on the rise-again, *Science*, **343**, 493-495, doi:10.1126/science.1247828, 2014.

Novelli, P. C., K. A. Masarie, and P. M. Lang, Distributions and recent changes of carbon monoxide in the lower troposphere, *J. Geophys. Res.*, **103**, 19015–19033, 1998.

Novelli, P. C., K. A. Masarie, P. M. Lang, B. D. Hall, R. C. Myers, and J. W. Elkins, Reanalysis of tropospheric CO trends: Effects of the 1997–1998 wildfires, *J. Geophys. Res.*, **108**, 4464, doi:10.1029/2002JD003031, 2003.

Prinn, R. G., J. Huang, R. F. Weiss, D. M. Cunnold, P. J. Fraser, P. G. Simmonds, A. McCulloch, C. Harth, P. Salameh, S. O'Doherty, R. H. J. Wang, L. Porter, and B. R. Miller, Evidence for substantial variations of atmospheric hydroxyl radicals in the past two decades, *Science*, **292**, 1882–1888, 2001.

Rayner, P. J., I. G. Enting, R. J. Francey, and R. Langenfelds, Reconstructing the recent carbon cycle from atmospheric CO_2, $\delta^{13}C$ and O_2/N_2 observations, *Tellus*, **51B**, 213–232, 1999.

Ravishankara, A. R., J. S. Daniel, and R. W. Portmann, Nitrous Oxide (N_2O): the dominant ozone-depleting substance emitted in the 21st century, *Science*, **326**, 123-125, 2009.

Rigby, M., R. G. Prinn, P. J. Fraser, P. G. Simmonds, R. L. Langenfelds, J. Huang, D. M. Cunnold, L. P. Steele, P. B. Krummel, R. F. Weiss, S. O'Doherty, P. K. Salameh, H. J. Wang, C. M. Harth, J. Mühle, and L. W. Porter, Renewed growth of atmospheric methane, *Geophys. Res. Lett.*, **35**, L22805, 2008.

Saunois M., P. Bousquet, B. Poulter, A. Peregon, P. Ciais, J. G. Canadell, E. J. Dlugokencky, G. Etiope, D. Bastviken, S. Houweling, G. Janssens-Maenhout, F. N. Tubiello, S. Castaldi, R. B. Jackson, M. Alexe, V. K. Arora, D. J. Beerling, P. Bergamaschi, D. R. Blake, G. Brailsford, V. Brovkin, L. Bruhwiler, C. Crevoisier, P. Crill, K. Covey, C. Curry, C. Frankenberg, N. Gedney, L. Höglund-Isaksson, M. Ishizawa, A. Ito, F. Joos, H. Kim, T. Kleinen, P. Krummel, J. Lamarque, R. Langenfelds, R. Locatelli, T. Machida, S. Maksyutov, K. C. McDonald, J. Marshall, J. R. Melton, I. Morino, V. Naik, S. O'Doherty, F. W. Parmentier, P. K. Patra, C. Peng, S. Peng, G. P. Peters, I. Pison, C. Prigent, R. Prinn, M. Ramonet, W. J. Riley, M. Saito, M. Santini, R. Schroeder, I. J. Simpson, R. Spahni, P. Steele, A. Takizawa, B. F. Thornton, H. Tian, Y. Tohjima, N. Viovy, A.

Voulgarakis, M. van Weele, G. R. van der Werf, R. Weiss, C. Wiedinmyer, D. J. Wilton, A. Wiltshire, D. Worthy, D. Wunch, X. Xu, Y. Yoshida, B. Zhang, Z. Zhang, and Q. Zhu, The global methane budget 2000–2012, *Earth Syst. Sci. Data*, **8**, 697–751, doi:10.5194/essd-8-697-2016, 2016.
(Further information is available on: http://www.globalcarbonproject.org/)

Seinfeld, J. H., and S. N. Pandis, Atmospheric Chemistry and Physics: From Air Pollution to Climate Change, *John Wiley & Sons, Inc., New York*, 1326 pp., 1998.

Solomon, S., G-K. Plattner, R. Knutti and P. Friedlingstein, Irreversible climate change due to carbon dioxide emissions, *Proc. Natl. Acad. Sci. USA*, **106**, 1704-1709, 2009.

Stenchikov, G., A. Robock, V. Ramaswamy, M. D. Schwarzkopf, K. Hamilton, and S. Ramachandran, Arctic Oscillation response to the 1991 Mount Pinatubo eruption: Effects of volcanic aerosols and ozone depletion, *J. Geophys. Res.*, **107**, 4803, doi:10.1029/2002JD002090, 2002.

Tans, P., An accounting of the observed increase in oceanic and atmospheric CO_2 and an outlook for the fiture, *Oceanography*, **22(4)**, 26-35, http://dx.doi.org/10.5670/oceanog.2009.94, 2009.

Thoning, K. W., P. P. Tans, and W. D. Komhyr, Atmospheric carbon dioxide at Mauna Loa observatory: 2. Analysis of the NOAA GMCC data, 1974-1985, *J. Geophys. Res.*, **94**, 8549–8565, 1989.

WMO, Scientific assessment of ozone depletion: 1998. WMO global ozone research and monitoring project—Report No. 44, 2-43, World Meteorological Organization, Geneva, 1999.

WMO, World Data Centre for Greenhouse Gases (WDCGG) Data Summary, WDCGG No. 22, 84pp, 2000.

WMO, World Data Centre for Greenhouse Gases Data Submission and Dissemination Guide, GAW Report No. 174, WMO TD No. 1416, 2007.

WMO, Technical Report of Global Analysis Method for Major Greenhouse Gases by the World Data Center for Greenhouse Gases, GAW Report No. 184, WMO TD No. 1473, 2009a.

WMO, Revision of the World Data Centre for Greenhouse Gases Data Submission and Dissemination Guide, GAW Report No. 188, WMO TD No. 1507, 2009b.
(http://www.wmo.int/pages/prog/arep/gaw/documents/GAW_188_web_20100128.pdf, accessed on 22 Feb. 2017)

WMO, WMO Greenhouse Gas Bulletin No.9, 2013. (http://www.wmo.int/pages/prog/arep/gaw/ghg/GHGbulletin.html, accessed on 22 Feb. 2017)

WMO, WMO Greenhouse Gas Bulletin No.10, 2014. (http://www.wmo.int/pages/prog/arep/gaw/ghg/GHGbulletin.html, accessed on 22 Feb. 2017)

WMO, WMO Greenhouse Gas Bulletin No.11, 2015. (http://www.wmo.int/pages/prog/arep/gaw/ghg/GHGbulletin.html, accessed on 22 Feb. 2017)

WMO, 18th WMO/IAEA Meeting on Carbon Dioxide, Other Greenhouse Gases and Related Tracers Measurement Techniques (GGMT-2015), ed. P. Tans and C. Zellweger, GAW Report No.229, 2016a.

WMO, WMO Greenhouse Gas Bulletin No.12, 2016b. (http://www.wmo.int/pages/prog/arep/gaw/ghg/GHGbulletin.html, accessed on 22 Feb. 2017)

WMO, WMO Global Atmosphere Watch (GAW) Implementation Plan: 2016-2023, GAW Report No.228, 2017.

Yoon, J., and A. Pozzer, Model-simulated trend of surface carbon monoxide for the 2001–2010 decade, *Atmos. Chem. Phys.*, **14**, 10465–10482, 2014.

APPENDICES

CALIBRATION AND STANDARD SCALES

1. Calibration System in the GAW Programme

Under the Global Atmosphere Watch (GAW) Programme, the Central Calibration Laboratories (CCLs) are assigned to host a Primary (Reference) Standard/scale, while the World Calibration Centres (WCCs) are responsible for the scale propagation to the stations via distribution of calibration standards for certain compounds, conducting instrument calibrations, comparison campaigns, station audits and providing training to the station personnel. A Reference Standard/scale is designated for each variable to be used for all GAW measurements of that variable. Table 1 lists the organizations that serve as WCCs and CCLs for GAW (WMO, 2017). For CFCs, no central facilities or quality control systems have so far been established within the GAW Programme.

Table 1. Overview of the GAW Central Calibration Laboratories (GAW-CCL, Reference Standard) and World Calibration Centres for greenhouse and other related gases. The World Calibration Centres have assumed global responsibilities, except where indicated (Am, Americas; E/A, Europe and Africa; A/O, Asia and the South-West Pacific)

Compounds	Central Calibration Laboratory (Host of Primary Standard)	World Calibration Centre
Carbon Dioxide (CO_2)	NOAA/ESRL	NOAA/ESRL (Round Robin) Empa (audits)
Carbon Dioxide (CO_2) isotopes	MPI-BGC	
Methane (CH_4)	NOAA/ESRL	Empa (Am, E/A) JMA (A/O)
Nitrous Oxide (N_2O)	NOAA/ESRL	KIT/IMK-IFU
Chlorofluorocarbons (CFCs)		
Sulfur Hexafluoride (SF_6)	NOAA/ESRL	KMA
Molecular Hydrogen (H_2)	MPI-BGC	
Carbon Monoxide (CO)	NOAA/ESRL	Empa

2. Carbon Dioxide (CO_2)

In 1995, the National Oceanic and Atmospheric Administration's Earth System Research Laboratory (NOAA/ESRL, formerly CMDL; Climate Monitoring and Diagnostics Laboratory) in Boulder, Colorado, USA, took over the role of the Central Calibration Laboratory (CCL) from the Scripps Institution of Oceanography (SIO) in San Diego, California, USA. Since then, NOAA/ESRL has served as the CCL responsible for the maintenance of the GAW Primary Standard for CO_2. As CCL for CO_2, NOAA/ESRL maintains a high-precision manometric system for absolute calibration of CO_2 as the reference for GAW measurements throughout the world (Zhao *et al.*, 1997), as well as carrying out Round Robin in the function of WCC. It has been recommended that the standards of the GAW measurement laboratories be calibrated at least every three years at the CCL (WMO, 2016).

Under the WMO calibration system, there have been several calibration scales for CO_2, *e.g.*, SIO-based X74, X85, X87, X93 and X2002 scales and the NOAA/ESRL-based WMO Mole Fraction Scale partially based on previous SIO scales. The CCL adopted the WMO X2005 scale, reflecting historical manometric calibrations of the CCL's set of cylinders and the possible small differences between SIO and NOAA/ESRL calibrations. The most current WMO Mole Fraction Scale is the WMO X2007 scale.

To assess the differences in standard scales among measuring laboratories, about every three years NOAA/ESRL organizes intercomparisons or Round Robin experiments endorsed by WMO. Many laboratories participated in the experiments organized in 1991–1992, 1995–1997, 1999–2000, 2002–2006, 2009-2012 and 2014-2015. Table 2 shows the results of the experiments performed in 2014-2015, in which the mole fractions measured by various laboratories are compared with the mole fractions measured by NOAA/ESRL (http://www .esrl.noaa.gov/gmd/ccgg/wmorr/wmorr_results.php). In addition, many laboratories compare their standards

bilaterally or multilaterally.

Table 3 lists laboratories and sites that contributed to the present issue of the *Data Summary* with standard scales of reported data and history of participation in WMO intercomparison experiments.

Table 2. Round Robin results for the mole fraction of carbon dioxide. Differences between the mole fractions measured by various laboratories and the mole fractions measured by NOAA (Laboratory minus NOAA, ppm).

Laboratory	Measurement Date	Mole Fraction Difference (ppm)	
		Low 375-380 ppm	High 400-415 ppm
NCAR	Mar-14 & Jun-15	–0.01 ~ 0.02	–0.05
NOAA-CSD	Apr-14	0.06	0.03
NEON	May-14	0.01	0.02
NIST	Jul-14	–0.37	–0.49
HU	Jul & Dec-14	0.05	0.01
PSU	Aug-14	0.03	-0.02
CALTECH	Sep-14	-0.02	-0.04
BLG	Oct-14	0.06	-0.09
AMERIFLUX	Nov-14	-0.01	-0.02
EC	Dec-14	0.09	0.06
HMS	Jun-15	0.03	0.02
AEMET	Aug-15	-0.01	-0.01
CSIRO	May-14	0.04	0.00
NIWA	Jun-14	0.08	-0.08
SAWS	Aug-14	0.16	0.14
CMA	Oct-14	0.02	-0.02
KMA	Jan-15	0.03	0.04
MGO	Aug-15	0.00	-0.03
LSCE	May-14	-0.05	-0.00
WCC-Empa	Jun-14	-0.10	-0.06
Empa	Jul-14	-0.07	-0.06
FMI	Sep-14 & Jul-15	0.01	-0.10
RUG	Dec-14	0.03	0.06
ECN	Jan-15	0.31	0.51
UEA	Mar-15	-0.31	-0.25
RHUL	Apr-15	-0.10	-0.02
UHEI-IUP	Jun-14	-0.03	-0.06
UBA-SCHAU	Jul-14	0.05	-0.04
UBA/ZUG	Sep-14	0.03	0.02
MPI-BGC	Nov-14	-0.01	-0.02
RSE	Jan-15	0.07	-0.08
IAFMC	Feb-15	-1.63	-1.62
ENEA	May-15	-0.01	-0.05
ICOS	Jul-15	-0.01	-0.03
JMA	Oct-13	-0.04	-0.04
MRI	Nov-13	-0.15	-0.14
AIST	Jan-14	0.13	0.18
NIES	Jan-14	-0.09	-0.04
TU	Feb-14	0.16	0.25

Table 3. Status of standard scales and calibration/intercomparison for CO_2 at laboratories.

Laboratory	WDCGG Filename Code	Calibration Scale	WMO Inter-comparison
AEMET	IZO128N0000	WMO	91/92, 96/97, 99/00, 09/12, 14/15
Aichi	MKW234N0000	WMO	
AIST	TKY236N0000	AIST	96/97, 99/00, 02/06, 09/12, 14/15
BMKG & Empa	BKT500S0000	WMO	
BoM & CSIRO	CGO540S0000, CGO540S0010	WMO	
CMA	WLG236N0000	WMO	96/97, 99/00, 02/06, 09/12, 14/15
CMA & NOAA/ESRL	SDZ240N0000, WLG236N0001	WMO	
CNR-ICES & DNA-IAA	JBN762S0000	WMO	
CSIRO	ALT482N0003, CFA519S0003, CGO540S0003, CRI215N0000, CYA766S0001, ESP449N0003, MAA767S0003, MLO519N0003, MQA554S0003, SIS660N0003, SPO789S0003	WMO	91/92, 96/97, 99/00, 02/06, 09/12, 14/15
DMC & Empa	TLL330S0000	WMO	
EC	ALT482N0000, ALT482N0005, CDL453N0000,CHM449N0000, CSJ451N0000, EGB444N0100 , ESP449N0000, ETL454N0000 , FSD449N0000, LLB454N0100, WSA443N0000, WSA443N0001	WMO	91/92, 96/97, 99/00, 02/06, 09/12, 14/15
EMA	CAI130N0000		
Empa	JFJ646N0000	WMO	09/12, 14/15
Empa & NHMS	PDI221N0000	WMO	
ENEA	LMP635N0001	WMO	91/92, 96/97, 99/00, 02/06, 09/12, 14/15
FMI	PAL667N0000	WMO	02/06, 09/12 14/15
HKO	HKG222N0001	WMO	
	HKO222N0000, HKO222N0001	NIST WMO	
HMS	HUN646N0000, KPS646N0000	WMO	91/92, 96/97, 99/00, 02/06, 09/12, 14/15
IAFMS	CMN644N0001, CMN644N0002	WMO	91/92, 96/97, 02/06, 14/15
IGP	HUA312S0000	WMO	
IMK-IFU	WNK647N0000, ZUG647N0014	WMO	99/00
INRNE	BEO642N0000	WMO	
IOEP	DIG654N0000	IOEP	
ISAC	CGR637N0000		

ITM	ZEP678N0000	WMO	96/97, 99/00, 09/12
JMA	MNM224N0000, RYO239N0000, YON224N0000	WMO	91/92, 96/97, 99/00, 02/06, 09/12, 14/15
KMA	AMY236N0000	WMO KRISS	02/06, 09/12 14/15
	KSG762S0000	KRISS	
KSNU	ISK242N0000		
KUP	JFJ646N0003	WMO	09/12
LSCE	AMS137S0000, BGU641N0000, LPO648N0000, MHD653N0002, PDM642N0000, PUY645N0000	WMO	91/92, 96/97, 99/00, 02/06, 09/12, 14/15
	FIK635N0000		
MGO	BER255N0001, KOT276N0001, KYZ240N0001, STC652N0001, TER669N0001, TIK271N0000	WMO	14/15
MMD	DMV504N0000	WMO	
MRI	TKB236N0002		91/92, 96/97, 99/00, 02/06, 09/12, 14/15
NIER	GSN233N0103	WMO	
NIES	COI243N0000, HAT224N0000	NIES 95**	96/97, 99/00, 02/06, 09/12, 14/15
NIMR	GSN233N0001	WMO	96/97
NIPR & Tohoku Univ.	SYO769S0000		Tohoku Univ.: 91/92, 96/97, 99/00, 02/06, 09/12
NIWA	BHD541S0000	WMO	91/92, 96/97, 99/00, 02/06, 09/12, 14/15
NMA	FDT645N0002		
NOAA/ESRL	BRW471N0000, MLO519N0000, SMO514S0000, SPO789S0000, NOAA/ESRL flask network*	WMO	91/92, 96/97, 99/00, 02/06, 09/12, 14/15
Osaka Univ.	SUI234N0000		
RIVM	KMW653N0000	NIST	
RSE	PRS645N0000	WMO	99/00, 02/06 14/15
Saitama	DDR236N0000, KIS236N0000, URW235N0000	WMO	
SAWS	CPT134S0000	WMO	99/00, 02/06, 09/12, 14/15
Shizuoka Univ.	HMM234N0000		
UBA	BRT648N0000, DEU649N0000, LGB652N0000, NGL653N0000, SNB647N0000, SSL647N0000, SSL647N0002, WES654N0000, ZGT654N0000, ZSF647N0001, ZUG647N0000	WMO	91/92, 96/97, 99/00, 02/06, 09/12, 14/15
Univ. Malta	GLH636N0000		

* NOAA/ESRL flask network:
ABP312S0001,ALT482N0001,AMS137S0001,ASC107S0001,ASK123N0001,AVI417N0001,AZR638N0001,BAL655N0001,BHD541S0001,
BKT500S0001,BME432N0001,BMW432N0001,BRW471N0001,BSC644N0001,CBA455N0001,CGO540S0001,CHR501N0001,CMO445N0001,
CPT134S0001,CRZ146S0001,EIC327S0001,GMI513N0001,GOZ636N0001,HBA775S0001,HPB647N0003,HUN646N0001,ICE663N0001,
ITN435N0001,IZO128N0001,KCO204N0001,KEY425N0001,KUM519N0001,KZD244N0001,KZM243N0001,LEF445N0001,LLB454N0001,
LLN223N0001,LMP635N0003,MBC476N0001,MEX419N0001,MHD653N0001,MID528N0001,MKN100S0001,MLO519N0001,NAT306S0001,
NMB123S0001,NWR440N0101,OPW448N0001,OXK650N0001,PAL667N0001,POC900N0001,POC905N0001,POC905S0001,POC910N0001,
POC910S0001,POC915N0001,POC915S0001,POC920N0001,POC920S0001,POC925N0001,POC925S0001,POC930N0001,POC930S0001,
POC935S0001,PSA764S0001,PTA438N0001,RPB413N0001,SCS903N0001,SCS906N0001,SCS909N0001,SCS912N0001,SCS915N0001,
SCS918N0001,SCS921N0001,SEY104S0001,SGP436N0001,SHM452N0001,SMO514S0001,SPO789S0001,STC654N0001,STM666N0001,
SUM672N0001,SYO769S0001,TAP236N0001,THD441N0001,TIK271N0001,USH354S0001,UTA439N0001,UUM244N0001,
WIS631N0001,ZEP678N0001

**NIES 95 CO_2 scale is 0.10 to 0.14 ppm lower than that of WMO in the range 355 to 385 ppm. (Machida *et al*., WMO/GAW Report No. 186, 26-29, 2009.)

3. Methane (CH_4)

The GAW Programme has established two WCCs for CH_4, the Swiss Federal Laboratory for Materials Testing and Research (Empa), Dübendorf, Switzerland; and the Japan Meteorological Agency (JMA), Tokyo, Japan (WMO, 2017). In addition, the Central Calibration Laboratory for CH_4 has been established at NOAA/ESRL (Dlugokencky *et al.*, 2005; WMO, 2017).

The WMO X2004 (NOAA04) scale has been designated as the Primary scale of the GAW Programme. This scale results in CH_4 mole fractions that are a factor of 1.0124 higher than the previous scale (NOAA/CMDL83) used by NOAA/ESRL (Dlugokencky *et al.*, 2005). The new WMO X2004A (NOAA04A) scale was updated 7 July 2015. Revisions to conversion factors will be small, but must be re-evaluated. Until they are revised, use conversion factors for WMO X2004.

Table 4 summarizes the CH_4 standard scales used by laboratories contributing to the WDCGG and lists tentative multiplying conversion factors applied for analysis in this issue of the *Data Summary*. The standard is the WMO X2004 scale, and conversion factors were calculated from the results of comparisons with other laboratories performed bilaterally or multilaterally before the establishment of the GAW Standard.

The NOAA/CMDL83 scale is lower than an absolute gravimetric scale (Aoki *et al.*, 1992) by ~1.5% (Dlugokencky *et al.*, 1994) and lower than the AES (Atmospheric Environment Service, currently EC) scale by a factor of 1.0151 (Worthy *et al.*, 1998). The NOAA/CMDL83 scale can be converted to the Tohoku University standard by multiplying by 1.0121 (Dlugokencky *et al.*, 2005). The conversion factors 1.0124 / 1.0151 = 0.9973 and 1.0124 / 1.0121 = 1.0003 have been adopted for comparisons with the WMO X2004 scale.

Table 4. Status of the standard scales of CH_4 at laboratories with conversion factors.

Laboratory	WDCGG Filename Code	Calibration Scale	Conversion Factor
AEMET	IZO128N0000	WMO X2004	1
AGAGE	CGO540S0011, CGO540S0013, CMO445N0011, MHD653N0011, MHD653N0013, RPB413N0000, RPB413N0011, SMO514S0014, SMO514S0016, THD441N0000	Tohoku Univ.	1.0003
BMKG & Empa	BKT500S0000	WMO X2004	1
CHMI	KOS649N0000	CHMI	
CMA	WLG236N0000	WMO X2004	1
CMA & NOAA/ESRL	SDZ240N0000, WLG236N0001	WMO X2004A	1
CSIRO	ALT482N0003, CFA519S0003, CGO540S0003, CRI215N0000, CYA766S0001, ESP449N0003, MAA767S0003, MLO519N0003, MQA554S0003, SIS660N0003, SPO789S0003	WMO X2004A	1
DMC & Empa	TLL330S0000	WMO X2004	1

EC	ALT482N0000, CDL453N0000, CHM449N0000, EGB444N0100, ESP449N0000, ETL454N0000, FSD449N0000, LLB454N0100, WSA443N0000	WMO X2004	1
Empa	JFJ646N0000	WMO X2004	1
ENEA	LMP635N0001	WMO X2004	1
FMI	PAL667N0000	WMO X2004A	1
INSTAAR	SUM672N0003	WMO	1
ISAC	CGR637N0000		
JMA	MNM224N0000, RYO239N0000, YON224N0000	WMO X2004	1
KMA	AMY236N0000	KRISS	
KSNU	ISK242N0000		
LSCE	AMS137S0002, BGU641N0000, LPO648N0000, PDM642N0000, PUY645N0002	NOAA /CMDL83	1.0124
	FIK635N0000, MHD653N0007		
MGO	TER669N0001, TIK271N0000	WMO X2004A	1
MRI	TKB236N0000		0.9973
NHMS & Empa	PDI221N0000	WMO X2004	1
NIER	GSN233N0103	WMO X2004	1
NIES	COI243N0000, HAT224N0000	NIES	0.9973
NIMR	GSN233N0001	SIO X97	
NOAA/ESRL	BRW471N0000, MLO519N0000, NOAA/ESRL flask network*	WMO X2004A	1
	KPA431N0001, MCM777S0001, NZL543S0001, SGI354S0001,SIO432N0001	NOAA /CMDL83	1.0124
RIVM	KMW653N0000	NIST	0.9973
RSE	PRS645N0000	WMO X2004	1
SAWS	CPT134S0000	WMO X2004A	1
UBA	DEU649N0000, NGL653N0000, SSL647N0000, ZGT654N0000, ZSF647N0001, ZUG647N0000	WMO X2004	1
	SNB647N0000		
UNIURB	CMN644N0003	WMO X2004A	1
Univ. Malta	GLH636N0000		

* NOAA/ESRL flask network:
ABP312S0001,ALT482N0001,AMS137S0001,ASC107S0001,ASK123N0001,AVI417N0001,AZR638N0001,BAL655N0001, BHD541S0001, BKT500S0001,BME432N0001,BMW432N0001,BRW471N0001,BSC644N0001,CBA455N0001,CGO540S0001,CHR501N0001,CMO445N0001, CPT134S0001,CRZ146S0001,EIC327S0001,GMI513N0001,GOZ636N0001,HBA775S0001,HPB647N0003,HUN646N0001,ICE663N0001, ITN435N0001,IZO128N0001,KEY425N0001,KUM519N0001,KZD244N0001,KZM243N0001,LEF445N0001,LLB454N0001,LLN223N0001, LMP635N0003,MBC476N0001,MEX419N0001,MHD653N0001,MID528N0001,MKN100S0001,MLO519N0001,NAT306S0001,NMB123S0001, NWR440N0101,OPW448N0001,OXK650N0001,PAL667N0001,POC900N0001,POC905N0001,POC905S0001,POC910N0001,POC910S0001, POC915N0001,POC915S0001,POC920N0001,POC920S0001,POC925N0001,POC925S0001,POC930N0001,POC930S0001, POC935S0001, PSA764S0001,PTA438N0001,RPB413N0001,SCS903N0001,SCS906N0001,SCS909N0001,SCS912N0001,SCS915N0001,SCS918N0001, SCS921N0001,SEY104S0001,SGP436N0001,SHM452N0001,SMO514S0001,SPO789S0001,STM666N0001,SUM672N0001,SYO769S0001, TAP236N0001,THD441N0001,TIK271N0001,USH354S0001,UTA439N0001,UUM244N0001,WIS631N0001,WKT431N0001, ZEP678N0001

4. Nitrous Oxide (N_2O)

The Halocarbons and other Atmospheric Trace Species (HATS) Group of NOAA/ESRL maintains a set of standards for N_2O (Hall *et al.*, 2001) and serves as a CCL for N_2O. The WMO X2006 (NOAA-2006) scale (Hall *et al.*, 2007), revised and updated to WMO X2006A (NOAA-2006A) in 2011 to deal with drifting in secondary standards, has been designated as the Primary scale for the GAW Programme. CCL compares its standards with the ones of other laboratories, including those of Environment Canada (EC) and the Australian Commonwealth Scientific and Industrial Research Organisation (CSIRO). Karlsruhe Institute of Technology, Institute for Meteorology and Climate Research, Germany, serves

as the GAW WCC for N_2O.

The SIO 1998 scale is essentially equivalent to the WMO X2006 scale, with an average difference of 0.01% over the range of 299–319 ppb; the WMO X2000 (NOAA-2000) scale can be converted to the WMO X2006 scale by using the factor 0.999402 (Hall *et al.*, 2007).

Table 5. Status of the standard scales of N_2O at laboratories.

Laboratory	WDCGG Filename Code	Calibration Scale	Conversion Factor
AEMET	IZO128N0000	WMO X2006A	1
AGAGE	ADR651N0010, CGO540S0011, CGO540S0012, CGO540S0013, CMO445N0010, CMO445N0011, MHD653N0011, MHD653N0013, RPB413N0000, RPB413N0010, RPB413N0011, SMO514S0014, SMO514S0015, SMO514S0016, THD441N0000	SIO 1998	1
CSIRO	ALT482N0003, CFA519S0003, CGO540S0003, CRI215N0000, CYA766S0001, ESP449N0003, MAA767S0003, MLO519N0003, MQA554S0003, SIS660N0003, SPO789S0003	WMO X2006A	1
Empa	JFJ646N0000	SIO 1998	1
ENEA	LMP635N0001	WMO X2006	1
JMA	RYO239N0000	WMO X2006A	1
KMA	AMY236N0000	KRISS	
MRI	MMB243N0000		
Nagoya Univ.	NGY235N0000		
NIER	GSN233N0103	WMO X2006	1
NIES	COI243N0000, HAT224N0000	NIES 96*	1
NILU	ZEP678N0000		
NIMR	GSN233N0001	WMO X1997	
NOAA/ESRL	ALT482N0001, BRW471N0001, CGO540S0001, KUM519N0001, MLO519N0001, NWR440N0001, SMO514S0001, SPO789S0001	WMO X2000	0.999402
	ALT482N0006, BRW471N0005, BRW471N0011, CGO540S0014, MLO519N0006, MLO519N0011, NWR440N0004, NWR440N0011, SMO514S0009, SMO514S0011, SPO789S0006, SPO789S0011	WMO X2006	1
	ALT482N0004, BRW471N0003, BRW471N0010, CGO540S0009, HFM442N0000, ITN435N0000, KUM519N0002, LEF445N0000, MHD653N0008, MLO519N0005, MLO519N0010, NWR440N0003, NWR440N0010, PSA764S0000, SMO514S0008, SMO514S0010, SPO789S0005, SPO789S0010, SUM672N0000, SUM672N0002, THD441N0002, USH354S0002	WMO X2006A	1
SAWS	CPT134S0000	WMO X2000	0.999402
UBA	SSL647N0000, ZSF647N0001	SIO 1998	1
UNIURB	CMN644N0003	WMO X2006A	1

* NIES 96 N_2O scale is approximately 0.7 ppb lower than that of WMO X2006A in the range 325 to 326 ppb. (http://www.esrl.noaa.gov/gmd/ccgg/wmorr/wmorr_results.php?rr=rr6&param=n2o)

6. Carbon Monoxide (CO)

NOAA/ESRL is the WMO/GAW CCL for carbon monoxide. Due to lack of stability of CO in high pressure cylinders, the CO scale has historically been defined by repeated sets of gravimetric standards made in 1996/1997, 1999/2000, 2006 and 2011. The CCL make revisions in the CO scale whenever new gravimetric standard sets indicate a significant drift in the scale. Scale revisions are indicated with date codes (WMO CO X2000, WMO CO X2004, WMO CO X2014) with the most recent made in December 2015 being WMO CO X2014A (WMO, 2016).

The Swiss Federal Laboratory for Materials Testing and Research (Empa) serves as the WCC under GAW based on its secondary standards calibrated against the standard at NOAA/ESRL designated as the Primary Standard for GAW. Empa, as WCC for CO, has developed an audit system for CO measurements at GAW stations.

Table 7. Status of CO standard scales at laboratories

Laboratory	WDCGG Filename Code	Calibration Scale	Audit Empa-WCC
AEMET	IZO128N0000	WMO X2004	00, 04, 09, 13
AGAGE	CGO540S0011, MHD653N0011	CSIRO94	
ARSO	KVV646N0000	CHMI	
BAS	HBA775S0000	WMO X2004	
BMKG & Empa	BKT500S0000	WMO X2000	01, 04, 07, 08, 11, 14
CHMI	KOS649N0000	CHMI	
CMA & NOAA/ESRL	SDZ240N0000, WLG236N0001	WMO X2004	
CSIRO	ALT482N0003, CFA519S0003, CGO540S0003, CRI215N0000, CYA766S0001, ESP449N0003, MAA767S0003, MLO519N0003, MQA554S0003, SIS660N0003, SPO789S0003	CSIRO	Cape Grim: 02, 10
DMC & Empa	TLL330S0000	WMO X2004	
DWD	HPB647N0000	WMO X2004	97, 06, 11
EC	ALT482N0000, CDL453N0000, CHM449N0000, EGB444N0100, ESP449N0000, ETL454N0000, FSD449N0000, LLB454N0100, WSA443N0000	WMO	Alert: 04
Empa	JFJ646N0000	WMO	99, 06, 15
	PAY646N0000, RIG646N0000	NPL	
Empa &KMD	MKN100S0000	WMO X2000	05, 06, 08, 10, 15
Empa &NHMS	PDI221N0000	WMO X2004	
INRNE	BEO642N0000	WMO	
ISAC	CGR637N0000		
	CMN644N0000	WMO X2004	12
	CMN644N0004	WMO X2014A	
JMA	MNM224N0000, RYO239N0000, YON224N0000	WMO	
LA	PDM642N0001	EMD	
LAMP	PUY645N0001	EMD	
LSCE	AMS137S0000	WMO X2004	08

NOAA/ESRL	NOAA/ESRL flask network*	WMO	
ONM	ASK123N0000	WMO X2000	07
PolyU	HKG222N0000		
RIVM	KMW653N0000, KTB653N0000	NMI	
SAWS	CPT134S0002		98, 02
	CPT134S0003	WMO	06, 11
SMN	USH354S0010, USH354S0011	WMO	98, 03, 08, 16
SMNA	USH354S0000	WMO X2000	
UBA	NGL653N0000, SSL647N0000, ZSF647N0001, ZUG647N0000	WMO	Zugspitze: 97, 01 Zugspitze/Schneefernerhaus: 01, 06, 11 Sonnblick: 98
	SNB647N0000		
UNIURB	CMN644N0003	WMO X2014	
Univ. Malta	GLH636N0001, GLH636N0002		
Univ. York	CVO116N0001	WMO X2004	12

* NOAA/ESRL flask network:
ABP312S0001,ALT482N0001,ASC107S0001,ASK123N0001,AZR638N0001,BAL655N0001,BHD541S0001,BKT500S0001,BME432N0001, BMW432N0001,BRW471N0001,BSC644N0001,CBA455N0001,CGO540S0001,CHR501N0001,CMO445N0001,CPT134S0001,CRZ146S0001, EIC327S0001,GMI513N0001,GOZ636N0001,HBA775S0001,HPB647N0003,HUN646N0001,ICE663N0001,ITN435N0001,IZO128N0001, KEY425N0001,KUM519N0001,KZD244N0001,KZM243N0001,LEF445N0001,LLB454N0001,LLN223N0001,LMP635N0003,MBC476N0001, MEX419N0001,MHD653N0001,MID528N0001,MKN100S0001,MLO519N0001,NAT306S0001,NMB123S0001,NWR440N0101,OXK650N0001, PAL667N0001,POC900N0001,POC905N0001,POC905S0001,POC910N0001,POC910S0001,POC915N0001,POC915S0001, POC920N0001,POC920S0001,POC925N0001,POC925S0001,POC930N0001,POC930S0001,POC935N0000,POC935S0001,PSA764S0001, PTA438N0001,RPB413N0001,SCS903N0001,SCS906N0001,SCS909N0001,SCS912N0001,SCS915N0001,SCS918N0001,SCS921N0001, SEY104S0001,SGP436N0001,SHM452N0001,SMO514S0001,SPO789S0001,STM666N0001,SUM672N0001,SYO769S0001,TAP236N0001, THD441N0001,USH354S0001,UTA439N0001,UUM244N0001,WIS631N0001, ZEP678N0001

References

Aoki, S., T. Nakazawa, S. Murayama, and S. Kawaguchi, Measurements of atmospheric methane at the Japanese Antarctic station, Syowa, *Tellus*, **44B**, 273–281, 1992.

Dlugokencky, E. J., L. P. Steele, P. M. Lang, and K. A. Masarie, The growth rate and distribution of atmospheric methane, *J. Geophys. Res.*, **99**, 17021-17043, 1994.

Dlugokencky, E. J., R. C. Myers, P. M. Lang, K. A. Masarie, A. M. Crotwell, K. W. Thoning, B. D. Hall, J. W. Elkins, and L. P. Steele, Conversion of NOAA atmospheric dry air CH_4 mole fractions to a gravimetrically prepared standard scale, *J. Geophys. Res.*, **110**, D18306, doi: 10.1029/2005JD006035, 2005.

Hall, B. D. (ed.), J. W. Elkins, J. H. Butler, S. A. Montzka, T. M. Thompson, L. Del Negro, G. S. Dutton, D. F. Hurst, D. B. King, E. S. Kline, L. Lock, D. MacTaggart, D. Mondeel, F. L. Moore, J. D. Nance, E. A. Ray, and P. A. Romashkin, Halocarbons and Other Atmospheric Trace Species, Section 5 in Climate Monitoring and Diagnostics Laboratory Summary Report No. 25, 1998–1999, R. S. Schnell, D. B. King, R. M. Rosson (eds.), NOAA-CMDL, Boulder, CO., USA, 2001.

Hall, B. D., G. S. Dutton, and J. W. Elkins, The NOAA nitrous oxide standard scale for atmospheric observations, *J. Geophys. Res.*, **112**, D09305, doi:10.1029/2006JD007954, 2007.

WMO, 18th WMO/IAEA Meeting on Carbon Dioxide, Other Greenhouse Gases and Related Tracers Measurement Techniques (GGMT-2015), ed. P. Tans and C. Zellweger, GAW Report No.229, 2016.

WMO, WMO Global Atmosphere Watch (GAW) Implementation Plan: 2016-2023, GAW Report No.228, 2017.

Worthy, D. E. J., I. Levin, N. B. A. Trivett, A. J. Kuhlmann, J. F. Hopper, and M. K. Ernst, Seven years of continuous methane observations at a remote boreal site in Ontario, Canada, *J. Geophys. Res.*, **103**, 15995–16007, 1998.

Zhao, C. L., P. P. Tans, and K. W. Thoning, A high precision manometric system for absolute calibrations of CO_2 in dry air, *J. Geophys. Res.*, **102**, 5885–5894, 1997.

LIST OF ABBREVIATIONS
IN THE CALIBRATION AND STANDARD SCALES

AEMET	Agencia Estatal de Meteorología (Spain)
AGAGE	Advanced Global Atmospheric Gases Experiment
Aichi	Aichi Prefecture (Japan)
AIST	National Institute of Advanced Industrial Science and Technology (Japan)
AMERIFLUX	AmeriFlux Network (USA)
ARSO	Agencija Republike Slovenije za Okolje (Slovenia)
BAS	British Antarctic Survey (United Kingdom)
BLG	Bowling Lab Group, Terrestrial Biogeochemistry, Department of Biology, University of Utah (USA)
BMKG	Agency for Meteorology, Climatology and Geophysics (Indonesia)
BoM	Commonwealth Bureau of Meteorology (Australia)
CALTECH	California Institute of Technology, Division of Geological and Planetary Science (USA)
CHMI	Czech Hydrometeorological Institute (Czech Republic)
CMA	China Meteorological Administration (China)
CNR-ICES	International Centre for Earth Sciences, Consiglio Nazionale delle Ricerche (Italy)
CSIRO	Commonwealth Scientific and Industrial Research Organisation (Australia)
DMC	Dirección Meteorológica de Chile (Chile)
DNA-IAA	Direccion Nacional del Antartico-Instituto Antartico Argentino (Argentina)
DWD	Deutscher Wetterdienst (German Meteorological Service, Germany)
EC	Environment Canada (Canada)
ECN	Energy Research Centre of the Netherlands (Netherlands)
EMA	Egyptian Meteorological Authority (Egypt)
EMD	Ecole des Mines de Douai (France)
Empa	Swiss Federal Laboratories for Material Testing and Research (Switzerland)
ENEA	Italian National Agency for New Technology, Energy and the Environment (Italy)
FMI	Finnish Meteorological Institute (Finland)
GAGE	Global Atmospheric Gases Experiment
GAW	Global Atmosphere Watch (WMO)
HATS	Halocarbons and other Atmospheric Trace Species Group, NOAA/ESRL
HKO	Hong Kong Observatory (Hong Kong, China)
HMS	Hungarian Meteorological Service (Hungary)
HU	Harvard University (USA)
IAFMS	Italian Air Force Meteorological Service (Italy)
ICOS	Integrated Carbon Observation System
IGP	Instituto Geofísico del Perú (Peru)
IMK-IFU	Institut für Meteorologie und Klimatologie, Atmosphärische Umweltforschung, Forschungszentrum Karlsruhe (Germany)
INRNE	Institute for Nuclear Research and Nuclear Energy (Bulgaria)
INSTAAR	Institute of Arctic and Alpine Research (USA)
IOEP	Institute of Environmental Protection (Poland)
ISAC	Istituto di Scienze dell'Atmosfera e del Clima, Consiglio Nazionale delle Ricerche (Italy)
ITM	Department of Applied Environmental Science, Stockholm University, (Sweden)
JMA	Japan Meteorological Agency (Japan)

KIT	Karlsruhe Institute of Technology (Germany)
KMA	Korea Meteorological Administration (Republic of Korea)
KMD	Kenya Meteorological Department (Kenya)
KRISS	Korea Research Institute of Standards and Science (Republic of Korea)
KSNU	Kyrgyz State National University (Kyrgyzstan)
KUP	Physics Institute, Climate and Environmental Physics, University of Bern (Switzerland)
LA	Laboratoire d'Aérologie (France)
LAMP	Laboratoire de Météorologie Physique (France)
LSCE	Laboratoire des Sciences du Climat et de l'Environnement (France)
MGO	Main Geophysical Observatory, Roshydromet (Russian Federation)
MPI-BGC	Max-Planck Institute (MPI) for Biogeochemistry in Jena (Germany)
MMD	Malaysian Meteorological Department (Malaysia)
MRI	Meteorological Research Institute, JMA (Japan)
Nagoya Univ.	Nagoya University (Japan)
NCAR	National Center For Atmospheric Research (USA)
NEON	National Ecological Observatory Network (USA)
NHMS	National Hydro-Meteorological Service (Vietnam)
NIER	National Institute of Environmental Research (Republic of Korea)
NIES	National Institute for Environmental Studies (Japan)
NILU	Norwegian Institute for Air Research (Norway)
NIMR	National Institute of Meteorological Reserch, KMA (Republic of Korea)
NIPR	National Institute of Polar Research (Japan)
NIST	National Institute of Standards and Technology (USA)
NIWA	National Institute of Water & Atmospheric Research (New Zealand)
NMA	National Meteorological Administration (Romania)
NMI	Nederlands Meetinstituut (Netherlands)
NOAA	National Oceanic and Atmospheric Administration (USA)
NOAA-CSD	Chemical Sciences Division, NOAA (USA)
NOAA/ESRL	Earth System Research Laboratory, NOAA (USA)
NPL	National Physical Laboratory (United Kingdom)
ONM	Office National de la Météorologie (Algeria)
Osaka Univ.	Osaka University (Japan)
PolyU	Hong Kong Polytechnic University (Hong Kong, China)
PSU	Penn State University (USA)
RHUL	Royal Holloway University London (United Kingdom)
RIVM	National Institute for Health and Environment (Netherlands)
Roshydromet	Federal Service for Hydrometeorology and Environmental Monitoring (Russian Federation)
RSE	Ricerca sul Sistema Elettrico (Italy)
RUG	University of Groningen (RUG), Centre for Isotope Research (CIO) (Netherlands)
Saitama	Saitama Prefecture (Japan)
SAWS	South African Weather Service (South Africa)
Shizuoka Univ.	Shizuoka University (Japan)
SIO	Scripps Institution of Oceanography (USA)
SMN(SMNA)	Servicio Meteorológico Nacional (Argentina)
Tohoku Univ. (TU)	Tohoku University (Japan)
UBA	Umweltbundesamt (Germany)
UBA-SCHAU	Umweltbundesamt, Station Schauinsland (Germany)

UBA/ZUG	Umweltbundesamt, Zugspitze GAW Station (Germany)
UEA	University of East Anglia (United Kingdom)
UHEI-IUP	University of Heidelberg, Institut fuer Umweltphysik (Germany)
UNIURB	University of Urbino (Italy)
Univ. Malta	University of Malta (Malta)
Univ. York	University of York (United Kingdom)
WCC-Empa	World Calibration Centre (Empa)
WDCGG	World Data Centre for Greenhouse Gases, operated by JMA, Japan (WMO)
WMO	World Meteorological Organization

LIST OF OBSERVATIONAL STATIONS

Station	Country/Territory	Index Number	Location Latitude (° ')	Location Longitude (° ')	Altitude (m)	Parameter
REGION I (Africa)						
Amsterdam Island	France	AMS137S00	37 48 S	77 32 E	55	CH_4, CO_2
Amsterdam Island	France	AMS137S00	37 48 S	77 32 E	55	CH_4, CO, CO_2
Ascension Island	United Kingdom of Great Britain and Northern Ireland	ASC107S00	7 55 S	14 25 W	54	$^{13}CH_4$, $^{13}CO_2$, $C^{18}O_2$, CH_4, CO, CO_2, H_2
Assekrem	Algeria	ASK123N00	23 16 N	5 38 E	2710	CO
Assekrem	Algeria	ASK123N00	23 16 N	5 38 E	2710	$^{13}CO_2$, $C^{18}O_2$, CH_4, CO, CO_2, H_2
Cairo	Egypt	CAI130N00	30 05 N	31 17 E	35	CO_2
Cape Point	South Africa	CPT134S00	34 21 S	18 29 E	230	CH_4, CO, CO_2
Cape Point	South Africa	CPT134S00	34 21 S	18 29 E	230	CH_4, CO, CO_2, N_2O
Cape Point	South Africa	CPT134S00	34 21 S	18 29 E	230	^{222}Rn
Cape Verde Observatory	Cape Verde	CVO116N00	16 51 N	24 52 W	10	CO
Crozet	France	CRZ146S00	46 27 S	51 51 E	120	$^{13}CO_2$, $C^{18}O_2$, CH_4, CO, CO_2, H_2
Gobabeb	Namibia	NMB123S00	23 34 S	15 01 E	461	$^{13}CO_2$, $C^{18}O_2$, CH_4, CO, CO_2
Izaña (Tenerife)	Spain	IZO128N00	28 18 N	16 30 W	2367	CH_4, CO, CO_2, N_2O, SF_6
Izaña (Tenerife)	Spain	IZO128N00	28 18 N	16 30 W	2367	$^{13}CO_2$, $C^{18}O_2$, CH_4, CO, CO_2, H_2
Mahe Island	Seychelles	SEY104S00	4 40 S	55 10 E	7	$^{13}CO_2$, $C^{18}O_2$, CH_4, CO, CO_2, H_2
Mt. Kenya	Kenya	MKN100S00	0 04 S	37 18 E	3678	CO
Mt. Kenya	Kenya	MKN100S00	0 04 S	37 18 E	3678	$^{13}CO_2$, $C^{18}O_2$, CH_4, CO, CO_2
REGION II (Asia)						
Anmyeon-do	Republic of Korea	AMY236N00	36 32 N	126 19 E	47	CFCs, CH_4, CO_2, N_2O, SF_6
Bering Island	Russian Federation	BER255N00	55 12 N	165 59 E	13	CO_2
Cape Ochi-ishi	Japan	COI243N00	43 10 N	145 30 E	42.5	CFCs, CH_4, CO_2, HCFCs, HFCs, N_2O, SF_6
Cape Rama	India	CRI215N00	15 05 N	73 50 E	60	$^{13}CO_2$, CH_4, CO, CO_2, H_2, N_2O
Everest - Pyramid	Nepal	PYR227N00	27 57 N	86 49 E	5079	C_2Cl_4, C_2HCl_3, $CBrClF_2$, $CBrF_3$, CCl_4, CFCs, CH_2Br_2, CH_2Cl_2, CH_3Br, CH_3CCl_3, CH_3Cl, $CHBr_3$, $CHCl_3$, HCFCs, HFCs
Gosan	Republic of Korea	GSN233N00	33 17 N	126 10 E	72	CFCs, CH_4, CO_2, N_2O
Gosan	Republic of Korea	GSN233N00	33 17 N	126 10 E	72	$C_2Br_2F_4$, $CBrClF_2$, $CBrF_3$, CFCs, CH_3CCl_3, CH_3Cl, $CHCl_3$, HCFCs, HFCs, PFCs, SF_6, SO_2F_2
Gosan	Republic of Korea	GSN233N01	33 10 N	126 06 E	72	CFCs, CH_4, CO_2, N_2O
Hamamatsu	Japan	HMM234N00	34 43 N	137 43 E	35	CO_2
Hateruma	Japan	HAT224N00	24 04 N	123 49 E	10.8	CFCs, CH_4, CO_2, HCFCs, HFCs, N_2O, SF_6
Hok Tsui	Hong Kong, China	HKG222N00	22 13 N	114 15 E	60	CO_2
Hok Tsui	Hong Kong, China	HKG222N00	22 13 N	114 15 E	60	CO
Issyk-Kul	Kyrgyzstan	ISK242N00	42 37 N	76 59 E	1640	CH_4, CO_2
Kaashidhoo	Maldives	KCO204N00	4 58 N	73 28 E	1	$^{13}CO_2$, CH_4, CO_2
King's Park	Hong Kong, China	HKO222N00	22 19 N	114 10 E	65	CO_2
Kisai	Japan	KIS236N00	36 05 N	139 33 E	13	CO_2
Kotelny Island	Russian Federation	KOT276N00	76 00 N	137 52 E	5	CO_2
Kyzylcha	Uzbekistan	KYZ240N00	40 52 N	66 09 E	340	CO_2
Lulin	China	LLN223N00	23 28 N	120 52 E	2867	$^{13}CO_2$, $C^{18}O_2$, CH_4, CO, CO_2
Memanbetsu	Japan	MMB243N00	43 55 N	144 12 E	32.9	N_2O
Mikawa-Ichinomiya	Japan	MKW234N00	34 51 N	137 26 E	50	CO_2
Minamitorishima	Japan	MNM224N00	24 17 N	153 59 E	8	CH_4, CO, CO_2
Mt. Dodaira	Japan	DDR236N00	36 00 N	139 11 E	840	CO_2

LIST OF OBSERVATIONAL STATIONS (continued)

Station	Country/Territory	Index Number	Location Latitude (° ')	Location Longitude (° ')	Altitude (m)	Parameter
Mt. Waliguan	China	WLG236N00	36 17 N	100 54 E	3810	CH_4, CO_2
Mt. Waliguan	China	WLG236N00	36 17 N	100 54 E	3810	$^{13}CH_4$, $^{13}CO_2$, $C^{18}O_2$, CH_4, CO, CO_2, H_2
Nagoya	Japan	NGY235N00	35 09 N	136 58 E	35	N_2O
Pha Din	Viet Nam	PDI221N00	21 34 N	103 31 E	1466	CH_4, CO, CO_2
Plateau Assy	Kazakhstan	KZM243N00	43 15 N	77 52 E	2519	$^{13}CO_2$, $C^{18}O_2$, CH_4, CO, CO_2, H_2
Ryori	Japan	RYO239N00	39 02 N	141 49 E	260	CCl_4, CFCs, CH_3CCl_3, CH_4, CO, CO_2, N_2O
Sary Taukum	Kazakhstan	KZD244N00	44 27 N	75 34 E	412	$^{13}CO_2$, $C^{18}O_2$, CH_4, CO, CO_2, H_2
Shangdianzi	China	SDZ240N00	40 39 N	117 07 E	287	CH_4, CO, CO_2
Ship between Ishigaki Island and Hateruma Island	Japan	SIH224N00	24 07 N	123 50 E	5	CO_2
South China Sea (03N)	N/A	SCS903N00	3 00 N	105 00 E	15	$^{13}CO_2$, $C^{18}O_2$, CH_4, CO, CO_2, H_2
South China Sea (06N)	N/A	SCS906N00	6 00 N	107 00 E	15	$^{13}CO_2$, $C^{18}O_2$, CH_4, CO, CO_2, H_2
South China Sea (09N)	N/A	SCS909N00	9 00 N	109 00 E	15	$^{13}CO_2$, $C^{18}O_2$, CH_4, CO, CO_2, H_2
South China Sea (12N)	N/A	SCS912N00	12 00 N	111 00 E	15	$^{13}CO_2$, $C^{18}O_2$, CH_4, CO, CO_2, H_2
South China Sea (15N)	N/A	SCS915N00	15 00 N	113 00 E	15	$^{13}CO_2$, $C^{18}O_2$, CH_4, CO, CO_2, H_2
South China Sea (18N)	N/A	SCS918N00	18 00 N	113 00 E	15	$^{13}CO_2$, $C^{18}O_2$, CH_4, CO, CO_2, H_2
South China Sea (21N)	N/A	SCS921N00	21 00 N	114 00 E	15	$^{13}CO_2$, $C^{18}O_2$, CH_4, CO, CO_2, H_2
Suita	Japan	SUI234N00	34 49 N	135 31 E	63	CO_2
Tae-ahn Peninsula	Republic of Korea	TAP236N00	36 43 N	126 07 E	20	$^{13}CH_4$, $^{13}CO_2$, $C^{18}O_2$, CH_4, CO, CO_2, H_2
Takayama	Japan	TKY236N00	36 09 N	137 25 E	1420	CO_2
Tiksi	Russian Federation	TIK271N00	71 35 N	128 55 E	8	CH_4, CO_2
Tiksi	Russian Federation	TIK271N00	71 35 N	128 55 E	8	CH_4, CO_2
Tsukuba	Japan	TKB236N00	36 03 N	140 08 E	26	CH_4, CO_2
Ulaan Uul	Mongolia	UUM244N00	44 27 N	111 05 E	914	$^{13}CO_2$, $C^{18}O_2$, CH_4, CO, CO_2, H_2
Urawa	Japan	URW235N00	35 52 N	139 36 E	10	CO_2
Yonagunijima	Japan	YON224N00	24 28 N	123 01 E	30	CH_4, CO, CO_2
REGION III (South America)						
Arembepe	Brazil	ABP312S00	12 46 S	38 10 W	0	CH_4, CO, CO_2, N_2O
Arembepe	Brazil	ABP312S00	12 46 S	38 10 W	0	$^{13}CO_2$, $C^{18}O_2$, CH_4, CO, CO_2
Bird Island	United Kingdom of Great Britain and Northern Ireland	SGI354S00	54 00 S	38 03 W	30	CH_4, CO_2
Easter Island	Chile	EIC327S00	27 08 S	109 27 W	50	$^{13}CO_2$, $C^{18}O_2$, CH_4, CO, CO_2, H_2
El Tololo	Chile	TLL330S00	30 10 S	70 48 W	2220	CH_4, CO, CO_2
Huancayo	Peru	HUA312S00	12 04 S	75 32 W	3313	CO_2
Natal	Brazil	NAT306S00	6 00 S	35 12 W	0	CH_4, CO, CO_2
Ushuaia	Argentina	USH354S00	54 51 S	68 19 W	18	$^{13}CO_2$, $C^{18}O_2$, CCl_4, CFCs, CH_3CCl_3, CH_4, CO, CO_2, H_2, N_2O, SF_6
Ushuaia	Argentina	USH354S00	54 51 S	68 19 W	18	CO
Ushuaia	Argentina	USH354S00	54 51 S	68 19 W	18	CO
REGION IV (North and Central America)						
Alert	Canada	ALT482N00	82 27 N	62 31 W	210	$^{13}CO_2$, CH_4, CO, CO_2, H_2, N_2O

LIST OF OBSERVATIONAL STATIONS (continued)

Station	Country/Territory	Index Number	Location Latitude (° ')	Location Longitude (° ')	Altitude (m)	Parameter
Alert	Canada	ALT482N00	82 27 N	62 31 W	210	$^{13}CO_2$, $C^{18}O_2$, CH_4, CO, CO_2, N_2O, SF_6
Alert	Canada	ALT482N00	82 27 N	62 31 W	210	$^{13}CH_4$, $^{13}CO_2$, $C^{18}O_2$, C_2Cl_4, $CBrClF_2$, $CBrF_3$, CCl_4, CFCs, CH_2Cl_2, CH_3Br, CH_3CCl_3, CH_3Cl, CH_4, CO, CO_2, H_2, HCFCs, HFCs, N_2O, SF_6
Argyle	United States of America	AMT445N00	45 02 N	68 41 W	50	$^{13}CO_2$, $C^{18}O_2$, CH_4
Barrow	United States of America	BRW471N00	71 19 N	156 36 W	11	$^{13}CH_4$, $^{13}CO_2$, $C^{18}O_2$, C_2Cl_4, $CBrClF_2$, $CBrF_3$, CCl_4, CFCs, CH_2Cl_2, CH_3Br, CH_3CCl_3, CH_3Cl, CH_4, CO, CO_2, H_2, HCFCs, HFCs, N_2O, SF_6
Candle Lake	Canada	CDL453N00	53 52 N	104 39 W	489	CH_4, CO, CO_2
Cape Meares	United States of America	CMO445N00	45 28 N	123 58 W	30	CCl_4, CFCs, CH_3CCl_3, CH_4, N_2O
Cape Meares	United States of America	CMO445N00	45 28 N	123 58 W	30	$^{13}CO_2$, $C^{18}O_2$, CH_4, CO, CO_2, H_2
Cape St. James	Canada	CSJ451N00	51 56 N	131 01 W	89	CO_2
Chibougamau	Canada	CHM449N00	49 41 N	74 21 W	393	CH_4, CO, CO_2
Churchill	Canada	CHL458N00	58 45 N	94 04 W	35	$^{13}CO_2$, $C^{18}O_2$, CH_4, CO_2, N_2O
Cold Bay	United States of America	CBA455N00	55 12 N	162 43 W	25	$^{13}CH_4$, $^{13}CO_2$, $C^{18}O_2$, CH_4, CO, CO_2, H_2
East Trout Lake	Canada	ETL454N00	54 21 N	104 59 W	492	$^{13}CO_2$, $C^{18}O_2$, CH_4, CO, CO_2
Egbert	Canada	EGB444N01	44 14 N	79 47 W	253	CH_4, CO, CO_2
Estevan Point	Canada	ESP449N00	49 23 N	126 33 W	39	$^{13}CO_2$, CH_4, CO, CO_2, H_2, N_2O
Estevan Point	Canada	ESP449N00	49 23 N	126 33 W	39	$^{13}CO_2$, $C^{18}O_2$, CH_4, CO, CO_2, N_2O, SF_6
Fraserdale	Canada	FSD449N00	49 53 N	81 34 W	210	$^{13}CO_2$, $C^{18}O_2$, CH_4, CO, CO_2
Grifton	United States of America	ITN435N00	35 21 N	77 23 W	505	$^{13}CO_2$, $C^{18}O_2$, CCl_4, CFCs, CH_3CCl_3, CH_4, CO, CO_2, H_2, N_2O, SF_6
Harvard Forest	United States of America	HFM442N00	42 54 N	72 18 W	340	C_2Cl_4, $CBrClF_2$, CCl_4, CFCs, CH_2Cl_2, CH_3Br, CH_3CCl_3, CH_3Cl, HCFCs, HFCs, N_2O, SF_6
Key Biscayne	United States of America	KEY425N00	25 40 N	80 12 W	3	$^{13}CO_2$, $C^{18}O_2$, CH_4, CO, CO_2, H_2
Kitt Peak	United States of America	KPA431N00	31 58 N	111 36 W	2083	CH_4
La Jolla	United States of America	SIO432N00	32 50 N	117 16 W	14	CH_4
Lac La Biche	Canada	LLB454N00	54 57 N	112 27 W	540	CH_4, CO, CO_2
Lac La Biche (Alberta)	Canada	LLB454N01	54 57 N	112 27 W	540	CH_4, CO, CO_2
Mex High Altitude Global Climate Observation Center, Mexico	Mexico	MEX419N00	19 59 N	97 10 W	4560	CH_4, CO, CO_2
Moody	United States of America	WKT431N00	31 19 N	97 19 W	708	$^{13}CO_2$, $C^{18}O_2$, CH_4
Mould Bay	Canada	MBC476N00	76 15 N	119 20 W	58	$^{13}CO_2$, $C^{18}O_2$, CH_4, CO, CO_2, H_2
Niwot Ridge (C-1)	United States of America	NWR440N00	40 02 N	105 32 W	3021	C_2Cl_4, $CBrClF_2$, $CBrF_3$, CCl_4, CFCs, CH_2Cl_2, CH_3Br, CH_3CCl_3, CH_3Cl, HCFCs, HFCs, N_2O, SF_6

LIST OF OBSERVATIONAL STATIONS (continued)

Station	Country/Territory	Index Number	Location Latitude (° ')	Location Longitude (° ')	Altitude (m)	Parameter
Niwot Ridge (T-van)	United States of America	NWR440N01	40 03 N	105 35 W	3523	$^{13}CH_4$, $^{13}CO_2$, $^{14}CO_2$, $C^{18}O_2$, CH_4, CO, CO_2, H_2, N_2O
Olympic Peninsula	United States of America	OPW448N00	48 15 N	124 25 W	488	CH_4, CO_2, H_2
Pacific Ocean (15N)	N/A	POC915N00	15 00 N	145 00 W	10	$^{13}CO_2$, $C^{18}O_2$, CH_4, CO, CO_2, H_2
Pacific Ocean (20N)	N/A	POC920N00	20 00 N	141 00 W	10	$^{13}CO_2$, $C^{18}O_2$, CH_4, CO, CO_2, H_2
Pacific Ocean (25N)	N/A	POC925N00	25 00 N	139 00 W	10	$^{13}CO_2$, $C^{18}O_2$, CH_4, CO, CO_2, H_2
Pacific Ocean (30N)	N/A	POC930N00	30 00 N	135 00 W	10	$^{13}CO_2$, $C^{18}O_2$, CH_4, CO, CO_2, H_2
Pacific Ocean (35N)	N/A	POC935N00	35 00 N	137 00 W	10	$^{13}CO_2$, $C^{18}O_2$, CO, H_2
Pacific Ocean (40N)	N/A	POC940N00	40 00 N	136 00 W	10	$^{13}CO_2$, H_2
Pacific Ocean (45N)	N/A	POC945N00	45 00 N	131 00 W	10	$^{13}CO_2$, H_2
Park Falls	United States of America	LEF445N00	45 55 N	90 16 W	868	$^{13}CO_2$, $C^{18}O_2$, C_2Cl_4, $CBrClF_2$, CCl_4, CFCs, CH_2Cl_2, CH_3Br, CH_3CCl_3, CH_3Cl, CH_4, CO, CO_2, H_2, HCFCs, HFCs, N_2O, SF_6
Point Arena	United States of America	PTA438N00	38 57 N	123 43 W	17	$^{13}CO_2$, $C^{18}O_2$, CH_4, CO, CO_2
Ragged Point	Barbados	RPB413N00	13 10 N	59 26 W	45	$C_2Br_2F_4$, C_2Cl_4, C_2HCl_3, $CBrClF_2$, $CBrF_3$, CCl_4, CFCs, CH_2Cl_2, CH_3Br, CH_3CCl_3, CH_3Cl, CH_4, $CHCl_3$, HCFCs, HFCs, N_2O, NF_3, PFCs, SF_6, SO_2F_2
Ragged Point	Barbados	RPB413N00	13 10 N	59 26 W	45	$^{13}CO_2$, $C^{18}O_2$, CH_4, CO, CO_2, H_2
Sable Island	Canada	WSA443N00	43 56 N	60 01 W	5	$^{13}CO_2$, $C^{18}O_2$, CH_4, CO, CO_2, N_2O, SF_6
Shemya Island	United States of America	SHM452N00	52 43 N	174 05 E	40	$^{13}CO_2$, $C^{18}O_2$, CH_4, CO, CO_2, H_2
Southern Great Plains	United States of America	SGP436N00	36 47 N	97 30 W	314	$^{13}CO_2$, $C^{18}O_2$, CH_4, CO, CO_2, H_2, N_2O, SF_6
St. Croix	United States of America	AVI417N00	17 45 N	64 45 W	3	CH_4, CO_2
St. David's Head	United Kingdom of Great Britain and Northern Ireland	BME432N00	32 22 N	64 39 W	30	$^{13}CO_2$, $C^{18}O_2$, CH_4, CO, CO_2, H_2
Trinidad Head	United States of America	THD441N00	41 03 N	124 09 W	120	$C_2Br_2F_4$, C_2Cl_4, C_2HCl_3, $CBrClF_2$, $CBrF_3$, CCl_4, CFCs, CH_2Cl_2, CH_3Br, CH_3CCl_3, CH_3Cl, CH_4, $CHCl_3$, HCFCs, HFCs, N_2O, PFCs, SF_6, SO_2F_2
Trinidad Head	United States of America	THD441N00	41 03 N	124 09 W	120	$^{13}CO_2$, $C^{18}O_2$, C_2Cl_4, $CBrClF_2$, CCl_4, CFCs, CH_2Cl_2, CH_3Br, CH_3CCl_3, CH_3Cl, CH_4, CO, CO_2, HCFCs, HFCs, N_2O, SF_6
Tudor Hill	United Kingdom of Great Britain and Northern Ireland	BMW432N00	32 16 N	64 52 W	30	$^{13}CO_2$, $C^{18}O_2$, CH_4, CO, CO_2, H_2
Wendover	United States of America	UTA439N00	39 53 N	113 43 W	1320	$^{13}CO_2$, $C^{18}O_2$, CH_4, CO, CO_2, H_2
West Branch	United States of America	WBI441N00	41 44 N	91 21 W	241.7	$^{13}CO_2$, $C^{18}O_2$

REGION V (South-West Pacific)

LIST OF OBSERVATIONAL STATIONS (continued)

Station	Country/Territory	Index Number	Location Latitude (° ')	Location Longitude (° ')	Altitude (m)	Parameter
Baring Head	New Zealand	BHD541S00	41 25 S	174 52 E	85	$^{13}CO_2$, $C^{18}O_2$, CH_4, CO, CO_2
Baring Head	New Zealand	BHD541S00	41 25 S	174 52 E	85	$^{13}CH_4$, $^{14}CO_2$, CH_4, CO, CO_2, N_2O
Bukit Koto Tabang	Indonesia	BKT500S00	0 12 S	100 19 E	864.5	CH_4, CO, CO_2
Bukit Koto Tabang	Indonesia	BKT500S00	0 12 S	100 19 E	864.5	$^{13}CO_2$, $C^{18}O_2$, CH_4, CO, CO_2, H_2, N_2O, SF_6
Cape Ferguson	Australia	CFA519S00	19 17 S	147 03 E	2	$^{13}CO_2$, CH_4, CO, CO_2, H_2, N_2O
Cape Grim	Australia	CGO540S00	40 41 S	144 41 E	94	CO_2
Cape Grim	Australia	CGO540S00	40 41 S	144 41 E	94	$C_2Br_2F_4$, C_2Cl_4, C_2HCl_3, $CBrClF_2$, $CBrF_3$, CCl_4, CFCs, CH_2Cl_2, CH_3Br, CH_3CCl_3, CH_3Cl, CH_4, $CHCl_3$, CO, H_2, HCFCs, HFCs, N_2O, NF_3, PFCs, SF_6, SO_2F_2
Cape Grim	Australia	CGO540S00	40 41 S	144 41 E	94	^{222}Rn
Cape Grim	Australia	CGO540S00	40 41 S	144 41 E	94	$^{13}CO_2$, CH_4, CO, CO_2, H_2, N_2O
Cape Grim	Australia	CGO540S00	40 41 S	144 41 E	94	$^{13}CH_4$, $^{13}CO_2$, $C^{18}O_2$, C_2Cl_4, $CBrClF_2$, $CBrF_3$, CCl_4, CFCs, CH_2Cl_2, CH_3Br, CH_3CCl_3, CH_3Cl, CH_4, CO, CO_2, H_2, HCFCs, HFCs, N_2O, SF_6
Cape Kumukahi	United States of America	KUM519N00	19 31 N	154 49 W	3	$^{13}CH_4$, $^{13}CO_2$, $C^{18}O_2$, C_2Cl_4, $CBrClF_2$, $CBrF_3$, CCl_4, CFCs, CH_2Cl_2, CH_3Br, CH_3CCl_3, CH_3Cl, CH_4, CO, CO_2, H_2, HCFCs, HFCs, N_2O, SF_6
Christmas Island	Kiribati	CHR501N00	1 42 N	157 10 W	3	$^{13}CO_2$, $C^{18}O_2$, CH_4, CO, CO_2, H_2
Danum Valley GAW Baseline Station	Malaysia	DMV504N00	4 58 N	117 50 E	426	CO_2
Guam	United States of America	GMI513N00	13 26 N	144 47 E	2	$^{13}CO_2$, $C^{18}O_2$, CH_4, CO, CO_2, H_2
Gunn Point	Australia	GPA512S00	12 15 S	131 03 E	25	$^{13}CO_2$, CH_4, CO, CO_2, H_2, N_2O
Kaitorete Spit	New Zealand	NZL543S00	43 50 S	172 38 E	3	CH_4
Lauder	New Zealand	LAU545S00	45 02 S	169 40 E	370	CH_4
Macquarie Island	Australia	MQA554S00	54 29 S	158 58 E	12	$^{13}CO_2$, CH_4, CO, CO_2, H_2, N_2O
Mauna Loa	United States of America	MLO519N00	19 32 N	155 35 W	3397	$^{13}CO_2$, CH_4, CO, CO_2, H_2, N_2O
Mauna Loa	United States of America	MLO519N00	19 32 N	155 35 W	3397	$^{13}CH_4$, $^{13}CO_2$, $C^{18}O_2$, C_2Cl_4, $CBrClF_2$, $CBrF_3$, CCl_4, CFCs, CH_2Cl_2, CH_3Br, CH_3CCl_3, CH_3Cl, CH_4, CO, CO_2, H_2, HCFCs, HFCs, N_2O, SF_6
Pacific Ocean (00N)	N/A	POC900N00	0 00 N	155 00 W	10	$^{13}CO_2$, $C^{18}O_2$, CH_4, CO, CO_2, H_2
Pacific Ocean (05N)	N/A	POC905N00	5 00 N	151 00 W	10	$^{13}CO_2$, $C^{18}O_2$, CH_4, CO, CO_2, H_2
Pacific Ocean (05S)	N/A	POC905S00	5 00 S	159 00 W	10	$^{13}CO_2$, $C^{18}O_2$, CH_4, CO, CO_2, H_2
Pacific Ocean (10N)	N/A	POC910N00	10 00 N	149 00 W	10	$^{13}CO_2$, $C^{18}O_2$, CH_4, CO, CO_2, H_2
Pacific Ocean (10S)	N/A	POC910S00	10 00 S	161 00 W	10	$^{13}CO_2$, $C^{18}O_2$, CH_4, CO, CO_2, H_2
Pacific Ocean (15S)	N/A	POC915S00	15 00 S	171 00 W	10	$^{13}CO_2$, $C^{18}O_2$, CH_4, CO, CO_2, H_2
Pacific Ocean (20S)	N/A	POC920S00	20 00 S	174 00 W	10	$^{13}CO_2$, $C^{18}O_2$, CH_4, CO, CO_2, H_2
Pacific Ocean (25S)	N/A	POC925S00	25 00 S	171 00 W	10	$^{13}CO_2$, $C^{18}O_2$, CH_4, CO, CO_2, H_2
Pacific Ocean (30S)	N/A	POC930S00	30 00 S	176 00 W	10	$^{13}CO_2$, $C^{18}O_2$, CH_4, CO, CO_2, H_2
Pacific Ocean (35S)	N/A	POC935S00	35 00 S	180 00 E	10	$^{13}CO_2$, $C^{18}O_2$, CH_4, CO, CO_2, H_2
Sand Island	United States of America	MID528N00	28 12 N	177 22 W	7.7	$^{13}CO_2$, $C^{18}O_2$, CH_4, CO, CO_2, H_2

LIST OF OBSERVATIONAL STATIONS (continued)

Station	Country/Territory	Index Number	Location Latitude (° ')	Location Longitude (° ')	Altitude (m)	Parameter
Tutuila (Cape Matatula)	United States of America	SMO514S00	14 14 S	170 34 W	42	$C_2Br_2F_4$, C_2Cl_4, C_2HCl_3, $CBrClF_2$, $CBrF_3$, CCl_4, CFCs, CH_2Cl_2, CH_3Br, CH_3CCl_3, CH_3Cl, CH_4, $CHCl_3$, HCFCs, HFCs, N_2O, PFCs, SF_6, SO_2F_2
Tutuila (Cape Matatula)	United States of America	SMO514S00	14 14 S	170 34 W	42	$^{13}CH_4$, $^{13}CO_2$, $C^{18}O_2$, C_2Cl_4, $CBrClF_2$, $CBrF_3$, CCl_4, CFCs, CH_2Cl_2, CH_3Br, CH_3CCl_3, CH_3Cl, CH_4, CO, CO_2, H_2, HCFCs, HFCs, N_2O, SF_6
REGION VI (Europe)						
Adrigole	Ireland	ADR651N00	51 41 N	9 44 W	50	CCl_4, CFCs, CH_3CCl_3, N_2O
BEO Moussala	Bulgaria	BEO642N00	42 11 N	23 35 E	2925	CO, CO_2
Baltic Sea	Poland	BAL655N00	55 21 N	17 13 E	28	$^{13}CO_2$, $C^{18}O_2$, CH_4, CO, CO_2, H_2
Begur	Spain	BGU641N00	41 58 N	3 14 E	13	CH_4, CO_2
Black Sea	Romania	BSC644N00	44 10 N	28 40 E	3	$^{13}CO_2$, $C^{18}O_2$, CH_4, CO, CO_2, H_2
Brotjacklriegel	Germany	BRT648N00	48 49 N	13 13 E	1016	CO_2
Capo Granitola	Italy	CGR637N00	37 40 N	12 39 E	5	CH_4, CO, CO_2
Deuselbach	Germany	DEU649N00	49 46 N	7 03 E	480	CH_4, CO_2
Dwejra Point	Malta	GOZ636N00	36 03 N	14 11 E	30	$^{13}CO_2$, $C^{18}O_2$, CH_4, CO, CO_2, H_2
Finokalia	Greece	FIK635N00	35 20 N	25 40 E	150	CH_4, CO_2
Fundata	Romania	FDT645N00	45 28 N	25 18 E	1383.5	CO_2
Giordan Lighthouse	Malta	GLH636N00	36 04 N	14 13 E	160	^{222}Rn, CH_4, CO, CO_2
Hegyhatsal	Hungary	HUN646N00	46 57 N	16 39 E	248	CO_2
Hegyhatsal	Hungary	HUN646N00	46 57 N	16 39 E	248	$^{13}CO_2$, $C^{18}O_2$, CH_4, CO, CO_2, H_2, N_2O, SF_6
Heimaey	Iceland	ICE663N00	63 24 N	20 17 W	100	$^{13}CO_2$, $C^{18}O_2$, CH_4, CO, CO_2, H_2
Hohenpeissenberg	Germany	HPB647N00	47 48 N	11 01 E	985	^{222}Rn, CH_4, CO, CO_2
Hohenpeissenberg	Germany	HPB647N00	47 48 N	11 01 E	985	$^{13}CO_2$, $C^{18}O_2$, CH_4, CO, CO_2
Ile Grande	France	LPO648N00	48 48 N	3 35 W	10	CH_4, CO_2
Jungfraujoch	Switzerland	JFJ646N00	46 33 N	7 59 E	3580	CO_2
Jungfraujoch	Switzerland	JFJ646N00	46 33 N	7 59 E	3580	CH_4, CO, CO_2, H_2, N_2O, SF_6
Jungfraujoch	Switzerland	JFJ646N00	46 33 N	7 59 E	3580	$C_2Br_2F_4$, C_2Cl_4, C_2HCl_3, $CBrClF_2$, $CBrF_3$, CCl_4, CFCs, CH_2Cl_2, CH_3Br, CH_3CCl_3, CH_3Cl, $CHCl_3$, HCFCs, HFCs, NF_3, PFCs, SF_6, SO_2F_2
K-puszta	Hungary	KPS646N00	46 58 N	19 33 E	125	CO_2
Kloosterburen	Netherlands (the)	KTB653N00	53 24 N	6 25 E	0	CO
Kollumerwaard	Netherlands (the)	KMW653N00	53 20 N	6 17 E	0	CH_4, CO, CO_2
Kosetice	Czech Republic	KOS649N00	49 35 N	15 05 E	534	CH_4, CO
Krvavec	Slovenia	KVV646N00	46 18 N	14 32 E	1720	CO
Lampedusa	Italy	LMP635N00	35 31 N	12 38 E	45	$CBrClF_2$, $CBrF_3$, CCl_4, CFCs, CH_2Br_2, CH_2Cl_2, CH_3Br, CH_3CCl_3, CH_3Cl, CH_3I, CH_4, $CHCl_3$, CO_2, HCFCs, HFCs, N_2O, SF_6
Lampedusa	Italy	LMP635N00	35 31 N	12 38 E	45	$^{13}CO_2$, $C^{18}O_2$, CH_4, CO, CO_2
Mace Head	Ireland	MHD653N00	53 20 N	9 54 W	8	CH_4, CO_2

LIST OF OBSERVATIONAL STATIONS (continued)

Station	Country/Territory	Index Number	Location Latitude (° ')	Location Longitude (° ')	Altitude (m)	Parameter
Mace Head	Ireland	MHD653N00	53 20 N	9 54 W	8	$C_2Br_2F_4$, C_2Cl_4, C_2HCl_3, $CBrClF_2$, $CBrF_3$, CCl_4, CFCs, CH_2Cl_2, CH_3Br, CH_3CCl_3, CH_3Cl, CH_4, $CHCl_3$, CO, H_2, HCFCs, HFCs, N_2O, NF_3, PFCs, SF_6, SO_2F_2
Mace Head	Ireland	MHD653N00	53 20 N	9 54 W	8	$^{13}CH_4$, $^{13}CO_2$, $C^{18}O_2$, C_2Cl_4, $CBrClF_2$, $CBrF_3$, CCl_4, CFCs, CH_2Cl_2, CH_3Br, CH_3CCl_3, CH_3Cl, CH_4, CO, CO_2, H_2, HCFCs, HFCs, N_2O, SF_6
Monte Cimone	Italy	CMN644N00	44 11 N	10 42 E	2165	CO_2
Monte Cimone	Italy	CMN644N00	44 11 N	10 42 E	2165	CO, H_2
Monte Cimone	Italy	CMN644N00	44 11 N	10 42 E	2165	CH_4, CO, N_2O, SF_6
Monte Cimone	Italy	CMN644N00	44 11 N	10 42 E	2165	C_2Cl_4, C_2HCl_3, $CBrClF_2$, $CBrF_3$, CCl_4, CFCs, CH_2Cl_2, CH_3Br, CH_3CCl_3, CH_3Cl, $CHCl_3$, HCFCs, HFCs, PFCs, SO_2F_2
Neuglobsow	Germany	NGL653N00	53 10 N	13 02 E	65	CH_4, CO, CO_2
Ocean Station "M"	Norway	STM666N00	66 00 N	2 00 E	5	$^{13}CO_2$, $C^{18}O_2$, CH_4, CO, CO_2, H_2
Ocean Station Charlie	Russian Federation	STC652N00	52 45 N	35 30 W	5	CO_2
Ocean Station Charlie	United States of America	STC654N00	54 00 N	35 00 W	6	CO_2
Ochsenkopf	Germany	OXK650N00	50 02 N	11 48 E	1185	$^{13}CO_2$, $C^{18}O_2$, CH_4, CO, CO_2
Pallas-Sammaltunturi	Finland	PAL667N00	67 58 N	24 07 E	560	CH_4, CO_2
Pallas-Sammaltunturi	Finland	PAL667N00	67 58 N	24 07 E	560	$^{13}CO_2$, $C^{18}O_2$, $CBrF_3$, CH_4, CO, CO_2
Payerne	Switzerland	PAY646N00	46 49 N	6 57 E	490	CO
Pic du Midi	France	PDM642N00	42 56 N	0 08 E	2877	CO
Pic du Midi	France	PDM642N00	42 56 N	0 08 E	2877	CH_4, CO_2
Plateau Rosa	Italy	PRS645N00	45 56 N	7 42 E	3480	CH_4, CO_2
Puszcza Borecka/Diabla Gora	Poland	DIG654N00	54 09 N	22 04 E	157	CO_2
Puy de Dome	France	PUY645N00	45 46 N	2 58 E	1465	CO
Puy de Dome	France	PUY645N00	45 46 N	2 58 E	1465	CH_4, CO_2
Ridge Hill	United Kingdom of Great Britain and Northern Ireland	RGL651N00	52 00 N	2 32 W	204	CH_4, CO_2, N_2O, SF_6
Rigi	Switzerland	RIG646N00	46 04 N	8 27 E	1031	CO
Schauinsland	Germany	SSL647N00	47 55 N	7 55 E	1205	CH_4, CO, CO_2, N_2O, SF_6
Sede Boker	Israel	WIS631N00	31 07 N	34 52 E	400	$^{13}CO_2$, $C^{18}O_2$, CH_4, CO, CO_2, H_2
Shetland	United Kingdom of Great Britain and Northern Ireland	SIS660N00	60 05 N	1 15 W	30	$^{13}CO_2$, CH_4, CO, CO_2, H_2, N_2O
Site J	Denmark	GRL666N00	66 30 N	46 12 W	2030	CH_4
Sonnblick	Austria	SNB647N00	47 03 N	12 57 E	3106	CH_4, CO, CO_2
Summit	Denmark	SUM672N00	72 35 N	38 29 W	3238	CH_4
Summit	Denmark	SUM672N00	72 35 N	38 29 W	3238	$^{13}CO_2$, $C^{18}O_2$, C_2Cl_4, $CBrClF_2$, CCl_4, CFCs, CH_2Cl_2, CH_3Br, CH_3CCl_3, CH_3Cl, CH_4, CO, CO_2, HCFCs, HFCs, N_2O, SF_6
Tacolneston Tall Tower	United Kingdom of Great Britain and Northern Ireland	TAC652N00	52 31 N	1 08 E	56	CH_4, CO_2

LIST OF OBSERVATIONAL STATIONS (continued)

Station	Country/Territory	Index Number	Location Latitude (° ')	Location Longitude (° ')	Altitude (m)	Parameter
Tacolneston Tall Tower	United Kingdom of Great Britain and Northern Ireland	TAC652N00	52 31 N	1 08 E	56	C_2Cl_4, C_2HCl_3, $CBrClF_2$, $CBrF_3$, CFCs, CH_2Cl_2, CH_3Br, CH_3CCl_3, CH_3Cl, CH_4, $CHCl_3$, CO, CO_2, H_2, HCFCs, HFCs, N_2O, PFCs, SF_6, SO_2F_2
Terceira Island	Portugal	AZR638N00	38 46 N	27 22 W	40	$^{13}CH_4$, $^{13}CO_2$, $C^{18}O_2$, CH_4, CO, CO_2, H_2
Teriberka	Russian Federation	TER669N00	69 12 N	35 06 E	40	CH_4, CO_2
Waldhof	Germany	LGB652N00	52 48 N	10 46 E	74	CO_2
Wank Peak	Germany	WNK647N00	47 31 N	11 09 E	1780	CO_2
Westerland	Germany	WES654N00	54 56 N	8 19 E	12	CO_2
Zeppelinfjellet (Ny-Alesund)	Norway	ZEP678N00	78 54 N	11 53 E	475	CO_2
Zeppelinfjellet (Ny-Alesund)	Norway	ZEP678N00	78 54 N	11 53 E	475	CCl_4, CFCs, CH_3CCl_3, N_2O
Zeppelinfjellet (Ny-Alesund)	Norway	ZEP678N00	78 54 N	11 53 E	475	$C_2Br_2F_4$, C_2Cl_4, C_2HCl_3, $CBrClF_2$, $CBrF_3$, CFCs, CH_2Cl_2, CH_3Br, CH_3CCl_3, CH_3Cl, $CHCl_3$, HCFCs, HFCs, PFCs, SF_6, SO_2F_2
Zeppelinfjellet (Ny-Alesund)	Norway	ZEP678N00	78 54 N	11 53 E	475	$^{13}CH_4$, $^{13}CO_2$, $C^{18}O_2$, CH_4, CO, CO_2, H_2
Zingst	Germany	ZGT654N00	54 26 N	12 44 E	1	CH_4, CO_2
Zugspitze	Germany	ZUG647N00	47 25 N	10 59 E	2960	CO_2
Zugspitze	Germany	ZUG647N00	47 25 N	10 59 E	2960	CH_4, CO, CO_2
Zugspitze / Schneefernerhaus	Germany	ZSF647N00	47 25 N	10 59 E	2656	CH_4, CO, CO_2, N_2O, SF_6
Zugspitze / Schneefernerhaus	Germany	ZSF647N00	47 25 N	10 59 E	2656	^{222}Rn

LIST OF OBSERVATIONAL STATIONS (continued)

Station	Country/Territory	Index Number	Location Latitude (° ')	Location Longitude (° ')	Altitude (m)	Parameter
ANTARCTICA						
Arrival Heights	New Zealand	ARH777S00	77 48 S	166 40 E	184	$^{13}CH_4$, CH_4, CO, N_2O
Casey Station	Australia	CYA766S00	66 17 S	110 32 E	60	$^{13}CO_2$, CH_4, CO, CO_2, H_2, N_2O
Halley Bay	United Kingdom of Great Britain and Northern Ireland	HBA775S00	75 34 S	26 30 W	33	CO
Halley Bay	United Kingdom of Great Britain and Northern Ireland	HBA775S00	75 34 S	26 30 W	33	$^{13}CO_2$, $C^{18}O_2$, CH_4, CO, CO_2, H_2
Jubany	Argentina	JBN762S00	62 14 S	58 40 W	15	CO_2
King Sejong	Republic of Korea	KSG762S00	62 13 S	58 47 W	0	CO_2
Mawson	Australia	MAA767S00	67 37 S	62 52 E	32	$^{13}CO_2$, CH_4, CO, CO_2, H_2, N_2O
McMurdo Station	United States of America	MCM777S00	77 49 S	166 35 E	11	CH_4
Mizuho	Japan	MZH770S00	70 42 S	44 18 E	2230	CH_4
Palmer Station	United States of America	PSA764S00	64 55 S	64 00 W	10	$^{13}CO_2$, $C^{18}O_2$, C_2Cl_4, $CBrClF_2$, CCl_4, CFCs, CH_2Cl_2, CH_3Br, CH_3CCl_3, CH_3Cl, CH_4, CO, CO_2, H_2, HCFCs, HFCs, N_2O, SF_6
South Pole	United States of America	SPO789S00	89 59 S	24 48 W	2810	$^{13}CO_2$, CH_4, CO, CO_2, H_2, N_2O
South Pole	United States of America	SPO789S00	89 59 S	24 48 W	2810	$^{13}CH_4$, $^{13}CO_2$, $C^{18}O_2$, C_2Cl_4, $CBrClF_2$, $CBrF_3$, CCl_4, CFCs, CH_2Cl_2, CH_3Br, CH_3CCl_3, CH_3Cl, CH_4, CO, CO_2, H_2, HCFCs, HFCs, N_2O, SF_6
Syowa Station	Japan	SYO769S00	69 00 S	39 35 E	16	CO_2
Syowa Station	Japan	SYO769S00	69 00 S	39 35 E	16	$^{13}CO_2$, $C^{18}O_2$, CH_4, CO, CO_2, H_2
MOBILE STATION						
Aircraft (over Bass Strait and Cape Grim)	Australia	AIA999900				$^{13}CO_2$, CH_4, CO, CO_2, H_2, N_2O
Aircraft Observation of Atmospheric trace gases by JMA	Japan	AOA999900				CH_4, CO, CO_2, N_2O
Aircraft: Orleans	France	ORL999900			150	CH_4, CO_2
Akademik Korolev, R/V	United States of America	AKD999900				CH_4
Alligator liberty, M/V	Japan	ALG999900				CO_2
Atlantic Ocean	United States of America	AOC9XXX00			10	CH_4, CO_2
Comprehensive Observation Network for TRace gases by AIrLiner (CONTRAIL)	Japan	EOM999900				CH_4, CO_2
Comprehensive Observation Network for TRace gases by AIrLiner (CONTRAIL)	Japan	EOM999900				$^{13}CH_4$, CH_3D
Discoverer 1983 & 1984, R/V	United States of America	DIS999900				CH_4

LIST OF OBSERVATIONAL STATIONS (continued)

Station	Country/Territory	Index Number	Location Latitude (° ')	Location Longitude (° ')	Altitude (m)	Parameter
Discoverer 1985, R/V	United States of America	DSC999900				CH_4
Drake Passage	United States of America	DRP999900				$^{13}CO_2$, $C^{18}O_2$, CH_4, CO, CO_2
HATS Ocean Projects	United States of America	HOP999900				HFCs
INSTAC-I (International Strato/Tropospheric Air Chemistry Project)	Japan	INS999900				$^{13}CO_2$, CH_4, CO_2
John Biscoe, R/V	United States of America	JBS999900				CH_4
Keifu Maru, R/V	Japan	KEF999900				CO_2, TIC
Kofu Maru, R/V	Japan	KOF999900				CO_2
Korolev, R/V	United States of America	KOR999900				CH_4
Long Lines Expedition, R/V	United States of America	LLE999900				CH_4
MRI Research, 1978-1986, R/V	Japan	MRI999900				CH_4
MRI Research, Hakuho Maru, R/V	Japan	HKH999900				CO_2
MRI Research, Kaiyo Maru, R/V	Japan	KIY999900				CO_2
MRI Research, Mirai, R/V	Japan	MMR999900				CO_2
MRI Research, Natushima, R/V	Japan	NTU999900				CO_2
MRI Research, Ryofu Maru, R/V	Japan	RFM999900				CO_2
MRI Research, Wellington Maru, R/V	Japan	WLT999900				CO_2
Mexico Naval H-02, R/V	United States of America	MXN999900				CH_4
NOPACCS - Hakurei Maru -	Japan	HAK999900				TIC
Observation of Atmospheric Chemistry Over Japan	Japan	OAJ999900				CFCs, N_2O
Oceanographer, R/V	United States of America	OCE999900				CH_4
Pacific Ocean	New Zealand	BSL999900				$^{13}CH_4$, CH_4
Pacific Ocean	United States of America	POC9XXX00			10	$^{13}CO_2$, $C^{18}O_2$, CH_4, CO, CO_2, H_2
Pacific-Atlantic Ocean	United States of America	PAO999900				CH_4, CO_2
Polar Star, R/V	United States of America	PLS999900				CH_4
Ryofu Maru, R/V	Japan	RYF999900				CFCs, CH_4, CO_2, N_2O, TIC
Santarem	Brazil	SAN999900				CH_4, CO, CO_2, N_2O, SF_6
South China Sea	United States of America	SCS9XXX00			15	$^{13}CO_2$, $C^{18}O_2$, CH_4, CO, CO_2, H_2
Soyo Maru, R/V	Japan	SOY999900				CO_2
Surveyor, R/V	United States of America	SUR999900				CH_4

LIST OF OBSERVATIONAL STATIONS (continued)

Station	Country/Territory	Index Number	Location Latitude (° ')	Location Longitude (° ')	Altitude (m)	Parameter
The Observation of Atmospheric Methane Over Japan	Japan	OAM999900				CH_4
The Observation of Atmospheric Sulfur Hexafluoride Over Japan	Japan	OAS999900				SF_6
WEST COSMIC - Hakurei Maru No.2 -	Japan	HAK999901				TIC
Wakataka-Maru	Japan	WAK999900				CO_2
Western Pacific	United States of America	WPC9XXX00			10	$^{13}CH_4$, $^{13}CO_2$, $C^{18}O_2$, CH_4, CO_2
northern and western Pacific	Japan	NWP999900				N_2O
over Japan between Sendai and Fukuoka	Japan	TDA999900				CH_4
over the Pacific Ocean 20-50 km off the coast of the Sendai plain	Japan	PIP999900				CH_4

LIST OF CONTRIBUTORS

Station Country/Territory	Name	Address
REGION I (Africa)		
Cairo (Egypt)	AbdElhamid Gouda Elawadi	Egyptian Meteorological Authority Department of Air Pollution Study Egyptian Meteorological Authority P.O.Box:11784 - Cairo, Egypt
Cape Point (South Africa)	Alastair Williams	Australian Nuclear Science and Technology Organisation, Institute for Environmental Research, Atmospheric Mixing and Pollution Transport Group Locked Bag 2001, Kirrawee DC, NSW 2232, Australia
Izaña (Tenerife) (Spain)	Angel J. Gomez-Pelaez	Izana Atmospheric Research Center, Meteorological State Agency of Spain (AEMET) C/ La Marina, 20, Planta 6. 38001 Santa Cruz de Tenerife, Spain
Cape Point (South Africa)	Casper Labuschagne	South African Weather Service (Climate Division) SA Weather Service, c/o CSIR (Environmentek), P.O. Box 320,Stellenbosch 7599, South Africa
	Thumeka Mkololo	South African Weather Service (Climate Division) SAWS, c/o CSIR (Environmentek), P.O. Box 320,Stellenbosch 7599, South Africa
	Lynwill Martin	South African Weather Service (Climate Division) SAWS, c/o CSIR (Environmentek), P.O. Box 320,Stellenbosch 7599, South Africa
Mt. Kenya (Kenya)	Constance Okuku	Kenya Meteorological Department Kenya Meteorological Department MT KENYA GAW STATION P.O. Box 192 10400 NANYUKI Kenya
	Jörg Klausen	Federal Office of Meteorology and Climatology MeteoSwiss 8058 ZH,Zürich-Flughafen Operation Center 1, Switzerland
	Stephan Henne	Empa, Swiss Federal Laboratories for Materials Science and Technology Ueberlandstrasse 129 8600 Duebendorf, Switzerland
Amsterdam Island (France)	Jean Sciare	LSCE (Laboratoire des Sciences du Climat et de l'Environnement) UMR CEA-CNRS LSCE - CEA Saclay - Orme des Merisiers - Bat.701 91191 Gif-sur-Yvette, France

LIST OF CONTRIBUTORS (continued)

Station Country/Territory	Name	Address
	Michel Ramonet	LSCE (Laboratoire des Sciences du Climat et de l'Environnement) UMR CEA-CNRS-UVSQ LSCE - CEA Saclay - Orme des Merisiers - 91191 Gif-sur-Yvette, France
Cape Verde Observatory (Cape Verde)	Katie Read	Department of Chemistry, University of York Department of Chemistry, University of York, Heslington, York, Y010 5DD, United Kingdom
	Zoë Fleming	National Centre for Atmospheric Science (NCAS) Department of Chemistry University of Leicester National Centre for Atmospheric Science (NCAS) Department of Chemistry University of Leicester Leicester LE1 7RH, UK
Assekrem (Algeria)	Mimouni Mohamed	Office National de la Meteorologie POBox 31 Tamanrasset 11000, Algeria
REGION II (Asia)		
Nagoya (Japan)	A. Matsunami	Research Center for Advanced Energy Conversion, Nagoya University Furo-cho, Chikusaku, Nagoya 464-8603, Japan
Minamitorishima Ryori Yonagunijima (Japan)	Atsushi TAKIZAWA	Atmospheric Environment Division, Global Environment and Marine Department, Japan Meteorological Agency (JMA) 1-3-4 Otemachi, Chiyoda-ku, Tokyo 100-8122, Japan
Pha Din (Viet Nam)	Martin Steinbacher	Empa - Swiss Federal Laboratories for Materials Science and Technology Ueberlandstrasse 129 8600 Duebendorf Switzerland
	Duong Hoang Long	National Hydro-Meteorological Service NHMS No. 3 Dang Thai Than street 100000 Hanoi Viet Nam
Anmyeon-do Gosan (Republic of Korea)	Haeyoung Lee	Climate Change Monitoring Division, Korea Meteorological Administration 61 Yeouidaebang-ro 16 gil, Dongjak-gu, Seoul, 07062, Republic of Korea

LIST OF CONTRIBUTORS (continued)

Station Country/Territory	Name	Address
	Park Hyo-Jin	Climate Change Monitoring Division, Korea Meteorological Administration 61 Yeouidaebang-ro 16 gil, Dongjak-gu, Seoul, 07062, Republic of Korea
Cape Ochi-ishi Hateruma (Japan)	Hitoshi MUKAI	Center for Global Environmental Research, National Institute for Environmental Studies 16-2, Onogawa, Tsukuba-shi, Ibaraki 305-8506, Japan
	Takuya Saito	Center for Environmental Measurement and Analysis, National Institute for Environmental Studies
	Yasunori TOHJIMA	Center for Global Environmental Research, National Institute for Environmental Studies 16-2, Onogawa, Tsukuba-shi, Ibaraki 305-8506, Japan
Everest - Pyramid (Nepal)	Jgor Arduini	Università degli Studi di Urbino Istituto di Scienze Chimiche, piazza Rinascimento 6, 61029 Urbino - Italy
Hok Tsui (Hong Kong, China)	Ka Se Lam	Department of Civil and Structural Engineering,Hong Kong Polytechnic University Hung Hom, Kowloon, Hong Kong, China
Mikawa-Ichinomiya (Japan)	Koji Ohno	Aichi Air Environment Division 1-2 Sannomaru-3chome, Naka-ku, Nagoya, Aichi 460-8501, Japan
Memanbetsu (Japan)	Michio Hirota	Geochemical Research Department, Meteorological Research Institute 1-1, Nagamine, Tsukuba, Ibaraki 305-0052, Japan
Tsukuba (Japan)	Michio Hirota	Geochemical Research Department, Meteorological Research Institute 1-1, Nagamine, Tsukuba, Ibaraki 305-0052, Japan
	Yousuke Sawa	Geochemical Research Department, Meteorological Research Institute 1-1, Nagamine, Tsukuba, Ibaraki 305-0052, Japan
Hamamatsu (Japan)	Mitsuo TODA	Shizuoka University 3-5-1 Jyohoku, Hamamatsu 432-8561, Japan
Bering Island Kotelny Island Tiksi (Russian Federation)	Nina Paramonova	Main Geophysical Observatory (MGO) Karbyshev Street 7, St. Petersburg, 194021, Russian Federation
Kyzylcha (Uzbekistan)		

LIST OF CONTRIBUTORS (continued)

Station Country/Territory	Name	Address
Hok Tsui King's Park (Hong Kong, China)	Olivia S.M. Lee	Hong Kong Observatory 134A, Nathan Road, Kowloon, Hong Kong
	David H.Y. Lam	Hong Kong Observatory 134A, Nathan Road, Kowloon, Hong Kong
Gosan (Republic of Korea)	Seung-Yeon Kim	National Institute of Environmental Research Environmental Research Complex, Gyeongseo-dong, Seo-gu, Incheon, 404-708, Republic of Korea
	Kyung-Jung Moon	National Institute of Environmental Research Environmental Research Complex, Gyeongseo-dong, Seo-gu, Incheon, 404-708, Republic of Korea
Takayama (Japan)	Shohei Murayama	Research Institute for Environmental Management Technology, National Institute of Advanced Industrial Science and Technology (AIST) AIST Tsukuba West, 16-1 Onogawa, Tsukuba, Ibaraki 305-8569, Japan
Mt. Waliguan (China)	Shuangxi FANG	Meteorological Observation Centre (MOC), China Meteorological Administration (CMA) 46 Zhongguancun Nandajie Beijing 100081, China
Ship between Ishigaki Island and Hateruma Island (Japan)	Takakiyo Nakazawa	Center for Atmospheric and Oceanic Studies, Graduate School of Science, Tohoku University Aoba, Sendai 980-8578, Japan
	Shuji Aoki	Center for Atmospheric and Oceanic Studies, Graduate School of Science, Tohoku University Aoba, Sendai 980-8578, Japan
Suita (Japan)	Tomohiro Oda	Division of Sustainable Energy and Environmental Engineering, Graduate School of Engineering, Osaka Universiy, Japan Green Engieering Lab Division of Sustainable Energy and Environmental Engineering 2-1 Yamadaoka, Suita, Osaka 565-0871 Japan
Issyk-Kul (Kyrgyzstan)	V. Sinyakov	Laboratory of Geophysics, Institute of Fundamental sciences at the Kyrgyz National University Manas Street 101, Bishkek, 720033, Kyrgyz Republic
Mt. Dodaira Kisai Urawa (Japan)	Yosuke MUTO	Center for Environmental Science in Saitama 914 Kamitanadare, Kisai-machi, Kita-Saitama-gun, Saitama 347-0115, Japan

LIST OF CONTRIBUTORS (continued)

Station Country/Territory	Name	Address
REGION III (South America)		
El Tololo (Chile)	Martin Steinbacher	Empa - Swiss Federal Laboratories for Materials Science and Technology Ueberlandstrasse 129 8600 Duebendorf Switzerland
	Gaston Torres	
Arembepe (Brazil)	Luciana Vanni Gatti	IPEN Atmospheric Chemistry Laboratory Av. Prof. Lineu Prestes, 2242, Cidade Universitaria, Sao Paulo, SP- BRAZIL CEP 05508-900
Ushuaia (Argentina)	Manuel Cupeiro	National Weather Service 245 Viviendas Tira 8A, Dpto 10. Ushuaia, Tierra del Fuego, Argentina
	Maria Elena Barlasina	National Weather Service Observatorio Central Villa Ortuzar División Radiación Av. de Los Constituyentes 3454 Cp 1427, Argentina
	Ricardo Sanchez	National Weather Service Observatorio Central Villa Ortuzar División Radiación Av. de Los Constituyentes 3454 Cp 1427, Argentina
Huancayo (Peru)	Mutsumi Ishitsuka	Observatorio de Huancayo, Instituto Geofisico del Peru Apartado 46, Huancayo, Peru
Ushuaia (Argentina)	Sergio Luppo	Servicio Meteorológico Nacional - Gobierno de Tierra del Fuego Estación VAG Ushuaia Subsecretaria de Ciencia y Tecnología, Ministerio de Educación, Cultura, Ciencia y Tecnología Gobierno de Tierra del Fuego 9410 Ushuaia, Tierra del Fuego, Argentina
REGION IV (North and Central America)		
Candle Lake Chibougamau Cape St. James Egbert Lac La Biche (Alberta) (Canada)	Doug Worthy	Environment Canada (EC) 4905 Dufferin Street, Toronto, Ontario, Canada, M3H 5T4

LIST OF CONTRIBUTORS (continued)

Station Country/Territory	Name	Address
Alert Churchill Estevan Point East Trout Lake Fraserdale Sable Island (Canada)	Doug Worthy	Environment Canada (EC) 4905 Dufferin Street, Toronto, Ontario, Canada, M3H 5T4
	Lin Huang	Environment & Climate Change Canada 4905 Dufferin Street, Toronto, Ontario, Canada, M3H 5T4
REGION V (South-West Pacific)		
Cape Grim (Australia)	Alastair Williams	Australian Nuclear Science and Technology Organisation, Institute for Environmental Research, Atmospheric Mixing and Pollution Transport Group Locked Bag 2001, Kirrawee DC, NSW 2232, Australia
Cape Grim (Australia)	Bruce Forgan	Commonwealth Bureau of Meteorology 700 Collins St, Docklands GPO Box 1289K, Melbourne, Victoria 3001, Australia
Lauder (New Zealand)	Dan Smale	National Institute of Water & Atmospheric Research Ltd. NIWA, Private Bag 50061, Omakau, Central Otago 9320, New Zealand
	Sylvia Nichol	National Institute of Water & Atmospheric Research Ltd. 301 Evans Bay Parade, Greta Point, Private Bag 14-901, Kilbirnie, Wellington, New Zealand
	Gordon Brailsford	National Institute of Water & Atmospheric Research Ltd. 301 Evans Bay Parade, Greta Point,Private Bag 14-901, Kilbirnie, Wellington, New Zealand
Bukit Koto Tabang (Indonesia)	Mangasa Naibaho	The Indonesia Agency for Meteorology Climatology and Geophysics (BMKG) Jl.Angkasa 1,No.2,Kemayoran Jakarta 10720,Indonesia
	Nahas, Alberth Christian	The Indonesia Agency for Meteorology Climatology and Geophysics (BMKG) Jl. Raya Bukittinggi-Medan Km. 17 Palupuh, District Agam, West Sumatera, Indonesia PO BOX 11 Bukittinggi 26100
	Ilahi, Asep Firman	Global GAW Bukit Kototabang Jl. Raya Bukittinggi-Medan Km. 17 Palupuh, District Agam, West Sumatera, Indonesia PO BOX 11 Bukittinggi 26100

LIST OF CONTRIBUTORS (continued)

Station Country/Territory	Name	Address
	Jörg Klausen	Federal Office of Meteorology and Climatology MeteoSwiss 8058 ZH,Zürich-Flughafen Operation Center 1, Switzerland
	Martin Steinbacher	Empa - Swiss Federal Laboratories for Materials Science and Technology Ueberlandstrasse 129 8600 Duebendorf Switzerland
Danum Valley GAW Baseline Station (Malaysia)	Maznorizan Mohamad	Atmospheric Science and Cloud Seeding Division Malaysian Meteorological Department
	Aminah Ismail	Jalan Sultan, 46667, Petaling Jaya, Selangor MALAYSIA
Baring Head (New Zealand)	Sylvia Nichol	National Institute of Water & Atmospheric Research Ltd. 301 Evans Bay Parade, Greta Point, Private Bag 14-901, Kilbirnie, Wellington, New Zealand
	Gordon Brailsford	National Institute of Water & Atmospheric Research Ltd. 301 Evans Bay Parade, Greta Point,Private Bag 14-901, Kilbirnie, Wellington, New Zealand
	Ross Martin	National Institute of Water & Atmospheric Research Ltd. 301 Evans Bay Parade, Greta Point, Private Bag 14-901, Kilbirnie, Wellington, New Zealand
REGION VI (Europe)		
Puszcza Borecka/Diabla Gora (Poland)	Anna Degorska	Institute of Environmental Protection Kolektorska 4 01-692 Warsaw, Poland
Zeppelinfjellet (Ny-Alesund) (Norway)	Birgitta Noone	Department of Applied Environmental Science (ITM) Stockholm University SE-10691 Stockholm
	Hans-Christen Hansson	Department of Applied Environmental Science (ITM) Stockholm University SE-10691 Stockholm

LIST OF CONTRIBUTORS (continued)

Station Country/Territory	Name	Address
Payerne Rigi (Switzerland)	Brigitte Buchmann	Empa - Swiss Federal Laboratories for Materials Science and Technology Überlandstrasse 129 CH-8600 Dübendorf Switzerland
	Thomas Seitz	Empa - Swiss Federal Laboratories for Materials Science and Technology Überlandstrasse 129 CH-8600 Dübendorf Switzerland
Hohenpeissenberg (Germany)	Dagmar Kubistin	Deutscher Wetterdienst (DWD, German Meteorological Service) Meteorologisches Observatorium Hohenpeissenberg Albin-Schwaiger-Weg 10 D-82383 Hohenpeissenberg Germany
	Lindauer Matthias	Deutscher Wetterdienst (DWD, German Meteorological Service) Meteorologisches Observatorium Hohenpeissenberg Albin-Schwaiger-Weg 10 82383 Hohenpeissenberg
Summit (Denmark)	Detlev Helmig	Institute of Arctic and Alpine Research (INSTAAR) INSTAAR, Univ. of Colorado 1560, 30th Street UCB 450 Boulder, CO 80309 U.S.A.
	Jacques Hueber	Institute of Arctic and Alpine Research (INSTAAR) INSTAAR, Univ. of Colorado 1560, 30th Street UCB 450 Boulder, CO 80309 U.S.A.
Jungfraujoch (Switzerland)	Martin Steinbacher	Empa - Swiss Federal Laboratories for Materials Science and Technology Ueberlandstrasse 129 8600 Duebendorf Switzerland
	Thomas Seitz	Empa - Swiss Federal Laboratories for Materials Science and Technology Überlandstrasse 129 CH-8600 Dübendorf Switzerland

LIST OF CONTRIBUTORS (continued)

Station Country/Territory	Name	Address
Fundata (Romania)	Florin Nicodim	National Meteorological Administration Sos. Bucuresti-Ploiesti nr. 97, 71552 Bucharest, Romania
Giordan Lighthouse (Malta)	Francelle Azzopardi	
	Raymond Ellul	Atmospheric Research Unit / Physics Department /University of Malta Msida MSD 06, Malta
	Martin Saliba	
Plateau Rosa (Italy)	Francesco Apadula	Ricerca sul Sistema Energetico - RSE S.p.A. via Rubattino 54, 20134 Milano, Italy
	Daniela Heltai	Ricerca sul Sistema Energetico - RSE S.p.A. via Rubattino 54, 20134 Milano, Italy
	Andrea Lanza	Ricerca sul Sistema Energetico - RSE S.p.A. via Rubattino 54, 20134 Milano, Italy
Zugspitze / Schneefernerhaus (Germany)	Gabriele Frank	Deutscher Wetterdienst (DWD, German Meteorological Service) Frankfurter Str. 135 63067 Offenbach Germany
Site J (Denmark)	Gen Hashida	National Institute of Polar Research Kaga 1-9-10, Itabashi-ku, Tokyo 173-8515, Japan
	Shinji Morimoto	National Institute of Polar Research Kaga 1-9-10, Itabashi-ku, Tokyo 173-8515, Japan
	Shuji Aoki	Center for Atmospheric and Oceanic Studies, Graduate School of Science, Tohoku University Aoba, Sendai 980-8578, Japan
Kloosterburen (Netherlands (the))	Hans Berkhout	RIVM - Centre for Environmental Monitoring (MIL) PO Box 1 3720 BA Bilthoven the Netherlands
Kollumerwaard (Netherlands (the))	Hans Berkhout	RIVM - Centre for Environmental Monitoring (MIL) PO Box 1 3720 BA Bilthoven the Netherlands
	Ronald Spoor	RIVM - Centre for Environmental Monitoring (MIL) PO Box 1 3720 BA Bilthoven the Netherlands

LIST OF CONTRIBUTORS (continued)

Station Country/Territory	Name	Address
Wank Peak (Germany)	Hans-Eckhart Scheel	Karlsruhe Institute of Technology (KIT), IMK-IFU 82467 Garmisch-Partenkirchen, Germany
BEO Moussala (Bulgaria)	Ivo Kalapov	INRNE Institute for Nuclear Research and Nuclear Energy Tsarigradsko shose Blvd. 1784 Sofia Bulgaria
Monte Cimone (Italy)	Jgor Arduini	Università degli Studi di Urbino Istituto di Scienze Chimiche, piazza Rinascimento 6, 61029 Urbino - Italy
Monte Cimone (Italy)	Jgor Arduini	Università degli Studi di Urbino Istituto di Scienze Chimiche, piazza Rinascimento 6, 61029 Urbino - Italy
	Paolo Cristofanelli	ISAC-CNR ISAC-CNR, VIa Gobetti 101 - 40129 Bologna -Italy
Pallas-Sammaltunturi (Finland)	Juha Hatakka	Finnish Meteorological Institute P.O.Box 503,FI-00101 Helsinki, Finland
Hegyhatsal K-puszta (Hungary)	Laszlo Haszpra	Hungarian Meteorological Service P.O. Box 39, H-1675 Budapest, Hungary
Brotjacklriegel Deuselbach Waldhof Neuglobsow Schauinsland Westerland Zingst Zugspitze / Schneefernerhaus Zugspitze (Germany)	Ludwig Ries	Umweltbundesamt (UBA, Federal Environmental Agency) Air Monitoring Network
Monte Cimone (Italy)	Marco Alemanno	Italian Air Force Mountain Centre C.A.M.M. Mt. CIMONE,Via delle Ville 40, 41029-Sestola (MO), Italy
Krvavec (Slovenia)	Marijana Murovec	Slovenian Environment Agency Ministrstvo za okolje in prostor / Ministry of Environment andSpatial Planning Agencija RS za okolje / Slovenian Environment Agency Urad za meteorologijo / Meteorology Office Sektor za kakovost zraka / Air Quality Division Vojkova 1b, 1001 Ljubljana, p.p. 2608, Slovenia

LIST OF CONTRIBUTORS (continued)

Station Country/Territory	Name	Address
Sonnblick (Austria)	Marina Fröhlich	Federal Environment Agency Austria Spittelauer Lände 5, A-1090 Wien, Austria
	Wolfgang Spangl	Federal Environment Agency Austria Spittelauer Lände 5, A-1090 Wien, Austria
	Elisabeth Friedbacher	Federal Environment Agency Austria Spittelauer Lände 5, A-1090 Wien, Austria
Jungfraujoch (Switzerland)	Markus Leunberger	University of Bern University of Bern Physics Institute Sidlerstrasse 5 CH-3012 Bern
Pic du Midi (France)	Meyerfeld Yves	Laboratoire d'Aérologie
	Gheusi Francois	
Ile Grande Pic du Midi Puy de Dome (France)	Michel Ramonet	LSCE (Laboratoire des Sciences du Climat et de l'Environnement) UMR CEA-CNRS-UVSQ LSCE - CEA Saclay - Orme des Merisiers - 91191 Gif-sur-Yvette, France
Finokalia (Greece)		
Mace Head (Ireland)		
Begur (Spain)		
Kosetice (Czech Republic)	Milan Vana	Czech Hydrometeorological Institute, Kosetice Observatory Na Sabatce 17, 143 06 Praha 4 - Komorany, Czech Republic
Ocean Station Charlie Teriberka (Russian Federation)	Nina Paramonova	Main Geophysical Observatory (MGO) Karbyshev Street 7, St. Petersburg, 194021, Russian Federation
Zeppelinfjellet (Ny-Alesund) (Norway)	Ove Hermansen	Norwegian Institute for Air Research (NILU) P. O. Box 100 Instituttveien 18, N-2027 Kjeller, Norway
Capo Granitola (Italy)	Paolo Cristofanelli	ISAC-CNR ISAC-CNR, VIa Gobetti 101 - 40129 Bologna -Italy
Puy de Dome (France)	Pichon Jean-Marc	Laboratoire de Météorologie Physique

LIST OF CONTRIBUTORS (continued)

Station Country/Territory	Name	Address
	Meyerfeld Yves	Laboratoire d'Aérologie
Lampedusa (Italy)	Salvatore Chiavarini	Italian National Agency for New Technology, Energy, and Sustainable Economic Development (ENEA) ENEA-UTPRA Via Anguillarese, 301 00123 Rome, Italy
	Salvatore Piacentino	Italian National Agency for New Technology, Energy, and Sustainable Economic Development (ENEA) Laboratory for Earth Observations and Analyses (UTMEA-TER) ENEA ACS-CLIMOSS, Via Catania 2, 90141 Palrmo, Italy.
	Damiano Sferlazzo	Italian National Agency for New Technology, Energy, and Sustainable Economic Development (ENEA) Laboratory for Earth Observations and Analyses (UTMEA-TER) Station for Climate Observations Contrada Capo Grecale 92010 Lampedusa Italy
	Alcide di Sarra	Italian National Agency for New Technology, Energy, and Sustainable Economic Development (ENEA) Laboratory for Earth Observations and Analyses (UTMEA-TER) Via Anguillarese, 301 00123 Rome, Italy.
Ridge Hill Tacolneston Tall Tower (United Kingdom of Great Britain and Northern Ireland)	Simon O'Doherty	Atmospheric Chemistry Research Group School of Chemistry University of Bristol Atmospheric Chemistry Research Group School of Chemistry University of Bristol Cantocks Close BS8 1TS Bristol United Kingdom
	Aoife Grant	Atmospheric Chemistry Research Group School of Chemistry University of Bristol Atmospheric Chemistry Research Group School of Chemistry University of Bristol Cantocks Close BS8 1TS Bristol United Kingdom
Zugspitze (Germany)	Thomas Trickl	Karlsruhe Institute of Technology (KIT), IMK-IFU Kreuzeckbahnstraße 19 82467 Garmisch-Partenkirchen, Germany

ANTARCTICA

LIST OF CONTRIBUTORS (continued)

Station Country/Territory	Name	Address
Jubany (Italy)	Claudio Rafanelli	ICES (Int.l Center for Earth Sciences) c/o CNR-Istituto di Acustica- Area della Ricerca di Roma Tor Vergata,via Fosso del Cavaliere 100, 00133 Rome, Italy
King Sejong (Republic of Korea)	Haeyoung Lee	Climate Change Monitoring Division, Korea Meteorological Administration 61 Yeouidaebang-ro 16 gil, Dongjak-gu, Seoul, 07062, Republic of Korea
	Taejin Choi	Division of Polar Climate Research, KOPRI Get-Pearl Tower, 12 Gaetbeol-ro, Yeonsu-gu, Incheon, 406-840, Republic of Korea
Halley Bay (United Kingdom of Great Britain and Northern Ireland)	Neil Brough	British Antarctic Survey http://www.antarctica.ac.uk High Cross, Madingley road, Cambridge, CB3 0ET
Arrival Heights (New Zealand)	Sylvia Nichol	National Institute of Water & Atmospheric Research Ltd. 301 Evans Bay Parade, Greta Point, Private Bag 14-901, Kilbirnie, Wellington, New Zealand
	Gordon Brailsford	National Institute of Water & Atmospheric Research Ltd. 301 Evans Bay Parade, Greta Point,Private Bag 14-901, Kilbirnie, Wellington, New Zealand
	Ross Martin	National Institute of Water & Atmospheric Research Ltd. 301 Evans Bay Parade, Greta Point, Private Bag 14-901, Kilbirnie, Wellington, New Zealand
Mizuho (Japan)	Takakiyo Nakazawa	Center for Atmospheric and Oceanic Studies, Graduate School of Science, Tohoku University Aoba, Sendai 980-8578, Japan
Syowa Station (Japan)	Takakiyo Nakazawa	Center for Atmospheric and Oceanic Studies, Graduate School of Science, Tohoku University Aoba, Sendai 980-8578, Japan
	Gen Hashida	National Institute of Polar Research Kaga 1-9-10, Itabashi-ku, Tokyo 173-8515, Japan
	Shinji Morimoto	National Institute of Polar Research Kaga 1-9-10, Itabashi-ku, Tokyo 173-8515, Japan

MOBILE STATION

LIST OF CONTRIBUTORS (continued)

Station Country/Territory	Name	Address
Aircraft Observation of Atmospheric trace gases by JMA (Japan)	Atsushi TAKIZAWA	Atmospheric Environment Division, Global Environment and Marine Department, Japan Meteorological Agency (JMA) 1-3-4 Otemachi, Chiyoda-ku, Tokyo 100-8122, Japan
NOPACCS - Hakurei Maru - WEST COSMIC - Hakurei Maru No.2 - (Japan)	General Environmental Texhnos	The General Environmental Technos Co., Ltd. (Old:Kansai Environmental Engineering Center, Co., Ltd.) 1-3-5, Azuchi machi, Chuo-ku, Osaka 541-0052, Japan
INSTAC-I (International Strato/Tropospheric Air Chemistry Project) (Japan)	Hidekazu Matsueda	Geochemical Research Department, Meteorological Research Institute Nagamine 1-1, Tsukuba, Ibaraki 305-0052, Japan
Comprehensive Observation Network for TRace gases by AIrLiner (CONTRAIL) (Japan)	Hidekazu Matsueda	Geochemical Research Department, Meteorological Research Institute Nagamine 1-1, Tsukuba, Ibaraki 305-0052, Japan
	Toshinobu Machida	National Institute for Environmental Studies 16-2 Onogawa, Tsukuba 305-8506, Japan
MRI Research, Mirai, R/V (Japan)	Hisayuki Yoshikawa-Inoue	Laboratory of Marine and Atmospheric GeochemistryGraduate School of Environmental Earth ScienceHokkaido University N10W5, Kita-ku, Sapporo 060-0810, Japan
northern and western Pacific (Japan)	Kentaro Ishijima	Japan Agency for Marine-earth Science and Technology (JAMSTEC) 3173-25 Showamachi, Kanazawa-ku, Yokohama, 236-0001, Japan
	Shuji Aoki	Center for Atmospheric and Oceanic Studies, Graduate School of Science, Tohoku University Aoba, Sendai 980-8578, Japan
	Takakiyo Nakazawa	Center for Atmospheric and Oceanic Studies, Graduate School of Science, Tohoku University Aoba, Sendai 980-8578, Japan
Santarem (Brazil)	Luciana Vanni Gatti	IPEN Atmospheric Chemistry Laboratory Av. Prof. Lineu Prestes, 2242, Cidade Universitaria, Sao Paulo, SP- BRAZIL CEP 05508-900

LIST OF CONTRIBUTORS (continued)

Station Country/Territory	Name	Address
MRI Research, Hakuho Maru, R/V MRI Research, Kaiyo Maru, R/V MRI Research, 1978-1986, R/V MRI Research, Natushima, R/V MRI Research, Ryofu Maru, R/V MRI Research, Wellington Maru, R/V (Japan)	Masao Ishii	Geochemical Research Department, Meteorological Research Institute Nagamine 1-1, Tsukuba, Ibaraki 305-0052, Japan
Aircraft: Orleans (France)	Michel Ramonet	LSCE (Laboratoire des Sciences du Climat et de l'Environnement) UMR CEA-CNRS-UVSQ LSCE - CEA Saclay - Orme des Merisiers - 91191 Gif-sur-Yvette, France
Observation of Atmospheric Chemistry Over Japan The Observation of Atmospheric Methane Over Japan The Observation of Atmospheric Sulfur Hexafluoride Over Japan (Japan)	Michio Hirota	Geochemical Research Department, Meteorological Research Institute 1-1, Nagamine, Tsukuba, Ibaraki 305-0052, Japan
Alligator liberty, M/V Kofu Maru, R/V (Japan)	Shu Saito	Marine Division, Global Environment and Marine Department, Japan Meteorological Agency (JMA) 1-3-4 Otemachi, Chiyoda-ku, Tokyo 100-8122, Japan
Keifu Maru, R/V Ryofu Maru, R/V (Japan)	Shu Saito	Marine Division, Global Environment and Marine Department, Japan Meteorological Agency (JMA) 1-3-4 Otemachi, Chiyoda-ku, Tokyo 100-8122, Japan
	Keizo Sakurai	Marine Division, Global Environment and Marine Department, Japan Meteorological Agency (JMA) 1-3-4 Otemachi, Chiyoda-ku, Tokyo 100-8122, Japan
Pacific Ocean (New Zealand)	Sylvia Nichol	National Institute of Water & Atmospheric Research Ltd. 301 Evans Bay Parade, Greta Point, Private Bag 14-901, Kilbirnie, Wellington, New Zealand
	Gordon Brailsford	National Institute of Water & Atmospheric Research Ltd. 301 Evans Bay Parade, Greta Point,Private Bag 14-901, Kilbirnie, Wellington, New Zealand

LIST OF CONTRIBUTORS (continued)

Station Country/Territory	Name	Address
Comprehensive Observation Network for TRace gases by AIrLiner (CONTRAIL) over the Pacific Ocean 20-50 km off the coast of the Sendai plain over Japan between Sendai and Fukuoka (Japan)	Taku Umezawa	National Institute for Environmental Studies
	Shuji Aoki	Center for Atmospheric and Oceanic Studies, Graduate School of Science, Tohoku University
Soyo Maru, R/V Wakataka-Maru (Japan)	Tsuneo Ono	Hokkaido National Fisheries Research Institute 116 Katsurakoi, Kushiro 085-0802, Japan

LIST OF CONTRIBUTORS (continued)

Station Country/Territory	Name	Address
NOAA/ESRL Flask Network		
Assekrem (Algeria)	Bruce Vaughn** James White** ($^{13}CH_4$, $^{13}CO_2$ and $C^{18}O_2$)	(*)NOAA/ESRL Global Monitoring Division 325 Broadway R/GMD1 Boulder, CO 80305-3328, U.S.A.
Ushuaia (Argentina)	Jocelyn Turnbull ($^{14}CO_2$)	(**)Institute of Arctic and Alpine Research (INSTAAR) Campus box 450, University of Colorado, Boulder, CO 80309-0450, U.S.A.
Cape Grim (Australia)	Edward J.Dlugokencky* (CH_4 and CO_2)	
Ragged Point (Barbados)	Paul C. Novelli* (CO and H_2)	
Arembepe Natal (Brazil)	Bruce Vaughn** (N_2O and SF_6)	
Alert Lac La Biche Mould Bay (Canada)		
Easter Island (Chile)		
Lulin Shangdianzi Mt. Waliguan (China)		
Summit (Denmark)		
Pallas-Sammaltunturi (Finland)		
Amsterdam Island Crozet (France)		
Hohenpeissenberg Ochsenkopf (Germany)		
Hegyhatsal (Hungary)		
Heimaey (Iceland)		
Bukit Koto Tabang (Indonesia)		

LIST OF CONTRIBUTORS (continued)

Station Country/Territory	Name	Address
Mace Head (Ireland)		
Sede Boker (Israel)		
Lampedusa (Italy)		
Syowa Station (Japan)		
Sary Taukum Plateau Assy (Kazakhstan)		
Mt. Kenya (Kenya)		
Christmas Island (Kiribati)		
Kaashidhoo (Maldives)		
Dwejra Point (Malta)		
Mex High Altitude Global Climate Observation Center, Mexico (Mexico)		
Ulaan Uul (Mongolia)		
Gobabeb (Namibia)		
Baring Head Kaitorete Spit (New Zealand)		
Ocean Station "M" Zeppelinfjellet (Ny-Alesund) (Norway)		
Baltic Sea (Poland)		

LIST OF CONTRIBUTORS (continued)

Station Country/Territory	Name	Address
Terceira Island (Portugal)		
Tae-ahn Peninsula (Republic of Korea)		
Black Sea (Romania)		
Tiksi (Russian Federation)		
Mahe Island (Seychelles)		
Cape Point (South Africa)		
Izaña (Tenerife) (Spain)		
Ascension Island St. David's Head Tudor Hill Halley Bay Bird Island Tacolneston Tall Tower (United Kingdom of Great Britain and Northern Ireland)		
Akademik Korolev, R/V		
Argyle		
Atlantic Ocean		
St. Croix		
Barrow		
Cold Bay		
Cape Meares		
Discoverer 1983 & 1984, R/V		
Drake Passage		
Discoverer 1985, R/V		
Guam		

LIST OF CONTRIBUTORS (continued)

Station Country/Territory	Name	Address
Grifton		
John Biscoe, R/V		
Key Biscayne		
Korolev, R/V		
Kitt Peak		
Cape Kumukahi		
Park Falls		
Long Lines Expedition, R/V		
McMurdo Station		
Sand Island		
Mauna Loa		
Mexico Naval H-02, R/V		
Niwot Ridge (T-van)		
Oceanographer, R/V		
Olympic Peninsula		
Pacific-Atlantic Ocean		
Polar Star, R/V		
Pacific Ocean		
Palmer Station		
Point Arena		
South China Sea		
Southern Great Plains		
Shemya Island		
La Jolla		
Tutuila (Cape Matatula)		
South Pole		

LIST OF CONTRIBUTORS (continued)

Station Country/Territory	Name	Address
Ocean Station Charlie		
Surveyor, R/V		
Trinidad Head		
Wendover		
West Branch		
Moody		
Western Pacific		
(United States of America)		
NOAA/ESRL/HATS Network		
Ushuaia (Argentina)	Geoffrey S. Dutton James W. Elkins Stephen A. Montzka	Halocarbons and Other Atmosphere Trace Species Group (HATS)/NOAA/ESRL Global Monitoring Division 325 Broadway R/GMD1 Boulder, CO 80305-3328, U.S.A.
Cape Grim (Australia)		
Alert (Canada)		
Summit (Denmark)		
Mace Head (Ireland)		
BACPAC 99		
BLAST1		
BLAST2		
BLAST3		
Barrow		
CLIVAR 01		
Gas Change Experiment		
Harvard Forest		
HATS Ocean Projects		

LIST OF CONTRIBUTORS (continued)

Station Country/Territory	Name	Address
Grifton		
Cape Kumukahi		
Park Falls		
Mauna Loa		
Niwot Ridge (C-1)		
PHASE I-04		
Palmer Station		
Tutuila (Cape Matatula)		
South Pole		
Trinidad Head		
(United States of America)		

LIST OF CONTRIBUTORS (continued)

Station Country/Territory	Name	Address
CSIRO Flask Network		
Aircraft (over Bass Strait and Cape Grim) Cape Ferguson Cape Grim Casey Station Gunn Point Mawson Macquarie Island (Australia)	Ray Langenfelds Paul Krummel Marcel van der Schoot Paul Steele Colin Allison	Commonwealth Scientific and Industrial Research Organisation (CSIRO) CSIRO Marine and Atmospheric Research Private Bag 1 Aspendale, Vic, Australia 3195
Alert Estevan Point (Canada)		
Cape Rama (India)		
Shetland (United Kingdom of Great Britain and Northern Ireland)		
Mauna Loa South Pole (United States of America)		
ALE/GAGE/AGAGE Network		
Cape Grim (Australia)	Michela Maione Martin Vollmer Stefan Reimann	Scripps Institute of Oceanography Scripps Institution of Oceanography UCSD, La Jolla, CA 92093-0244 USA
Ragged Point (Barbados)	Simon O'Doherty Paul Krummel Jgor Arduini	
Adrigole Mace Head (Ireland)	Paul Steele Ray Wang Ray F. Weiss	
Monte Cimone (Italy)		
Zeppelinfjellet (Ny-Alesund) (Norway)		
Gosan (Republic of Korea)		
Jungfraujoch (Switzerland)		

LIST OF CONTRIBUTORS (continued)

Station Country/Territory	Name	Address
Cape Meares Tutuila (Cape Matatula) Trinidad Head (United States of America)		

ACRONYMS

ATMOSPHERIC SPECIES:

CCl_4	tetrachloromethane (carbon tetrachloride)
C_2Cl_4	tetrachloroethylene
CFC-11	chlorofluorocarbon-11 (trichlorofluoromethane, CCl_3F)
CFC-12	chlorofluorocarbon-12 (dichlorodifluoromethane, CCl_2F_2)
CFC-113	chlorofluorocarbon-113 (1,1,2-trichlorotrifluoroethane, CCl_2FCClF_2)
CFCs	chlorofluorocarbons
CH_4	methane
$CHBr_3$	tribromomethane (bromoform)
CH_2Br_2	dibromomethane
CH_3Br	bromomethane
CH_3CCl_3	1,1,1-trichloroethane (methyl chloroform)
$CHCl_3$	trichloromethane (chloroform)
CH_2Cl_2	dichloromethane (methylene chloride)
CH_3Cl	chloromethane (methyl chloride)
C_2HCl_3	trichloroethylene
CO	carbon monoxide
CO_2	carbon dioxide
H_2	hydrogen
Halon-1211	chlorodifluorobromomethane ($CBrClF_2$)
Halon-1301	bromotrifluoromethane ($CBrF_3$)
HCFC-141b	hydrochlorofluorocarbon-141b (1,1-dichloro-1-fluoroethane, CH_3CCl_2F)
HCFC-142b	hydrochlorofluorocarbon-142b (1,1-difluoro-1-chloroethane, CH_3CClF_2)
HCFC-22	hydrochlorofluorocarbon-22 (chlorodifluoromethane, $CHClF_2$)
HCFCs	hydrochlorofluorocarbons
HFC-134a	hydrofluorocarbon-134a (1,1,1,2-tetrafluoroethane, CH_2FCF_3)
HFC-152a	hydrofluorocarbon-152a (1,1-difluoroethane, CHF_2CH_3)
HFCs	hydrofluorocarbons
N_2O	nitrous oxide
NO_X	nitrogen oxides
O_3	ozone
PFCs	perfluorocarbons
Rn	radon
SF_6	sulphur hexafluoride
SO_2	sulphur dioxide
TIC	total inorganic carbon
VOCs	volatile organic compounds

UNITS:

ppm	parts per million
ppb	parts per billion
ppt	parts per trillion

Others:

ENSO	El Niño-Southern Oscillation
M/V	merchant vessel
R/V	research vessel

LIST OF WMO/WDCGG PUBLICATIONS

DATA REPORTING MANUAL:

WDCGG No. 1	January	1991

WMO WDCGG DATA REPORT:

			(period of data accepted)				
WDCGG No. 2 Part A	October	1992	October	1990	~	August	1992
WDCGG No. 2 Part B	October	1992	October	1990	~	August	1992
WDCGG No. 3	October	1993	September	1992	~	March	1993
WDCGG No. 5	March	1994	April	1993	~	September	1993
WDCGG No. 6	September	1994	September	1993	~	March	1994
WDCGG No. 7	March	1995	April	1994	~	December	1994
WDCGG No. 9	September	1995	January	1995	~	June	1995
WDCGG No.10	March	1996	July	1995	~	December	1995
WDCGG No.11	September	1996	January	1996	~	June	1996
WDCGG No.12	March	1997	July	1996	~	November	1996
WDCGG No.14	September	1997	December	1996	~	June	1997
WDCGG No.16	March	1998	July	1997	~	December	1997
WDCGG No.17	September	1998	January	1998	~	June	1998
WDCGG No.18	March	1999	July	1998	~	December	1998
WDCGG No.20	September	1999	January	1999	~	June	1999
WDCGG No.21	March	2000	July	1999	~	December	1999
WDCGG No.23	September	2000	January	2000	~	June	2000
WDCGG No.25	March	2001	July	2000	~	December	2000

WMO WDCGG DATA CATALOGUE:

WDCGG No. 4	December	1993
WDCGG No.13	March	1997
WDCGG No.19	March	1999
WDCGG No.24	March	2001

WMO WDCGG DATA SUMMARY:

WDCGG No. 8	October	1995
WDCGG No.15	March	1998
WDCGG No.22	March	2000
WDCGG No.26	March	2002
WDCGG No.27	March	2003
WDCGG No.28	March	2004
WDCGG No.29	March	2005
WDCGG No.30	March	2006
WDCGG No.31	March	2007
WDCGG No.32	March	2008
WDCGG No.33	March	2009
WDCGG No.34	March	2010
WDCGG No.35	March	2011
WDCGG No.36	March	2012
WDCGG No.37	March	2013
WDCGG No.38	March	2014
WDCGG No.39	March	2015
WDCGG No.40	March	2016
WDCGG No.41	March	2017

WMO WDCGG CD-ROM: (period of data accepted)

CD-ROM No. 1	March	1995	October	1990	~	December	1994
CD-ROM No. 2	March	1996	October	1990	~	June	1995
CD-ROM No. 3	March	1997	October	1990	~	June	1996
CD-ROM No. 4	March	1998	October	1990	~	December	1997
CD-ROM No. 5	March	1999	October	1990	~	December	1998
CD-ROM No. 6	March	2000	October	1990	~	December	1999
CD-ROM No. 7	March	2001	October	1990	~	December	2000
CD-ROM No. 8	March	2002	October	1990	~	January	2002
CD-ROM No. 9	March	2003	October	1990	~	December	2002
CD-ROM No.10	March	2004	October	1990	~	December	2003
CD-ROM No.11	March	2005	October	1990	~	December	2004
CD-ROM No.12	March	2006	October	1990	~	December	2005
CD-ROM No.13	March	2007	October	1990	~	November	2006
CD-ROM No.14	March	2008	October	1990	~	November	2007

WMO WDCGG DVD: (period of data accepted)

DVD No. 1	March	2009	October	1990	~	November	2008
DVD No. 2	March	2010	October	1990	~	November	2009
DVD No. 3	March	2011	October	1990	~	November	2010
DVD No. 4	March	2012	October	1990	~	November	2011
DVD No. 5	March	2013	October	1990	~	November	2012
DVD No. 6	March	2014	October	1990	~	November	2013
DVD No. 7	March	2015	October	1990	~	November	2014
DVD No. 8	March	2016	October	1990	~	November	2015